

Radio-over-Fibre Systems
for
Body-Centric Communication Measurements

Sunny Dusara

A thesis submitted to
The University of Birmingham
for the degree of
MASTER OF RESEARCH

Electronic, Electrical and Computer Engineering
School of Engineering
The University of Birmingham
December 2010

UNIVERSITY OF
BIRMINGHAM

University of Birmingham Research Archive

e-theses repository

This unpublished thesis/dissertation is copyright of the author and/or third parties. The intellectual property rights of the author or third parties in respect of this work are as defined by The Copyright Designs and Patents Act 1988 or as modified by any successor legislation.

Any use made of information contained in this thesis/dissertation must be in accordance with that legislation and must be properly acknowledged. Further distribution or reproduction in any format is prohibited without the permission of the copyright holder.

ABSTRACT

Body-centric wireless communication devices are continually required to be smaller, lighter and thinner, and consequently the PCB, components, battery and antenna must become smaller.

The conventional method for measuring an antenna's performance requires an anechoic chamber coaxial cable measurement system. However, measuring the antenna's radiation pattern becomes difficult when the relative size of the antenna is smaller than the coaxial cable. Furthermore the difficulty increases when the antenna is in close proximity to the body due to the effects of detuning causing low antenna efficiency. A coaxial cable system produces poor measurement repeatability due to moving cables. This produces variable loss and phase and undesired coupling.

To solve this problem, this thesis describes the design of a novel radio-over-fibre antenna measurement system for on-body channel path measurements. The fibre system is employed to replace coaxial cables with fibre optic cables between the antennas and network analyser at 2.45 Gigahertz for the belt-to-head channel. The simulations are compared to measurements taken in the anechoic chamber. The radio-over-fibre system appears to improve measurement accuracy through an observable improvement in mean forward path gain (S_{21}) of 2.19 dB when compared with the coaxial system. This improvement is most desirable for repeatable on-body measurements.

DEDICATION

This work is dedicated to my parents, Ajay and Bhagwati, and family, Ketan, Sheila, Anisha and Sweta, as without their love, help and support this would not have been possible.

ACKNOWLEDGEMENTS

This project would not have been possible without help and support from others. I must commence by thanking my supervisor, Professor Peter Hall, for his support, guidance and constructive critique throughout the year.

Members of the Communications Engineering research group, Yuriy Nechayev, Lida Akhoondzadeh-Asl, and Elham Ebrahimi, contributed through assisting with on-body measurements. In addition, general technical support provided during the year by Alan Yates was appreciated.

Finally, I acknowledge with thanks, the financial support provided by the Engineering and Physical Sciences Research Council.

TABLE OF CONTENTS

Chapter 1	1
1 Introduction	1
1.1 Motivation	1
1.2 Objectives	5
1.3 Flowchart of the project	5
1.4 Contents of the Thesis	7
Chapter 2	8
2 Literature Review	8
2.1 Introduction	8
2.2 Body-centric Communications.....	8
2.2.1 Off-body to On-body Communication	10
2.2.2 On-body Communication.....	10
2.2.3 In-body Communication	10
2.2.4 Body Proximity effects on Antennas	11
2.2.5 Phantoms	14
2.2.6 On-body Simulation Techniques.....	16
2.3 Previous Radio-over-Fibre Systems for Antenna Measurements.....	17
2.4 Transmission Lines	21
2.4.1 Coaxial cable	21
2.4.2 Matching.....	29

2.4.3	Optical Transmission.....	29
2.5	Alternative Electromagnetic or Radio Frequency Interference Reduction Techniques for Antenna Measurements	33
2.6	Conclusions	35
Chapter 3	36
3	Design, Simulation and Results of Radio-over-Fibre System	36
3.1	Introduction	36
3.2	Radio-over-Fibre System.....	36
3.2.1	Architecture	36
3.2.2	Specification.....	37
3.2.3	Components.....	38
3.3	System Design.....	40
3.3.1	Electro-Optical Modulator Design	42
3.3.2	Opto-Electrical Modulator Design	43
3.4	Simulated Results.....	44
3.5	Measurement Results	46
3.6	Conclusions	54
Chapter 4	55
4	Integration and Characterisation of a Commercial Radio-over-Fibre System vs. Coaxial Cable System for Off-Body Chamber Measurements	55
4.1	Introduction	55
4.2	Power Supply Design	55

4.3	Radio-over-Fibre System Characterisation	58
4.3.1	System Link 1 (Transceiver to Receiver)	58
4.3.2	System Link 2 (Transmitter to Transceiver)	59
4.3.3	Full System Link 1 and 2 Link Budget	61
4.3.4	Temperature vs. Loss	61
4.4	Monopole Design and Build	65
4.5	Monopole Radiation Patterns with Coaxial Cable in the Anechoic Chamber	66
4.6	Comparison of Monopole Radiation Patterns using Coaxial Cable or Fibre Optic Cable in the Anechoic Chamber	68
4.7	Conclusions	70
Chapter 5		71
5	Simulation and Measurement Results of Commercial RoF System vs. Coaxial Cable for On-Body Measurements	71
5.1	Introduction	71
5.2	On-body Simulations – Comparison of Coaxial Cable vs. Fibre in CST MWS	71
5.3	On-body Measurements – Comparison of Coaxial Cable vs. Fibre in the Anechoic Chamber	73
5.4	Conclusions	83
Chapter 6		84
6	Conclusions and Suggestions for Further Work	84
6.1	Conclusions	84
6.2	Suggestions for Further Work	88

7	References.....	89
8	Appendices	91

Appendix A - Honeywell HFE4083-322/XBA Datasheet

Appendix B - Thorlabs FG04 Datasheet

Appendix C - Radio-over-Fibre 1-Stage Simulation Results (1 x MSA-0886)

Appendix D - Radio-over-Fibre 3-Stage Simulation Results (1 x MGA-81563 & 2 x MGA-86576)

Appendix E - Radio-over-Fibre 3-Stage Simulation Results (3 x MSA-0886)

Appendix F - Avago MSA-0866 Datasheet

Appendix G - Avago MGA-81563 Datasheet

Appendix H - Avago MGA-86576 Datasheet

Appendix I - Radio-over-Fibre 1-Stage Measurement Results (1 x MSA-0886)

Appendix J - Radio-over-Fibre 3-Stage Measurement Results (1xMGA-81563 & 2xMGA-86576)

Appendix K - Radio-over-Fibre 3-Stage Simulation Results (3 x MSA-0886)

Appendix L - Radio-over-Fibre System Characterisation

Appendix M - Ferrotec Single Stage Thermoelectric Cooler

Appendix N - Optical Zonu OZ600 Transceiver Datasheet

Appendix O - Optical Zonu OZ450 Transmitter/Receiver Datasheet

Appendix P - On-Body Simulation & Measurement Results

Appendix Q - Rhopase 160 Series Coaxial Cable Datasheet

LIST OF ILLUSTRATIONS

Figure 1.1 Example of typical wireless products available.....	1
Figure 1.2 Typical anechoic chamber measurement setup (a) diagram and (b) photograph, (c) Typical on-body antenna measurement setup photograph (RAM (Radio Absorbent Material), TX (Transmit), RX (Receive)).....	3
Figure 1.3 (a) Real life – Antenna & transceiver integrated into user equipment (b) Conventional measurement with braided coaxial cable – Antenna & coaxial cable (differs significantly to reality) (c) Novel measurement with fibre-optic system – Antenna, fibre module & fibre-optic cable (closer to reality).....	4
Figure 1.4 Flowchart of project (practical work (white font) and simulations (black font)).....	6
Figure 2.1 Medical monitoring example of wireless body area network (WBAN) and wireless personal area network (WPAN) [1].....	9
Figure 2.2 Cochlear Implant [3].....	11
Figure 2.3 Example of electrical characteristics of tissues over frequency range of 1 MHz to 100 GHz at 37 °C [5].....	11
Figure 2.4 Simulation & measurement of monopole efficiency in free space and on-body phantom material [6].....	12
Figure 2.5 Possible placement positions of wearable devices on the body [9].....	13
Figure 2.6 (a) Example of human-head dry phantom (b) Multi-postural realistic human-torso phantom at 900MHz (c) Realistic human-torso phantom (agar-based solid phantom) [5]	14
Figure 2.7 Mike Phantom [10].....	15
Figure 2.8 A voxel phantom NORMAN [5].....	15
Figure 2.9 James phantom in Poser 6 [11].....	16
Figure 2.10 Maximum deviations of three different cabling configurations for (a) vertical and (b) horizontal polarized antenna measurement [12].....	18

Figure 2.11 Diagram showing measurement system for the radiation pattern [13].....	19
Figure 2.12 (a) Measurement model showing orientation of axis and (b) diagram showing cable setting for radiation pattern measurement [13]	19
Figure 2.13 Radiation pattern measured by the (a) RF cable and (b) Fibre-optic cables at position B (Z-X plane) as per Figure 2.12 [13]	20
Figure 2.14 Typical coaxial cable showing internal structure	21
Figure 2.15 Coaxial Line Geometry [16]	22
Figure 2.16 EM information leakage from a braided shielded coaxial cable [17]	23
Figure 2.17 Simulated transfer impedance of differing cable types vs. frequency [18]	24
Figure 2.18 Measured transfer impedance of URM102 vs. frequency [18]	24
Figure 2.19 Cross-sectional view of coaxial cable immersed in an electric field [15].....	25
Figure 2.20 Coaxial cable immersed in a tangential magnetic field [15]	25
Figure 2.21 Cross-sectional view of cylindrical shell immersed in a uniform magnetic field [15]	26
Figure 2.22 Coaxial cable - Distribution of current in the conductors when current is injected into the shield [15].....	27
Figure 2.23 Layout of (a) braided shielded cable and (b) tape-wound shielded cable [15]	28
Figure 2.24 Theoretical transfer impedance vs. frequency for solid, perforated and tape-wound shield [15]	28
Figure 2.25 Measured transfer impedances for Tyco coaxial cables [19].....	28
Figure 2.26 Analogue Optical Link - Intensity Modulation Direct Detection (IMDD).....	30
Figure 2.27 VCSEL semiconductor laser structure [20]	32
Figure 2.28 Ferrite beads for EMI/RFI reduction	34
Figure 2.29 Quarter-wave balun sleeve for mobile phone handset [23].....	34
Figure 2.30 (a) Real life – Antenna & transceiver (user equipment) (b) Conventional measurement with coaxial cable – Antenna & braided coaxial cable (differs significantly to reality) (c)	

Novel measurement with fibre-optic system – Antenna, fibre-optic module & fibre-optic cable (closer to reality).....	35
Figure 3.1 On-body measurements employing novel radio-over-fibre system	37
Figure 3.2 Radio-over-fibre system without the body (OEM (opto-electrical modulator), EOM (electro-optical modulator))	37
Figure 3.3 Simple Electro-Optical Modulator (EOM) and Opto-Electrical Modulator (OEM) circuit....	40
Figure 3.4 Electro-Optical Modulator Microstrip layout.....	42
Figure 3.5 Stabilised voltage and current output.....	42
Figure 3.6 Opto-Electrical Modulator Circuit Diagram.....	43
Figure 3.7 1-Stage OEM Microstrip Layout	43
Figure 3.8 3-Stage OEM Microstrip Layout	43
Figure 3.9 Overview of the radio-over-fibre system with 1-stage amplifier (MSA0886) (Appendix C)	44
Figure 3.10 Example S-Parameter result of radio-over-fibre system with 1-stage amplifier at 28mA Bias (MSA-0886)	45
Figure 3.11 S-Parameter results of radio-over-fibre system with 1-stage and 3-stage amplifiers	45
Figure 3.12 Measurement setup to characterise the laser diode.....	46
Figure 3.13 Power Output (a) dBm and (b) uW vs. Forward Current (mA) for Laser Diode HFE4080-321/XBA.....	47
Figure 3.14 Laser Diode Frequency Modulation Response at $P_{RFIn} = 0$ dBm	49
Figure 3.15 RF Modulation vs. Optical Power for differing Fibre Types	49
Figure 3.16 Fibre coupling measurement setup between fibre optic cables and laser diode.....	49
Figure 3.17 Radio-over-Fibre System with 1-Stage MSA-0886 (FG04-1)	50
Figure 3.18 Measurement Results of 1-Stage System (MSA-0886/FG04-1)	51
Figure 3.19 Radio-over-Fibre System with 3-Stage 1x MGA-81563, 2x MGA-86576 (FG04-2).....	51
Figure 3.20 Results of 3-Stage System (1 x PA & 2 x LNA)	52
Figure 3.21 Radio-over-Fibre System with 3-Stage 3x MSA-0886 (FG04-2).....	52

Figure 3.22 Results of 3-Stage System (3 x PA)	53
Figure 4.1 Power Supply for Commercial Radio-over-Fibre System Modules	56
Figure 4.2 Loss of Gain with Voltage Dropout	56
Figure 4.3 DC Cables to OZ450 Radio-over-Fibre modules	57
Figure 4.4 Photos of whole system (Transceiver → Receiver→ Transmitter→ Transceiver)	58
Figure 4.5 Diagram of the measurement set up for System Link 1.....	58
Figure 4.6 Results of the Transceiver to Receiver (System Link 1).....	59
Figure 4.7 Diagram of the measurement set up for Transmitter to Transceiver (System Link 2)	60
Figure 4.8 Results of the Transmitter to Transceiver (System Link 2)	60
Figure 4.9 Gain Variation over Time for Commercial RoF System	62
Figure 4.10 40dB Attenuators in place of RF channel for controlled measurement analysis.....	62
Figure 4.11 (a) External heatsink, (b) 4.5cm x 4.5cm internal heatsink and ventilation holes.....	63
Figure 4.12 Gain/Loss over time for commercial RoF system 2 with 40dB attenuators	63
Figure 4.13 (a) 3D model and (b) return loss simulation result using CST MWS	65
Figure 4.14 Quarter-wave monopole.....	65
Figure 4.15 Bird’s eye view diagrams above and photographs below showing coaxial cable orientation and antenna polarisation (a) Vivaldi reference antenna (b) cable left co-polarisation (c) cable left cross-polarisation (d) cable right co-polarisation (e) cable right cross-polarisation	66
Figure 4.16 Influence of coaxial cable left vs. coaxial cable right on monopole antenna radiation pattern.....	67
Figure 4.17 (a) Coaxial system and (b) fibre system measurement set up with monopoles.....	68
Figure 4.18 Normalised radiation pattern for coaxial cable and fibre optic cable in H-Plane Co- Polarised.....	69
Figure 5.1 Mike phantom with two monopoles in CST MWS 2008	72

Figure 5.2 Photograph of measurement setup of vertical orientation coaxial cable with on-body Mike stance	74
Figure 5.3 Measurement & simulation results of vertical alignment coaxial cable on-body over 60 seconds in Mike stance as per Figure 5.2.....	74
Figure 5.4 Mean plot measurement & simulation results of vertical alignment coaxial cable on-body in Mike stance as per Figure 5.2.....	75
Figure 5.5 Photographs of measurement setup of (a) horizontal (90°) & (b) diagonal (45°) orientation coaxial cable with on-body in Mike stance	75
Figure 5.6 Measurement & simulation results of horizontal & diagonal orientation coaxial cable on-body over 60 seconds in Mike stance as per Figure 5.5	76
Figure 5.7 Mean plots of measurements & simulation results of horizontal & diagonal orientation coaxial cable on-body in Mike stance as per Figure 5.5.....	76
Figure 5.8 Photograph of measurement setup of fibre system on-body in Mike stance	77
Figure 5.9 Measurement & simulation results 1 of fibre system on-body over 60 seconds in Mike stance as per Figure 5.8	77
Figure 5.10 Measurement & simulation results 2 of fibre system on-body over 60 seconds in Mike stance as per Figure 5.8	78
Figure 5.11 Mean plot of measurement & simulation results of fibre system on-body in Mike stance as per Figure 5.8	79
Figure 5.12 Mean plot of matched pair simulated & measured results of coaxial cable vs. fibre system on-body in Mike stance.....	80
Figure 5.13 On-body measurement results of coaxial cable vs. fibre cable during an 18 posture set (IF bandwidth is 30 Hz).....	82

LIST OF TABLES

Table 2.1 Efficiency results for Monopole [6]	12
Table 2.2 Average On-body Path Loss (dB) with quarter-wave monopoles at 2.45GHz [4]	13
Table 3.1 Results Table for Laser Diode HFE4080-321/XBA.....	48
Table 3.2 Table of RF modulation signal in dBm/mW/V/mA.....	50
Table 5.1 Tabular results of $\Delta\langle S_{21} \rangle$ for various measurement arrangements ($\Delta\langle S_{21} \rangle$ is the difference between max and min of the means shown in Figure 5.3, Figure 5.6, Figure 5.9 and Figure 5.10)	81

CHAPTER 1

1 INTRODUCTION

1.1 Motivation

Body-centric wireless communication devices are becoming popular with the increasing number of wireless communication users. This has led to an increasing number of body-centric communication devices being manufactured for varying applications. The applications for such devices can be categorised into two groups, personal and commercial.

Personal users of wireless communications require the use for social and entertainment purposes. These devices come in the form of mobile phones, Personal Digital Assistants (PDA), Bluetooth headsets (mono and stereo), Bluetooth MP3 players. Some of these products have several wireless features integrated within them. An example would be the PDA, which has Wi-Fi (Wireless Fidelity), Bluetooth, Infrared, GPS (Global Positioning System), GSM (Groupe Spécial Mobile) and UMTS (Universal Mobile Telecommunications System). An example of a range of devices is shown in Figure 1.1.



Figure 1.1 Example of typical wireless products available

Commercial users rely critically on wireless communications. Many businesses and organisations such as the military, the emergency-services and the medical profession use these applications. The types of devices that are used by the professions above are body-worn computers and medical-sensor networks.

The concept of body-centric wireless communication encompasses a Personal Area Network (PAN) and a Body Area Network (BAN). PAN and BAN can be categorised into three communication components; off-body to on-body, on-body and in-body. An off-body device communicates to an on-body device (e.g. laptop to headset), two on-body devices communicating with each other (e.g. mobile phone to headset), and two in-body devices communicating with each other (e.g. medical implant and sensor network).

The popularisation of body-centric wireless devices has caused designers to miniaturise these devices, making them easy to carry, user friendly and fashionable. As devices are required to be smaller, lighter and thinner, consequently, the printed circuit board (PCB), components, battery and antenna must be smaller. As a result, this causes many challenges during design and testing procedures.

In particular, the designed antenna or antennae in a device require simulation and testing in order to evaluate their performance. The parameters that characterise the performance of an antenna are the radiation pattern, gain, directivity, efficiency, impedance, current distribution and polarisation. These parameters can be measured using several methods. The most common antenna range is the free-space range, which can be simulated using an anechoic chamber. Thus, the conventional method for measuring antenna performance requires the use of a braided coaxial cable to feed an antenna, which connects to a network analyser. However, as previously mentioned, the smaller the antenna the greater the measurement challenge due to the relative size difference between the antenna-under-test (AUT) and the braided coaxial cable. The coaxial cable emits and absorbs electromagnetic waves (egress/ingress), which causes perturbation of the antenna radiation pattern and the transmitted signal. The amount of egress or ingress depends on the braided coaxial cable properties such as transfer impedance, which will be introduced and discussed later.

On-body communication systems use a relatively small antenna for communication and a problem that occurs is the undesired influence of braided coaxial cable on measurements. On-body

measurements also involve taking measurements of static postures and the transitions between such postures. The on-body position of coaxial cable during the measurement process is critical and must remain identical throughout the process for accurate results. This is unachievable due to the dynamic nature of on-body measurements.

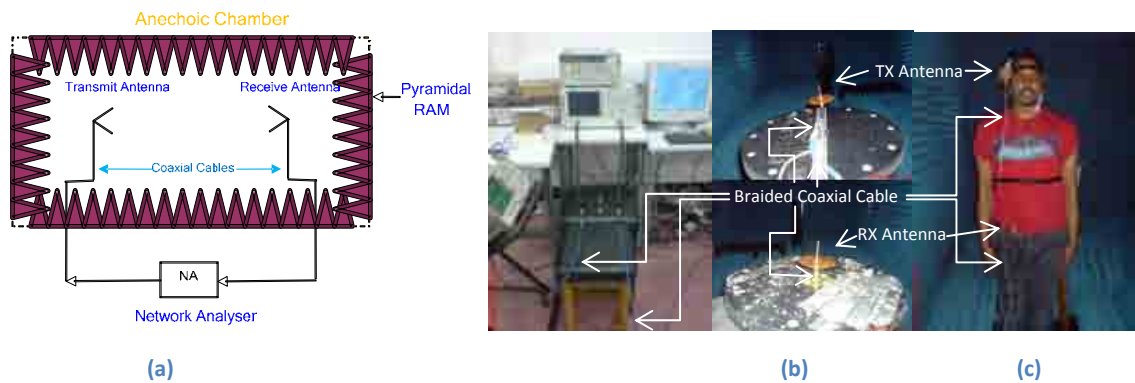


Figure 1.2 Typical anechoic chamber measurement setup (a) diagram and (b) photograph, (c) Typical on-body antenna measurement setup photograph (RAM (Radio Absorbent Material), TX (Transmit), RX (Receive))

The problems of on-body antenna measurements that need to be addressed are:

- The variation of coaxial cable position when the body moves, resulting in variable loss and phase. Even during a static posture the body moves slightly, therefore resulting in variable and unpredictable loss and phase
- The generation of current on the outer shield through radiation or absorption instigating superfluous coupling
- Metallic influence of coaxial cable perturbing the radiation from the antenna through attenuation of waves or scattering into different directions

This thesis explores a radio-over-fibre system to replace coaxial cables between an antenna and the network analyser as shown in Figure 1.2(a). The fibre system eliminates the use of braided coaxial cable hence removing electromagnetic emission and absorption from coaxial cables. This should enable an accurate measurement method for small antennas mounted on-body. There are no commercial products that address this problem specifically, as shielded coaxial cables used in most

measurement systems are assumed to be relatively loss free and confine the majority of the electromagnetic wave within the structure.

Figure 1.3 shows a diagram to highlight the problems of on-body antenna measurements which need to be addressed and depicts a novel method to improve measurement accuracy using an active fibre system.

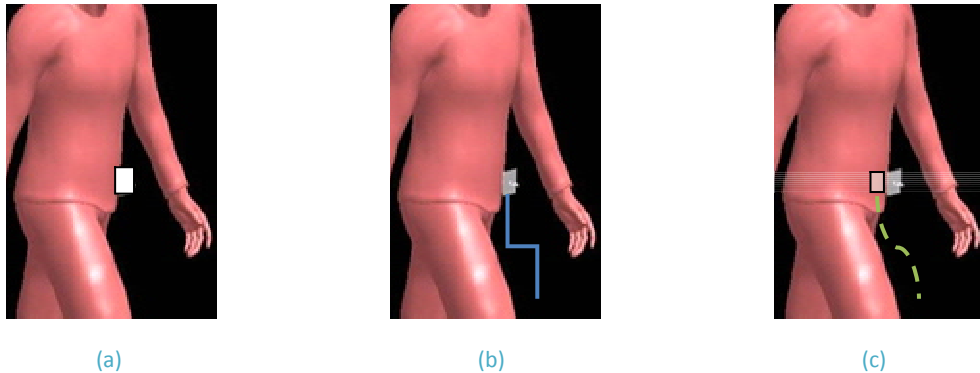


Figure 1.3 (a) Real life – Antenna & transceiver integrated into user equipment

(b) Conventional measurement with braided coaxial cable – Antenna & coaxial cable (differs significantly to reality)

(c) Novel measurement with fibre-optic system – Antenna, fibre module & fibre-optic cable (closer to reality)

Radio-over-fibre, (RoF), is a system that modulates an input radio frequency (RF) signal onto an optical signal. This is then carried via fibre optic cable to the destination, which demodulates the optical signal into the original input RF signal. The major advantage of using optical light as the carrier is that it is impervious to radio frequency interference (RFI) or electromagnetic interference (EMI). There are further advantages of using radio-over-fibre technologies over braided coaxial cable which will be discussed later.

1.2 Objectives

The main objective of this thesis is to design, build and evaluate an alternative system that removes coaxial cables from antenna measurements. The on-body components need to be free from coaxial cable and have low RF visibility. A summary of objectives are to:

- Explore the source of coaxial cable variable loss and phase, superfluous coupling and perturbation of the radiation pattern
- Research alternative antenna measurement methods using fibre-optics
- Design, build and evaluate the radio-over-fibre system
- Investigate the effects of coaxial cable on measurements
- Investigate the effects of radio-over-fibre on measurements
- Compare the results of the both methods and conclude findings.

1.3 Flowchart of the project

The project has been divided into smaller objectives in order to be completed over the period of study. It has also been subdivided into two categories; practical and simulation work, which is illustrated in the flowchart in Figure 1.4.

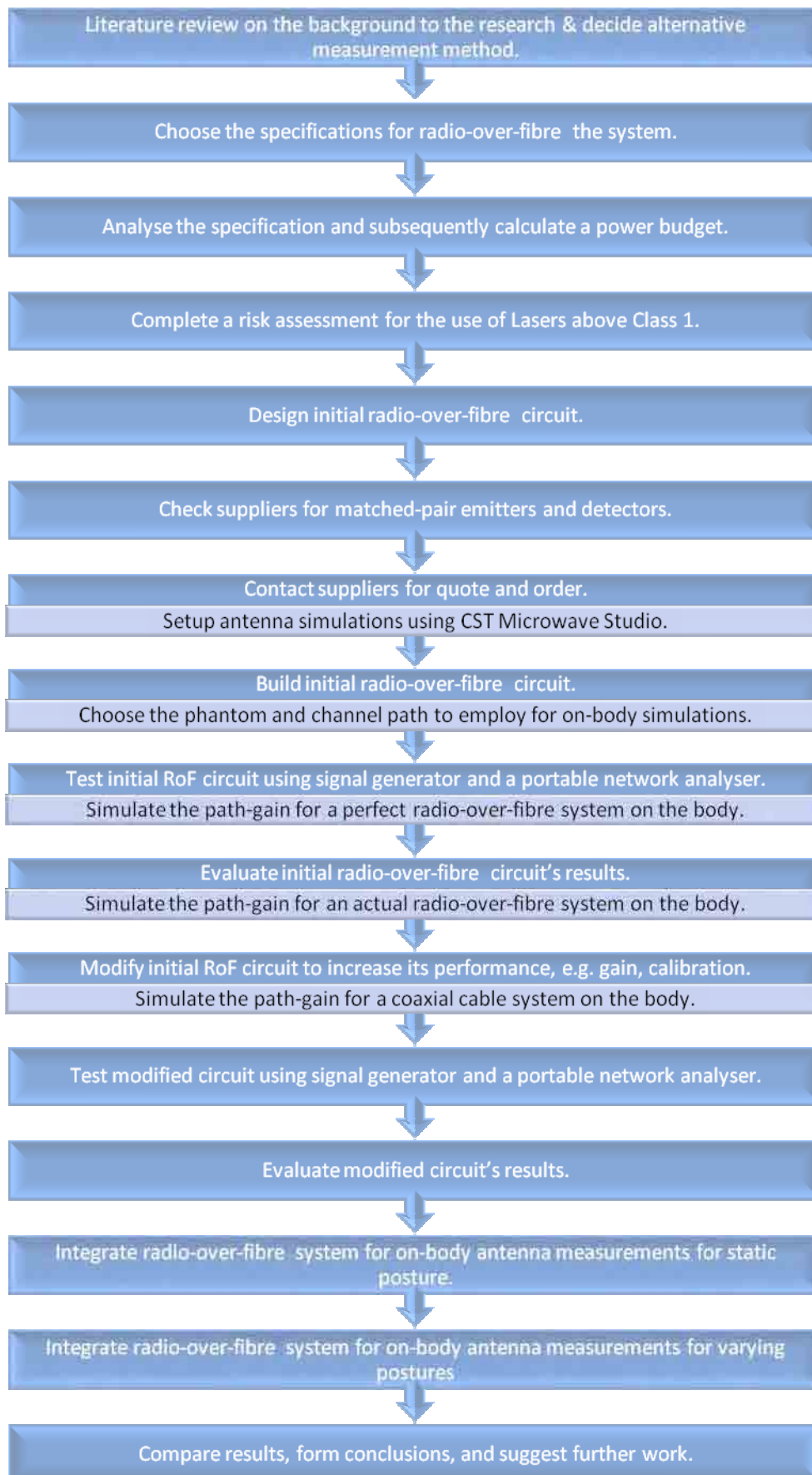


Figure 1.4 Flowchart of project (practical work (white font) and simulations (black font))

1.4 Contents of the Thesis

Chapter 2 discusses the background material of the project and introduces the fundamentals of body-centric communications and modelling, radio-frequency transmission and optical transmission. This is followed by a literature review of different antenna measurement methods and their method of reducing electromagnetic and radio-frequency interference.

Chapter 3 describes the design of a radio-over-fibre system for the purpose of antenna measurements. This design aims to replace the standard coaxial cable with optical cables for antenna measurements. The design is followed by simulation and measurements, thereafter conclusions are formulated.

Chapter 4 discusses the integration of a commercial radio-over-fibre system specifically for on-body antenna measurements. Power supply design is introduced, followed by coaxial and fibre system characterisation.

Chapter 5 presents simulations and measurements of the coaxial system and commercial radio-over-fibre system to assess feasibility for on-body channel path measurements.

Chapter 6 concludes the main body of the thesis. It summarises the findings and recommends further work that can be carried out.

The appendices include datasheets and relevant raw results from simulations and measurements, and are included as a source of reference for future research, however important results are summarised in tabular or graph form within the main body of the thesis.

CHAPTER 2

2 LITERATURE REVIEW

2.1 Introduction

A review of important fundamentals is presented in this Chapter. Body-centric communications form the basis of this thesis and are introduced. In addition, on-body simulation techniques including modelling methods are presented. Thereafter, a literature review of radio-over-fibre and Body-centric communications measurements is conducted. Last, an overview of transmission line theory including coaxial and optical transmission is presented.

2.2 Body-centric Communications

A huge demand for body-centric products has led to vast research being conducted into improving range, reliability and bandwidth as well as miniaturising designs. It is fair to say that most users would like to have the option for wired or wireless devices. The general business user would typically possess a laptop, PDA, mobile phone and Bluetooth headset. These products constitute a body/personal area network (BAN/PAN) and currently communicate using Bluetooth within the industrial, scientific and medical (ISM) band. Users would like to be able to connect these devices wirelessly as the wired option would be restrictive and disallow freedom of movement. In the future, more wireless devices will be added to BAN/PAN, such as body-worn computers, video headsets, body sensors and many more. Currently, these products are available but only with wired options, but with the development of Ultra-Wideband (UWB) and Cognitive Radio (CR) technologies, wireless options for these devices will be available soon. UWB and CR technologies will increase the throughput bandwidth and allocate usage of maximum radio spectrum in the local area.

The drawbacks of wireless technologies are reduced security, efficiency, reliability and increased power consumption. Some significant issues that need consideration are eavesdropping, dropouts, interference, distortion and fading. In addition, the body in proximity to the communication channel poses further challenges, which will be discussed later.

The other types of network are Wide Area Network (WAN), Metropolitan Area Network (MAN), Local Area Network (LAN), and Personal Area Network (PAN). A WAN connects two countries together via fibre-optic or satellite link. This is then distributed via a MAN to different cities via fibre-optic or wireless link provided by an Internet Service Provider (ISP). Each MAN termination can be connected to a LAN, which is always private. A LAN can be employed into either a business or a home for distribution to many computers. A PAN is a subset of LAN where only portable devices are allowed to network.

As mentioned earlier, BAN/PAN can be categorised into three communication components, off-body to on-body, on-body and in-body as shown in Figure 2.1. Each of these will be described in more detail highlighting the key challenges for antennas and propagation.

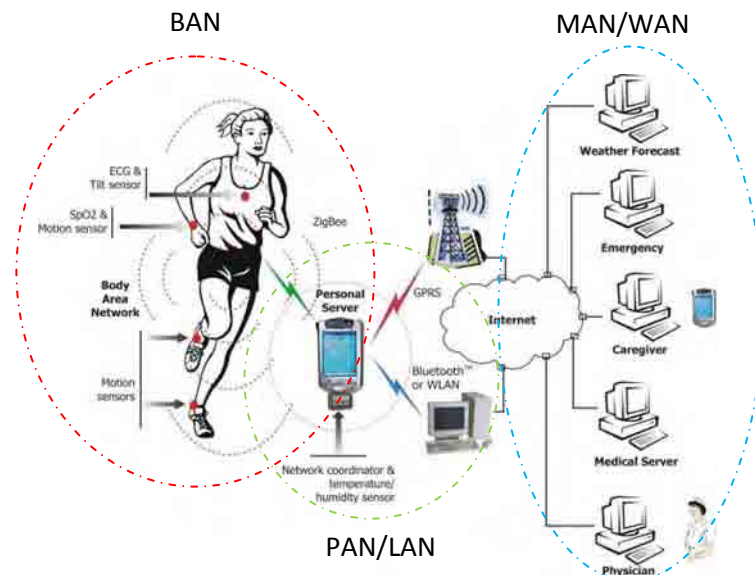


Figure 2.1 Medical monitoring example of wireless body area network (WBAN) and wireless personal area network (WPAN) [1]

2.2.1 Off-body to On-body Communication

This mode of communication comprises of a localised base station or off-body transceiver to on-body transceiver. The on-body antenna is of utmost importance as the body proximity and orientation directly affect the performance. Fabric-based antennas are very interesting as these are designed with a low profile to maximise antenna aperture whilst isolating the body via a large ground plane in order to prevent body tissue from reducing antenna efficiency [2]. Ideally, these antennas should radiate away from the body although maintain omni-directional characteristics. Several examples of on-body antenna are Planar Inverted-F Antenna (PIFA), Shorted Patch Antenna, U-slot Antenna, and Electromagnetic Bandgap (EBG) Antenna.

2.2.2 On-body Communication

On-body communication comprises of two transceivers in the local vicinity of the body, for example a mobile phone and Bluetooth headset. These antennas should be as small as possible; however, the drawbacks of this are reduction of input return loss and gain. The antennas are located very close to the human body and so the antenna should not detune. These antennas should radiate towards the ground plane, which creates a surface or creeping wave along the body surface. Such examples of antenna are the monopole antenna, disc-loaded monopole antenna, PIFA and folded planar.

2.2.3 In-body Communication

In-body communication comprises of a network of miniature implantable devices that communicate with each other and form a sensor network. The major application for these devices would be medical monitoring, such as the heart rate, blood and other vitals. These will collect information and pass it onto another sensor in the network or to an external sensor. A simple example of this is the cochlea implant as shown in Figure 2.2.

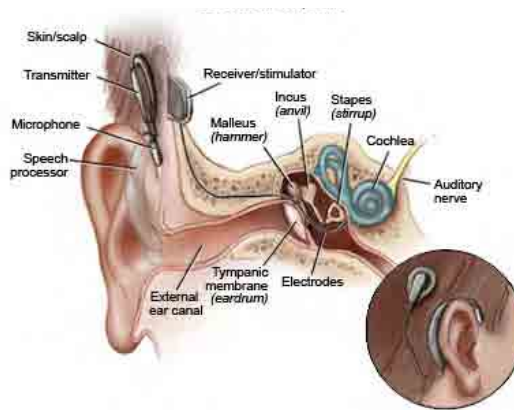


Figure 2.2 Cochlear Implant [3]

2.2.4 Body Proximity effects on Antennas

The proximity of the body causes an antenna to detune and losses occur due to interaction with the body. As the antenna is moved closer to the body there is a shift in the resonant frequency. Hall and Hao [4] have investigated the effects of a monopole in proximity to the human body at 2.45 GHz. Their measured results show a decrease in input return loss and a 300 MHz shift in resonant frequency when the distance between antenna and phantom is decreased from 10 mm to 0 mm. Also discovered is, the efficiency of this monopole antenna is 90% in free space, but reduced to 52% on the phantom. These results show the maximum losses due to the intimate contact with the body, however in most cases the antenna will not be intimately in contact with the body but separated by clothes hence the efficiency will be improved. Figure 2.3 shows the permittivity and conductivity of human tissue over 1 MHz to 100 GHz.

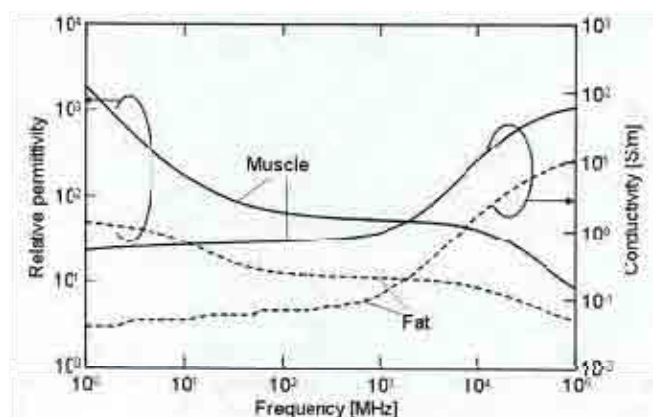


Figure 2.3 Example of electrical characteristics of tissues over frequency range of 1 MHz to 100 GHz at 37 °C [5]

Other aspects such as Specific Absorption Rate (SAR) show how antennas lose power into the body and the rate at which this occurs. Antenna radiation into the body has implications on human safety and the European limit for such exposure is limited to 2.0 Watts per kilogram.

Salim and Hall [6] have investigated the efficiency of a monopole antenna when a body is in proximity and both measured and simulated results compare well. When the monopole is positioned in proximity to the phantom, the mean efficiency drops from 93.3% to 56.9%. Figure 2.4 and Table 2.1 show the simulation and measurement results of antenna efficiency.

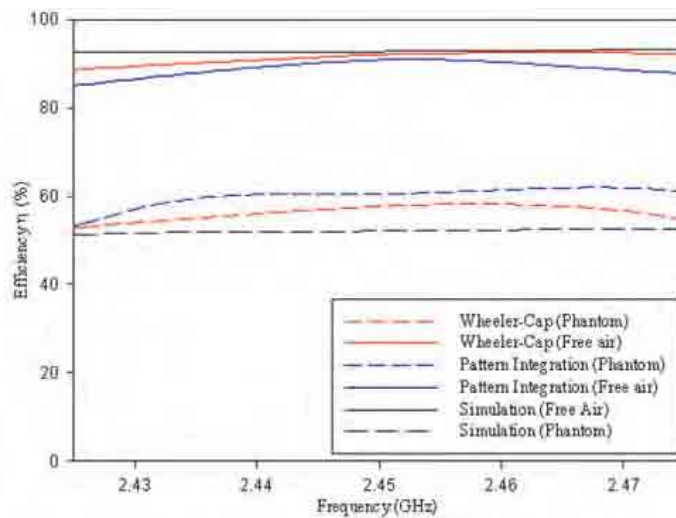


Figure 2.4 Simulation & measurement of monopole efficiency in free space and on-body phantom material [6]

	Wheeler-Cap	Anechoic Chamber	Simulation
Free Space	92.26%	91%	96.74%
Phantom	57.99%	60.61%	52.23%

Table 2.1 Efficiency results for Monopole [6]

Hall et al. [7] introduced on-body channel measurements and modelling which provides insight into key considerations of channel measurements such as multipath & fading. This showed that differing postures cause path loss variability from on-body multipath, and can vary as much as 50 dB as shown in Table 2.2.

Antenna Position \ Posture	Head Right	Head Left	Chest Right	Chest Left	Right Thigh	Left Thigh	Right Shank	Left Shank	Right Wrist	Left Wrist	Right Upper Arm	Left Upper Arm	Back Centre
Stand	59	45	39	37	40	36	46	44	42	29	51	41	49
Body Left	46	44	36	35	41	36	50	46	38	31	46	46	52
Body Right	75	43	42	36	33	33	43	43	50	27	60	37	46
Body Forward	62	46	37	32	36	34	49	45	45	31	53	40	48
Head Forward	51	40	38	38	40	36	48	43	43	29	52	41	50
Head Left	41	64	40	37	40	37	48	44	43	29	51	41	50
Head Right	60	42	38	37	40	37	48	44	43	29	51	40	50
Arms Sideways	58	44	38	35	40	37	48	43	73	65	59	40	52
Arms Upwards	53	43	38	36	40	36	48	44	58	51	60	46	52
Arms Forward	62	54	39	32	37	37	51	43	48	38	53	35	51
Forearms Forward	63	61	38	43	38	37	47	43	57	32	73	48	49
Sit	58	43	38	29	37	34	61	59	71	34	49	43	50

Table 2.2 Average On-body Path Loss (dB) with quarter-wave monopoles at 2.45GHz [4]

A space diversity antenna can be employed to overcome path loss variability. To increase gain further, a pattern switched diversity antenna can be employed as demonstrated by Kamarudin [8].

On-body channel measurements involve the placement of a transmit and receive antenna on the body. The positions of these antennas dictate which channel is being measured. Possible channel configurations are shown in Figure 2.5. To measure a channel's performance, an RF signal is passed through the transmit antenna and is broadcasted into the local atmosphere. The RF signal is reflected and absorbed by local objects such as the body and inanimate or moving objects, until it is received by the receive antenna. The received RF signal power is then measured and compared to the transmit power. This process characterises an on-body channel for measurement purposes.

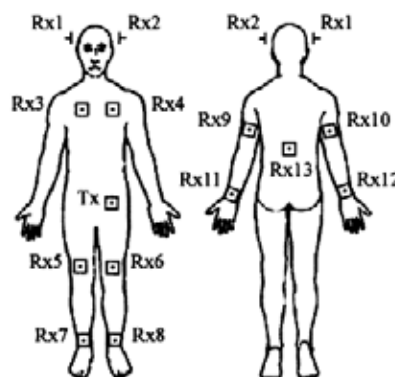


Figure 2.5 Possible placement positions of wearable devices on the body [9]

2.2.5 Phantoms

A phantom is an artificial human body, which approximately mimics the dielectric properties of an actual human body. The main properties that a phantom mimics are conductivity, relative permittivity, loss tangent and penetration depth. Some measurement scenarios require a controlled environment which can be achieved using a phantom. There are two types of phantom; physical and numerical.

There are physical phantoms of two types: dry phantom and semi-solid (gel) phantom. The phantom choice depends on the application required for the measurements.

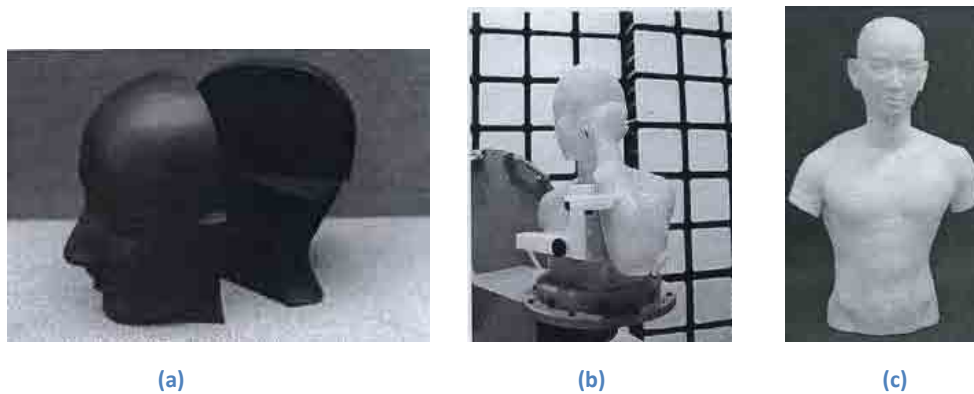


Figure 2.6 (a) Example of human-head dry phantom (b) Multi-postural realistic human-torso phantom at 900MHz (c) Realistic human-torso phantom (agar-based solid phantom) [5]

Numerical phantoms can be used for computational simulations. These phantoms can be imported into most electromagnetic (EM) antenna based software to calculate wave propagation around the body from a source. There are two types of numerical phantom: theoretical and voxel phantoms. Theoretical phantoms are simple approximated models formed from the human body. This can be a simple cylindroid modeling the body structure, or even a multi-layered cylindroid. An example of this would be Mike, a CST designed homogeneous phantom (Skin: conductivity = 0.7 S/m, relative permittivity = 41, relative permeability = 1) by Bai [10] as depicted in Figure 2.7.

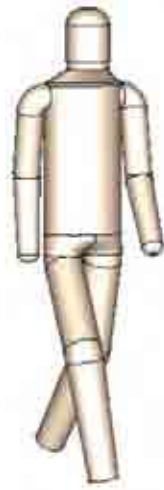


Figure 2.7 Mike Phantom [10]

Voxel phantoms are the type of phantoms formed from magnetic resonance imaging (MRI) of a human body. These are complex due to data collection in a volume, which is called a voxel. A voxel is a volume element, representing a value on a regular grid in three-dimensional space. The data is collected through a series of MRI's of the human body, of which NORMAN (normalised man, 170 cm and 70 kg) is most recognised as shown in Figure 2.8. NORMAN consists of 37 different tissue types, with a resolution of 2^3 mm^3 . A female equivalent of NORMAN was also developed, named NAOMI (anatomical model, 163 cm, 60 kg).



Figure 2.8 A voxel phantom NORMAN [5]

Although these high-resolution voxel phantoms seem to be useful, they are limited to static postures. In most cases, simulation requires specific postures that are used in radio communications,

such as mobile phone in hand, held to head. In this case, these phantoms would have been inadequate. Gallo et al [11] investigated moving phantoms and their solution was to use animation software. POSER created an animation of James in a walking motion. These frames were extracted and exported into XFDTD to produce a homogenous phantom. The phantom James is shown in Figure 2.9.



Figure 2.9 James phantom in Poser 6 [11]

2.2.6 On-body Simulation Techniques

On-body numerical modelling for antennas and propagation at microwave frequencies are incredibly interesting because the human body acts as a transmission medium, which guides a surface wave and acts as a reflector for space waves. On the body, antenna orientation, polarisation and body posture trigger large variation in path loss. Several numerical methods enable the solution of on-body electromagnetic problem by using the approximation that the body is a homogeneous lossy dielectric. Two of which are discussed below.

The Finite Element Method (FEM) is efficient for structures with curved boundaries. This technique uses rigorous mathematical formulation to converge to a solution. FEM splits the various objects into known geometric shapes and then applies calculations. The drawback of using FEM is that it is computationally time consuming due to the number of matrix calculations.

The Finite-Difference Time-Domain (FDTD) method dissects an object into small cells, forming a grid and then applying boundary conditions to solve the electromagnetic (EM) structures. It is apt for modelling complicated boundaries and inhomogeneous media such as the human body. Although, a weakness of this method is that before computation can commence, the area within the boundary must be meshed, and these cell dimensions must be smaller than the smallest wavelength within the structure. If the structure has many small curves, then the smallest cell dimension is very small, therefore increasing the computational time. The meshed grid cells are staircase mode, thus smooth surfaces are impossible to model.

To conclude, these two techniques are most suited for on-body radio propagation modelling. This thesis uses CST Microwave Studio (CST MWS) to solve electromagnetic (EM) fields around the phantom and antenna. CST MWS software simulates the EM fields within a three-dimensional boundary. It utilises finite integration technique (FIT) and perfect boundary approximation (PBA) which resolves the difficulty of smooth surface modelling using FEM.

2.3 Previous Radio-over-Fibre Systems for Antenna Measurements

Radio-over-fibre is the term given to an analogue optical transmission system that does not require re-modulation of the signal. It is specifically chosen for transmissions where a coaxial system interfaces with an optical system. The main purpose for a radio-over-fibre system would be to decrease signal transmission loss over long distance. A radio-over-fibre system does not emit EMI/RFI, nor is prone to such interference.

Antenna testing and measurements form the basis of this project and the fundamentals have not vastly changed in the last 50 years. There are several key measurement methods: far field, compact, near field and extrapolation range. Any measurement method can be used, however it must be chosen depending on the application. An anechoic chamber is lined with pyramidal radio absorbent material (RAM), which absorbs radio waves. This is useful for antenna measurements as it is undesirable to characterise an antenna in an open environment where reflections and interference

can influence results dramatically. There are several methods on how an antenna should be tested and a method should be chosen to suit the application. Typically, a far-field measurement method should be chosen for use in an anechoic chamber. The anechoic chamber provides a radio wave free zone. RAM is used on the walls to reduce specular reflections, thus it is possible to characterise antennas. The parameters that can be simulated using electromagnetic software or measured in an anechoic chamber are gain, effective isotropic radiation power (EIRP), directivity, beam pattern, beam width, side lobes, cross-polarisation, efficiency, voltage standing wave ratio (VSWR)/return path loss (S11), forward path gain (S21) and dynamic range.

Lao et al. [12] outlines an electro-optical antenna measurement system, which replaces the traditional RF cable with optical fibre. They state that this system can reduce the disturbance of an electromagnetic field around the receiving antenna caused by transmission cables. From their analysis of several papers, the disturbance variation of RF coaxial feeds ranges between 7 dB and 10 dB. This paper compares the results of the RF cable vs. optical fibre, with the RF cable in the horizontal and vertical axis. The results are shown in Figure 2.10. The results conclude that using an electro-optical link, the S21 deviation of RF cables can reach a maximum of 0.7 dB as compared to optical fibres of a maximum of 0.05 dB.

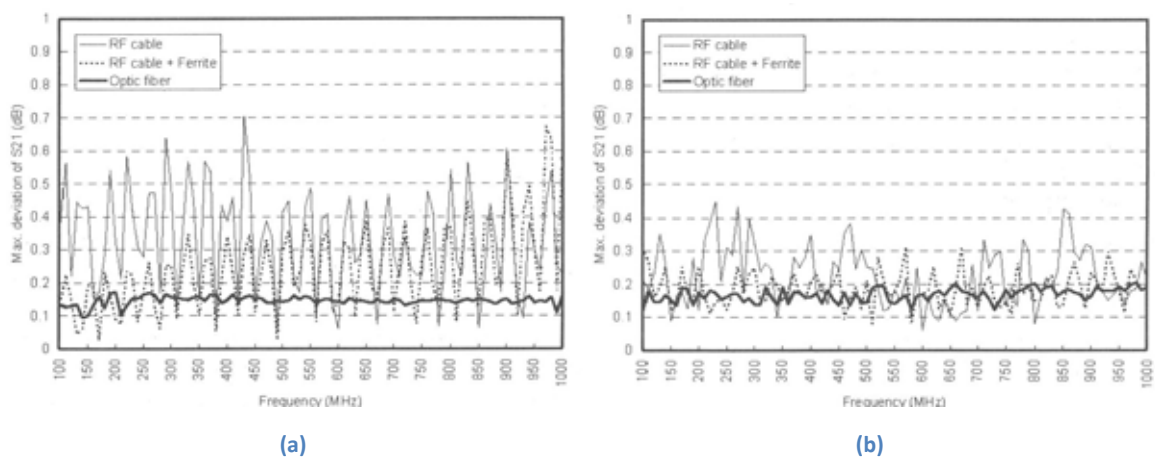


Figure 2.10 Maximum deviations of three different cabling configurations for (a) vertical and (b) horizontal polarized antenna measurement [12]

Fukasawa et al. [13] outlines a small antenna measurement method using fibre optics. The purpose of this paper is to highlight the inefficiencies of the conventional method using a Voltage Controlled Oscillator (VCO). The measurement setup and model is depicted in Figure 2.11 and Figure 2.12 respectively, showing the system diagram and measurement planes for the polar plot shown in Figure 2.13.

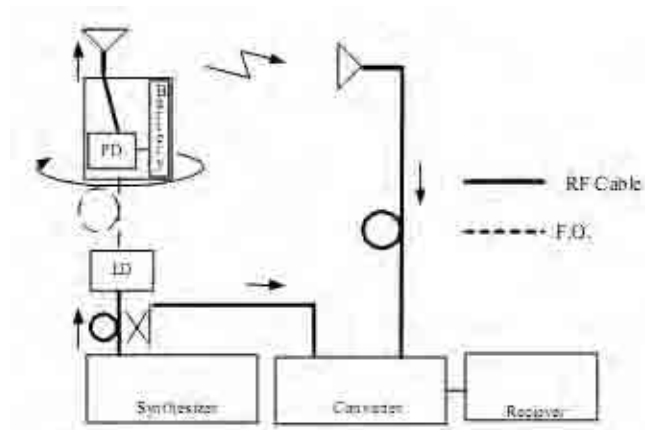


Figure 2.11 Diagram showing measurement system for the radiation pattern [13]

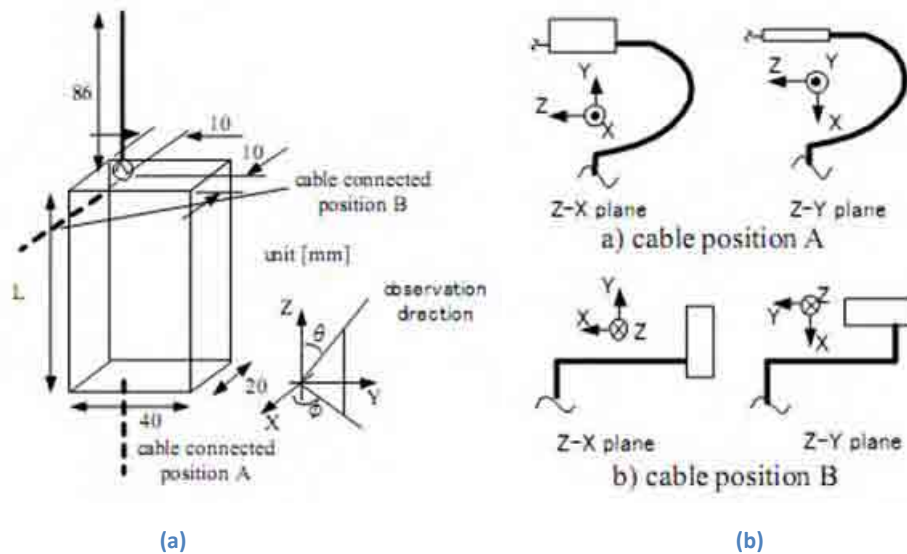


Figure 2.12 (a) Measurement model showing orientation of axis and (b) diagram showing cable setting for radiation pattern measurement [13]

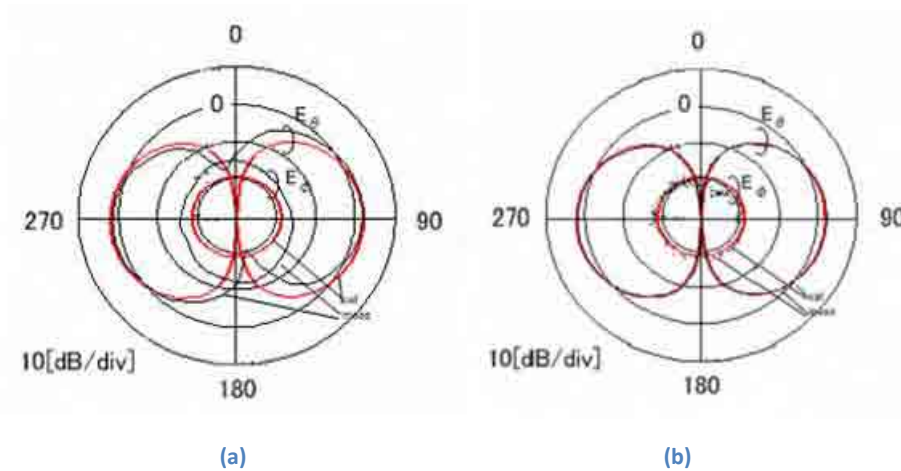


Figure 2.13 Radiation pattern measured by the (a) RF cable and (b) Fibre-optic cables at position B (Z-X plane) as per Figure 2.12 [13]

The polar plots in Figure 2.13 show the calculated and measured radiation pattern with RF cable compared to fibre optic cable. The polar plots show that between the calculated and measured pattern, the RF cable has a max variation of 5 dB. In the case of the fibre cable, the measured pattern almost perfectly overlaid the calculated pattern. This leads to the conclusion that the system used in the paper worked very well for a 900 MHz application, however this measurement setup would fail to operate within the unlicensed ISM band.

Cryan et al. [14] cover a different application although some of the concepts that they used may be useful to consider. The purpose of this paper is to build an active antenna to communicate between two laptops bi-directionally. A low cost Vertical-Cavity Surface-Emitting Laser (VCSEL) is integrated into the microstrip antenna. This proves the viability of the laser for operation at 2.45 GHz and only requires a modest bias of 7 mA.

To conclude, the radio-over-optical system for on-body measurement would pose greater difficulty because two cascaded optical links must be employed. In the papers discussed, only a single optical link is employed.

2.4 Transmission Lines

A transmission line is characterised by its propagation constant, characteristic impedance, and attenuation. There are several types of commonly used transmission lines and they can support a number of modes, such as transverse electromagnetic (TEM) waves, transverse electric (TE) waves or transverse magnetic (TM) waves. If a transmission line has two or more conductors, TEM mode propagation is possible due to the lack of longitudinal field components. Single conductor transmission lines can only support TE or TM modes. Examples of TE & TM guides are single conductor waveguides. An example of a TEM guide is coaxial cable, where electric (E_z) and magnetic (H_z) fields in z-axis as per geometry in Figure 2.15 is zero. This discussion has been primarily formed by Kaiser [15] and Pozar [16].

2.4.1 Coaxial cable

Coaxial cable is essentially made up of two parallel conductors and consists of an inner conductor surrounded by dielectric material (often $\epsilon_r \approx 2$), followed by an outer conductor and enclosed with an insulator. There are many varieties of coaxial cable available, with each type designed for common applications, although coaxial cables do not exist for all applications. The structure of a typical coaxial cable is shown in Figure 2.14.



Figure 2.14 Typical coaxial cable showing internal structure

2.4.1.1 Cable Modelling

Coaxial cable can be modelled in terms of its electrical characteristics. Figure 2.15 depicts the geometry and assigned labels used in the discussion.

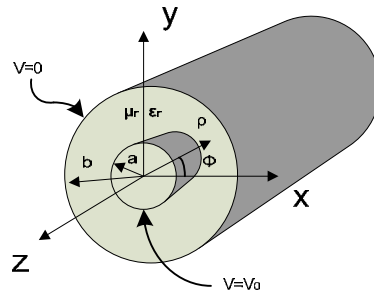


Figure 2.15 Coaxial Line Geometry [16]

The signal velocity of a lossless line is the function of its capacitance and inductance per unit length. The high frequency characteristic impedance for a coaxial cable is:

$$Z_0 = \sqrt{\frac{L}{C}} = \sqrt{\frac{\frac{\mu_r \mu_0}{2\pi} \ln\left(\frac{a}{b}\right)}{\frac{2\pi \epsilon_r \epsilon_0}{\ln\left(\frac{a}{b}\right)}}} \approx 60 \sqrt{\frac{\mu_r}{\epsilon_r}} \ln\left(\frac{a}{b}\right) \Omega \quad \text{Equation 1}$$

where, a defines inner radius, b defines outer radius, Φ defines radial angle, μ_r defines the dielectric permeability, ϵ_r defines the dielectric permittivity, ρ defines resistivity and Z_0 defines impedance as labelled in Figure 2.15.

As the medium between the inner and outer conductor is non-magnetic this implies μ_r is 1 and Equation 1 becomes Equation 2.

$$Z_0 = 60 \frac{1}{\sqrt{\epsilon_r}} \ln\left(\frac{a}{b}\right) \Omega \quad \text{Equation 2}$$

The velocity of propagation (v) is given by,

$$v = \frac{1}{\sqrt{LC}} = \frac{1}{\sqrt{\mu_r \mu_0 \epsilon_r \epsilon_0}} = \frac{1}{\sqrt{\mu_r \epsilon_r}} \frac{1}{\sqrt{\mu_0 \epsilon_0}} = \frac{3 \times 10^8 \text{ m}}{\sqrt{\epsilon_r}} \frac{1}{\pi} \quad \text{Equation 3}$$

where, L and C are the inductance and capacitance, respectively.

This shows that the dielectric constant and characteristic impedance are a function of the shape, size and position of the conductors.

This may initially imply that smaller diameter coaxial cables have smaller characteristic impedances since the distance between the two conductors is smaller. However, Z_0 is only the

function of the ratio between the outer to inner conductor radii. This implies if the radii ratio is constant so too is the characteristic impedance.

The attenuation (α) of coaxial cable due to conductor resistance is related by the frequency (f), relative permittivity/dielectric constant, inner and outer radii as shown by Equation 4.

$$\alpha \propto \frac{\sqrt{f \epsilon_r} \left(1 + \frac{a}{b}\right)}{a \lg\left(\frac{b}{a}\right)} \quad \text{Equation 4}$$

2.4.1.2 Cable Shielding & Crosstalk

Cable shielding performs an important role within a coaxial cable structure. The outer shield confines the electromagnetic signal inside the coaxial structure, and shunts any ingress radio and electromagnetic interference to ground. The perfect outer shield would consist of an infinitely conductive solid material. However, in reality, there are no such perfect cases and one is limited to solid copper shields, such as a semi-rigid cable. Other types of outer shield are braided or taped.

Zhang et al. [17] studied the electromagnetic leakage from a braided shielding cable using the finite-difference formulation for both inner and outer conductors. They simulated the transmission of a video signal through a braided shielded coaxial cable and then captured the leakage around the coaxial cable. They were then able to recover the video signal from this leakage through several processing techniques highlighted in the paper. Figure 2.16 shows the transmitted and recovered video signal images.

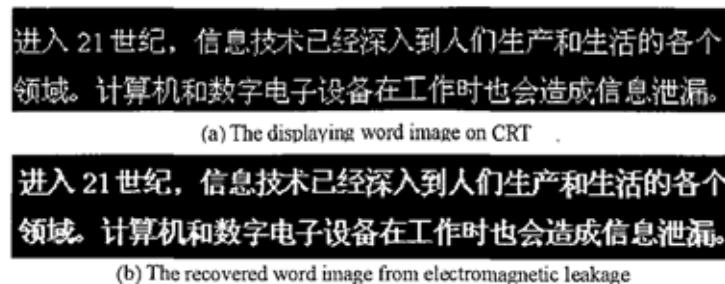


Figure 2.16 EM information leakage from a braided shielded coaxial cable [17]

Benson et al. [18] also studied the leakage from coaxial cable with similar results. Transfer impedance (Z_T) against frequency had been investigated and some results are shown in Figure 2.17 and Figure 2.18.

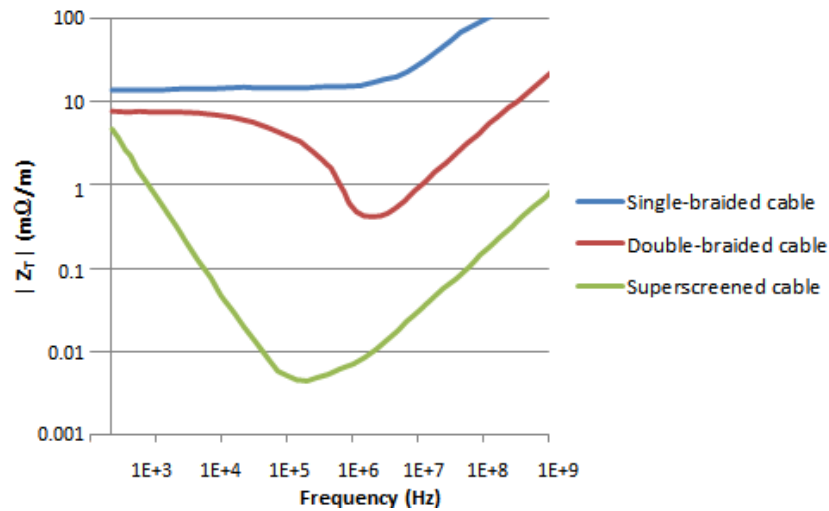


Figure 2.17 Simulated transfer impedance of differing cable types vs. frequency [18]

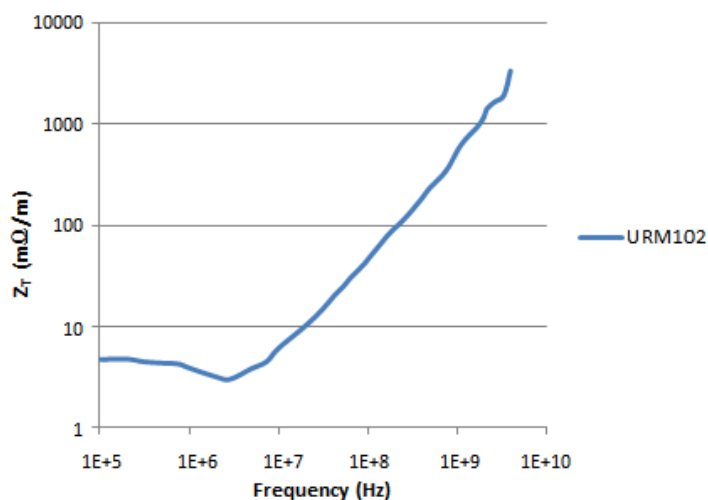


Figure 2.18 Measured transfer impedance of URM102 vs. frequency [18]

Benson et al. [18] highlight coaxial cable leakage having measured it from different cable shield types. Their results show that for higher quality shielding, the transfer impedance is lower thereby minimising ingress or egress. To add further immunity from radio & electromagnetic ingress, multiple shields in layers can be used. It is important to model a cable for its shield's effectiveness (Z_T) if it is being used in an electromagnetic or radio interference application. Experimental methods were developed by Kaiser (2006) [15] to reveal a shield's effectiveness by screening external electric and magnetic fields. A measure of a shield's effectiveness is its transfer impedance. Low transfer

impedance implies a low induced voltage along the coaxial cable, which will be observed later. A shield's effectiveness is measured through immersing the cable in an electric field, as shown in Figure 2.19. The cable conducts, hence distorting the imposed electric field.

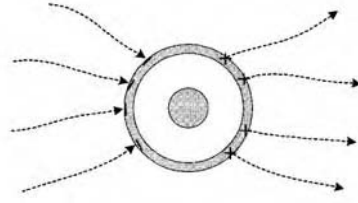


Figure 2.19 Cross-sectional view of coaxial cable immersed in an electric field [15]

If the shield is an excellent solid conductor then the electric field within the shield is very low, this is called Faraday shielding. Magnetic fields can be both normal and tangential to conductors, unlike its counterpart. Figure 2.20 below shows a coaxial cable with tangential fields, H_{Tint} and H_{Text} .

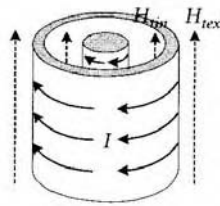


Figure 2.20 Coaxial cable immersed in a tangential magnetic field [15]

The external magnetic field H_{Text} is tangential to the outer coaxial structure, and the internal magnetic field H_{Tint} is tangential to the inner coaxial structure. The internal magnetic field strength is a function of the outer shield thickness, radius, conductivity, permeability and the frequency of the magnetic field. If the magnetic field is time varying, an induced circulating current on the outer and inner shield is produced. Therefore, the magnetic field and induced current are not parallel, and these currents generate ohmic power loss. The longitudinal magnetic fields between the two conductors result in induced electromotive force (EMF) or voltage. Faraday's law states that the induced voltage produced by a time varying magnetic field passing through a closed loop is proportional to the area of the loop and the applied field strength and frequency. The outer

conductor is a one-turn loop, thus having an inductance and impedance. With current passing, a voltage drop occurs. This leakage field through the shield is modelled as inductance.

A low frequency magnetic field transverse to the axis of a coaxial cable easily penetrates the shield but it cannot do this at higher frequencies. A cylindrical shell immersed within a uniform magnetic field is shown in Figure 2.21.

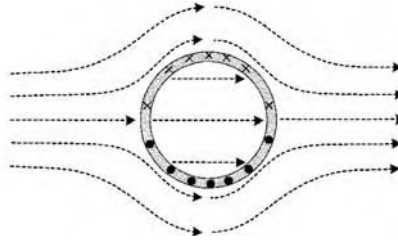


Figure 2.21 Cross-sectional view of cylindrical shell immersed in a uniform magnetic field [15]

If both ends are short circuiting caps or have end effects through parasitic capacitance then the current can pass through one end (x) and return down the other side (•) of the cylinder. If an inner conductor is within the cylindrical shell, the longitudinal current can also be induced down it if there is an outer shield or external circuit return path. The longitudinal induced current will attribute to the power loss within the cylinder.

The transfer impedance (Z_t) of an electrically small cable of length in the z direction is defined as,

$$Z_t = \frac{1}{I_e} \frac{dV_t}{dz} \Omega/m \tag{Equation 5}$$

where, I_e is the injected current into the outer shield and V_t is the voltage across the inner surface of the outer shield.

The transfer impedance of an electrically large cable of length (l_{th}) in the z direction is defined as,

$$Z_t = \frac{1}{I_e} \frac{V_t}{l_{th}} \Omega m^{-1} \Rightarrow V_t = I_e l_{th} Z_t \tag{Equation 6}$$

One method of measuring the voltage induced down the inner shield is to inject current into the shield whilst shorting one end of the coaxial cable and measure the voltage V_t across the

inner conductor and the outer shield at the other end, as shown in Figure 2.22. Therefore, if V_t , I_e and I_{th} are known, then the transfer impedance can be found using Equation 6.

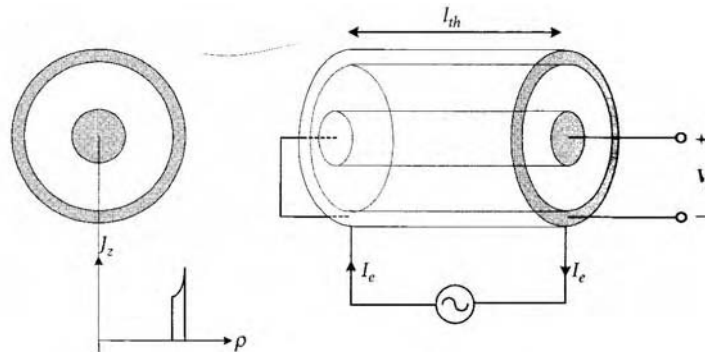


Figure 2.22 Coaxial cable - Distribution of current in the conductors when current is injected into the shield [15]

At higher frequencies, the current distribution is not uniform over the outer shield thickness. In the case shown in Figure 2.22 above, the injected current has a greater current density (J_z), along the outer surface and decreases as the distance into the shield increases.

At very high frequencies, where skin depth δ is smaller than the thickness of the shield, the inner surface current density is small. The skin depth δ is given by:

$$\delta = \frac{1}{\sqrt{\pi f \mu \sigma}}$$

Equation 7

For a solid shield, the transfer impedance decreases with frequency (f). A smaller Z_t implies that only a little energy from the induced current is passed from the outer to inner shield. This can be calculated by complex equations 5.25 onwards [15]. This solid-shield transfer impedance is important as it highlights the ideal transfer impedance and can be used as a reference.

Real or braided shields have openings or apertures throughout the structure, usually found in most types of coaxial cable. Braids are made up of weaved parallel wires or strands. A braided and tape-wound diagram is shown in Figure 2.23.

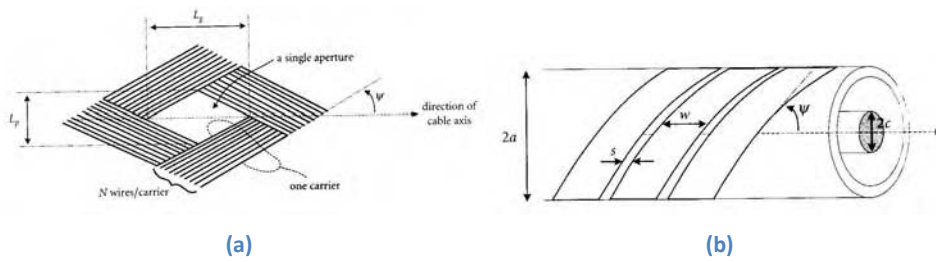


Figure 2.23 Layout of (a) braided shielded cable and (b) tape-wound shielded cable [15]

The graphs in Figure 2.24 and Figure 2.25 show how transfer impedance changes with frequency for different shield types.

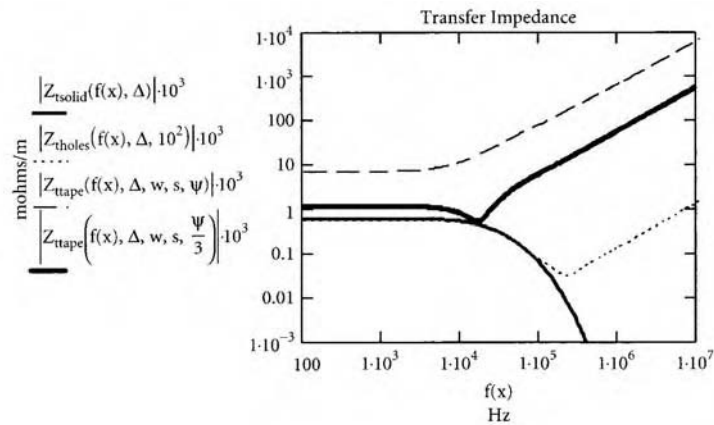


Figure 2.24 Theoretical transfer impedance vs. frequency for solid, perforated and tape-wound shield [15]

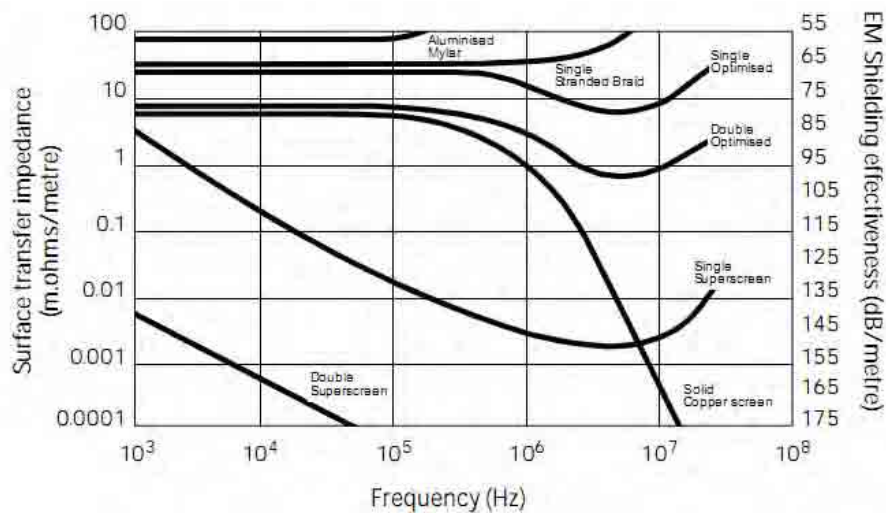


Figure 2.25 Measured transfer impedances for Tyco coaxial cables [19]

Other methods can also determine a shields' effectiveness, such as loss impedance, transfer admittance and the coupling model. However, manufacturers most commonly use transfer impedance method to determine shield effectiveness.

To conclude, there are many methods to improve the transfer impedance of coaxial cable. Some solutions are to increase shield thickness and conductivity, increase the coverage of the shield (fewer holes and tighter braid weave), use multiple layers of differing shield types (braid, foil and tape), use a combination of non-magnetic and magnetic layers (“superscreened” cables), and isolate shield layers (triaxial cable).

Each one of these methods increases complexity, diameter, cost, weight and stiffness of the cable as well as other important factors such as power handling capability, capacitance and bandwidth. For on-body applications the diameter, weight and flexibility are of most importance. A cable that is thick, heavy and inflexible results in difficulties in use for on-body applications.

2.4.2 Matching

Transmission lines such as coaxial cable require matched impedances at the end of a line, as this enables maximum power transfer and minimises reflections from the input to the output. There are several techniques to match impedances, such as the use of resistors, capacitors, transformers and inductors in combination. An impedance mismatch can be resolved in three ways; using resistive, complex conjugate or complex impedance loads. Impedance mismatch examples are a lumped network, a single-stub tuner, a double-stub tuner and a quarter-wave transformer. These methods can be found in many textbooks [16] and can be applied to form a matching network of the required type and specification for a transmission line.

2.4.3 Optical Transmission

Optical transmission lines use light waves to carry signals instead of microwaves. A typical analogue optical fibre system is shown in Figure 2.26.

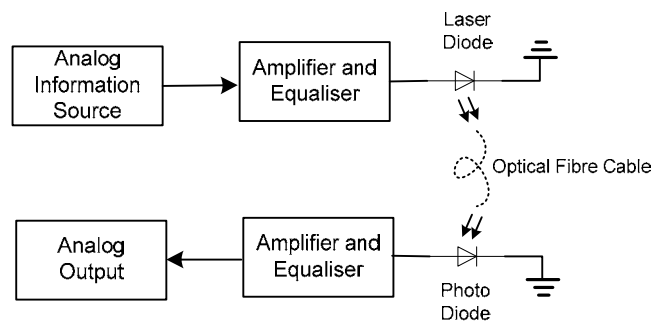


Figure 2.26 Analogue Optical Link - Intensity Modulation Direct Detection (IMDD)

The analogue laser diode modulates the information in a continuous sinusoidal mode and is simple to implement. Analogue links require a higher signal to noise ratio (SNR) at the receiver than digital links do. Hence, analogue optical links are primarily used for short distance and low bandwidth links.

The advantages of optical fibre over conventional electrical communications are the enormous potential bandwidth, small diameter, lightweight and flexible fibres, electrical isolation, Interference and crosstalk immunity, signal security, low loss and reliability & ease of maintenance. The optical carrier frequency is approximately 10^{13} to 10^{16} Hz, hence the potential bandwidth is very wide. Although currently this huge bandwidth cannot be utilised, in the future this may be possible using wavelength division multiplexing (WDM). For comparison, coaxial cable bandwidth is approximately several Gigahertz, however an optical link can carry greater bandwidth over longer distances than coaxial cable. Optical fibres have very small diameters of approximately 9 to 50 μm including protective coatings totalling approximately 125 μm , which are very small and light. They are also manufactured for flexibility, as glass or plastic can be bent to small radii or even twisted without damage. Optical fibres are fabricated from plastic or glass, therefore they are electrical insulators, and do not cause earth or shorting issues. Due to the dielectric waveguide structure of fibres, they do not emit RFI nor are they affected by EMI. This makes them very attractive for replacing coaxial cable for use in antenna measurements as they can be placed in very close vicinity of the antenna without the worry of ingress or egress. However, any electrical circuitry or RF port within the system is potentially susceptible to radio interference, which may be modulated onto the optical carrier. The

optical fibre cables available are very low loss (0.2 dB/km) and this is a major advantage. The low loss per distance means fewer amplifiers are required, hence a more reliable and robust system. The lifespan of optical components is approximately 10 to 20 years.

The disadvantage of optical fibre over conventional electrical communications is that the initial system cost can be high, especially for high performance semiconductor lasers and detector photodiodes. However, optical fibres are relatively cheaper than coaxial cable, so there are particular trade-offs.

2.4.3.1 Optical Fibre

There are several types of optical fibre waveguides; Plastic, Plastic Clad Silica (PCS) and Silica, which are all used in different applications. These waveguides couple power to and from optical sources and detectors.

2.4.3.2 Laser Diodes

Laser diodes come in two packages, either surface emitting or edge emitting. Laser diodes have the advantage of high-speed operation due to their fast rise and fall times although manufacturing costs are very high. A laser diodes' performance relies upon several key factors as listed below. However, noise is a major factor for signal distortion, especially for analogue transmission. The sources of noise are relaxation oscillations, phase or frequency noise/relative intensity noise (RIN), self-pulsation and back reflection of light. Phase noise poses the greatest threat for optical transmission and cannot be removed, as it is an intrinsic property of manufactured lasers

There are essentially four types of laser diodes, Fabry-Perot (FP), Distributed Feedback (DFB), Distributed Bragg Reflectors (DBR) and Vertical Cavity (VCSEL). A vertical cavity design allows surface emission, which meant it could be easily tested during the fabrication process. This unique structure has highly reflective mirrors in the short vertical cavity. A vertical cavity laser structure is shown in Figure 2.27.

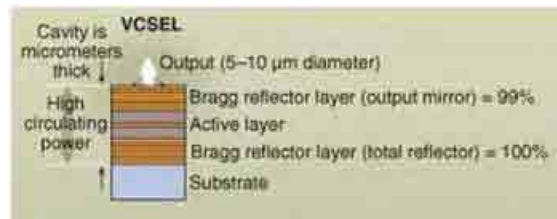


Figure 2.27 VCSEL semiconductor laser structure [20]

This device is designed for small signal modulation, thus consume less power, have a lower threshold current, a long lifetime and larger small signal bandwidth.

2.4.3.3 Photodiode

The optical detector is an important component of an optical fibre link and in most cases dictates the overall system performance. Its purpose is to convert the received optical light into an electrical signal. The electrical signal current created by the photodiode is very small and must be amplified before further processing. The strict requirements of a photodiode are high sensitivity at the operating wavelength, high fidelity or linearity, maximal electrical response to the received optical signal, fast response time, minimum detector noise from low dark currents, high stability over temperature range, small dimensions, low bias voltages and high reliability.

For this reason, semiconductor photodiodes seem to be most viable for most applications. An important property of a photodiode is the responsivity and is defined as the output photocurrent over the incident optical power. This states the quantum efficiency, which is the number of photons that are converted into electrons. The noise considerations for photodiodes consist of thermal noise, dark current and quantum or shot noise. Thermal noise causes spontaneous fluctuations in the received signal. Dark noise current is the small reverse leakage current when no incident optical light is present. This creates spontaneous fluctuations in the received signal. Quantum or shot noise is due to photons giving rise to detectable statistical fluctuations in the received signal. The photodiode has an inherent capacitance, which dictates the achievable bandwidth. For maximum bandwidth, the photodiode capacitance and resistance must be reduced, however this leads to greater thermal noise, hence a compromise between bandwidth and thermal noise occurs.

2.4.3.4 Optical Modulation

The two types of optical modulation are intensity modulation/direct detection (IMDD), and coherent modulation. This only uses the amplitude of the signal and therefore forms a simple and effective optical communication system. A laser diode has input power requirements of 5 mA to 300 mA for forward current and between 1.5 to 2.5 Volts of forward voltage, resulting in an optical output power between 0.1 mW to 1.0 W. The linearity of the input current to optical power is important as nonlinearities can cause severe distortions to optical signal. Most lasers are operated above threshold current where the device operates linearly. The thermal effects of a laser limit the performance and at higher temperatures, more current is required to compensate for output stability. Analogue transmission using intensity modulation uses a small electrical input signal such as a sine wave imposed onto the laser diode threshold current bias, which causes a large sine wave optical signal.

2.5 Alternative Electromagnetic or Radio Frequency Interference Reduction Techniques for Antenna Measurements

There are alternative techniques that can reduce electromagnetic and radio frequency interference, which do not use fibre optic systems. Coaxial cable examples are shielded coaxial cable, ferrite beads and quarter-wave balun sleeves. It must be noted that these passive methods only reduce these effects and cannot eliminate all coaxial cable influences.

Superscreened coaxial cable seem to reduce this interference on the signal however, it is not perfect. Shielded coaxial cable consists of several layers of shielding and braiding around the dielectric, and functions by effectively shunting to ground any incoming or outgoing interference. Superscreened coaxial cable is undesirable for on-body measurements as they are heavy, thick and inflexible. On-body measurement cables are required to be small, light and flexible. Sali [21] showed that as frequency increases towards 3.5 GHz the transfer impedance continues linearity. In theory,

higher frequencies should have less of an effect on coaxial cable, thus we see this is invalid. The problem of this emission and absorption with coaxial cables remains.

Ferrite beads are utilised by surrounding the coaxial cable with beads as shown in Figure 2.28. Ferrite beads operate by imposing high impedance to high frequency EMI/RFI. This induces currents within the ferrite beads, which creates and dissipates heat as a result. Ferrite beads are limited to several hundred Megahertz, thus are inadequate for antenna measurements at higher frequencies. Massey and Boyle [22] measured results of the reduction of perturbations, using different feedline techniques and ferrite beads.

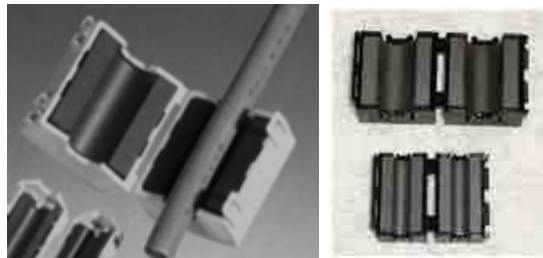


Figure 2.28 Ferrite beads for EMI/RFI reduction

The last technique involves incorporating a quarter-wave balun sleeve to the coaxial cable feed as shown in Figure 2.29. This prevents undesired interference by eliminating feedline common mode currents and radiation. It also helps reduce interference being picked-up by the coaxial shield. The drawback of this method is that the balun sleeve is narrowband and more than one sleeve is required for differing frequencies. Icheln et al. [23] successfully used this method for small mobile antennas and reduced perturbations on the radiation patterns by 10 %. It is found that the use of multiple baluns or multiple ferrites reduces the effect of scattering by the coaxial cable.

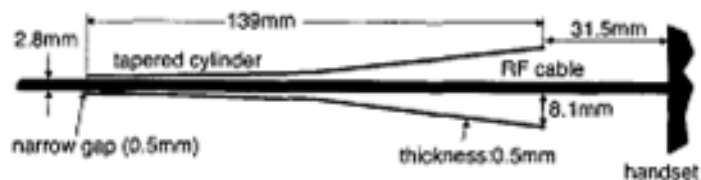


Figure 2.29 Quarter-wave balun sleeve for mobile phone handset [23]

2.6 Conclusions

In the conventional antenna measurement application, a double shielded coaxial cable is used and this is acceptable for electrically medium to large antennas. For electrically small antennas, it becomes difficult to measure their characteristics accurately. Therefore, a cascadable radio-over-fibre system with a wide dynamic range is designed to replace the coaxial cables with fibre-optic cables. This will overcome the problems associated with antenna measurements such as moving cables that causes fluctuation in loss and phase, spurious coupling from currents on outer shield from incoming/outgoing radiation, and radiation pattern perturbation from attenuation of waves or scattering in different directions.

The conventional antenna measurement method uses an antenna and a braided coaxial cable as depicted in Figure 2.30(b), which differs greatly in reality. In reality, the antenna is integrated very close to the PCB and transceiver as depicted in Figure 2.30(a), thus, results differ from the conventional antenna measurement method shown in Figure 2.30(b). To bridge the gap between these two extreme cases a radio-over-fibre system is proposed. The radio-over-fibre system's aim is to increase measurement accuracy, as the system will closely model reality as shown in Figure 2.30(c). This system will aim to remove the metallic influence of the coaxial cable as shown in Figure 2.30(b).

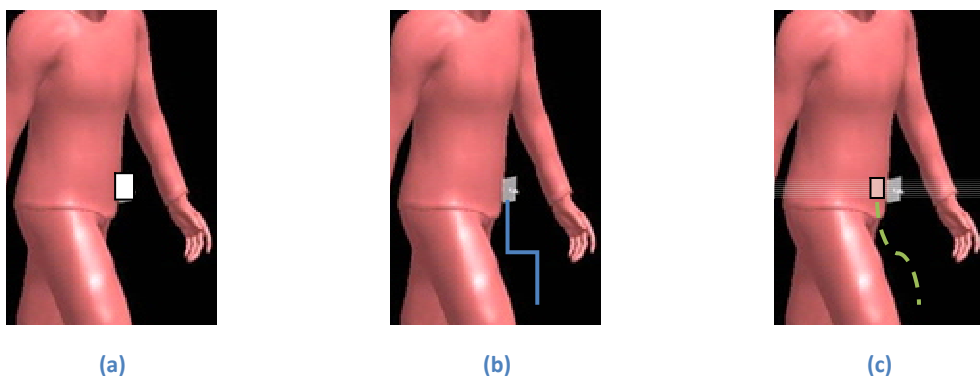


Figure 2.30 (a) Real life – Antenna & transceiver (user equipment)

(b) Conventional measurement with coaxial cable – Antenna & braided coaxial cable (differs significantly to reality)

(c) Novel measurement with fibre-optic system – Antenna, fibre-optic module & fibre-optic cable (closer to reality)

CHAPTER 3

3 DESIGN, SIMULATION AND RESULTS OF RADIO-OVER-FIBRE SYSTEM

3.1 Introduction

The review in Chapter 2 suggests that a radio-over-fibre system is designed in order to reduce the influence of coaxial cables on antenna measurements. Radio-over-fibre, (RoF), is a system that modulates an input radio frequency signal into an optical signal. This is then carried via fibre optic cable to the destination, which demodulates the optical signal into the original input radio frequency signal. The system is designed to replace coaxial cables. A top-down design approach is taken with attention for on-body integration. The simulation and measurement results of the radio-over-fibre system are also presented.

3.2 Radio-over-Fibre System

The design of the system took into account many considerations discussed in Chapter 2. These include the interfaces between components, analogue design, and required dynamic range.

3.2.1 Architecture

The system consists of an optical link connected to an RF channel followed by another optical link, thus removing coaxial cables from on-body measurements. The proposed on-body architecture is depicted in Figure 3.1. The off-body architecture is depicted in Figure 3.2.

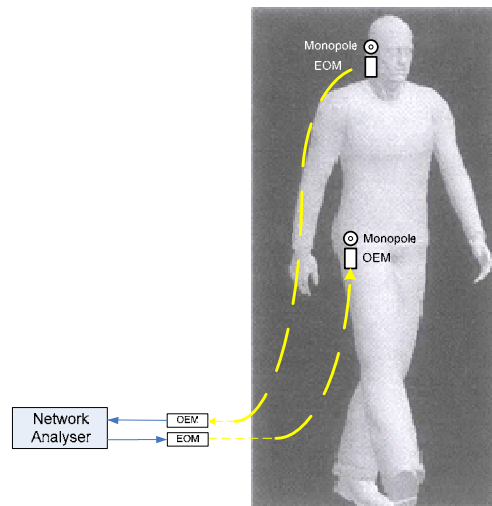


Figure 3.1 On-body measurements employing novel radio-over-fibre system

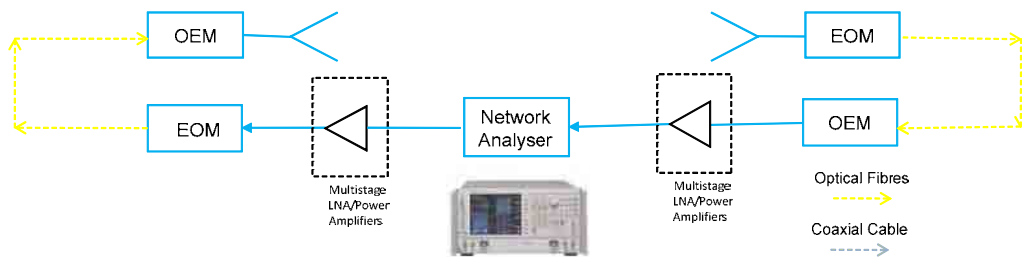


Figure 3.2 Radio-over-fibre system without the body (OEM (opto-electrical modulator), EOM (electro-optical modulator))

3.2.2 Specification

The most important system considerations. The optical fibre system should ideally be a simplex link that communicates unidirectionally. As the device is to be mounted on the body it should be battery powered, which means some form of voltage and current regulation will be required. The system should be portable, therefore requires approximately 15 metres of optical fibre. For measurement flexibility and repeatability, demountable connectors should be used. The system is required to operate primarily between 2.40–2.50 GHz, part of the unlicensed ISM band. This band holds many key wireless technologies such as Wi-Fi and Bluetooth. The electro-optical modulator is essentially a fast switching laser diode for analogue signals, which converts an electrical signal into an optical signal. For use at 2.45 GHz, the laser diode must be high speed and have a wide analogue bandwidth. The laser diode should ideally have a mate-able fibre connector to the photodiode. The electro-optical modulator should be impedance matched to the source or sink, usually at 50 Ω . From Figure 3.2, this is either a network analyser or an antenna. The optical fibre

cable should be either singlemode or multimode depending on the choice of laser diode and photodiode. The opto-electrical modulator is a combination of multi-stage amplifiers and a photodiode. For use at 2.45 GHz, the photodiode should be high speed and have a wide analogue bandwidth. It also must possess a high responsivity at 2.45 GHz. The photodiode should have a mate-able fibre connector to the laser diode and should be impedance matched to the source or sink.

3.2.3 Components

The important components in this system are the laser diode and photodiode of which the photodiode in most cases dictates the overall system performance.

3.2.3.1 Laser Diode

The laser diode is a Honeywell VCSEL multi-mode 850 nm laser diode. The part number is HFE4083-322/XBA. The specification of the laser diode is found in Appendix A. The bandwidth of the laser diode is undocumented, however, it can be calculated through the stated rise and fall times. The typical rise/fall time is 100 pS and maximum rise/fall time is 300 pS.

$$B_{\text{typ}} = 1/\tau$$

Equation 8

Thus using Equation 8, the typical and minimum bandwidth is 10 GHz and 3.3 GHz, respectively. For the application, this deems sufficient bandwidth. However, the laser diode is specifically designed for digital transmission with an interface of emitter-coupled (ECL) logic/positive emitter-coupled logic (PECL). Although ECL/PECL is the designed interface, it can still be driven using analogue methods. Some other important factors that need consideration are optical output power, threshold current, relative intensity noise (RIN) and series resistance. The optical power output of laser diode varies between 0.2 mW and 1.0 mW, which are ample for the application. This is dependent on the threshold current, which is typically 3.6 mA, but can be driven higher. The noise of the laser diode is -128 dB/Hz, which is a typical noise level for a standard laser diode and is acceptable for the application. The series resistance is 25-50 Ω that indicates it is designed for interface to standard RF devices therefore little or no matching is required. The laser diode also has a

monitor photodiode built into it for optical feedback. This enables safety features such as average optical power control to be implemented as to avoid optical saturation.

3.2.3.2 Photodiode

The type of photodiode is a Thorlabs InGaAs photodiode. The part number is FGA04. The specification of the photodiode is found in Appendix B. The photodiode bandwidth is 3.0 GHz and hence is able to demodulate a signal up to this frequency. The photodiode responsivity at 850 nm is 0.2 A/W. At this responsivity, the photodiode cannot operate efficiently, however all other commercial photodiodes are available as only bare dies. The other limitations of a photodiode's performance are the dark current and capacitance. When the photodiode is reverse biased at 5V the dark current is typically 0.5 nA, which is acceptable for the application. The photodiode capacitance is 1.0 pF and load resistance of 50 Ω . Using Equation 9, the operating bandwidth is 3.18 GHz.

$$f_{BW} = 1 / (2\pi R_{LOAD} C_J) \quad \text{Equation 9}$$

The laser diode and photodiode have different connector types as per their specification. Thus, it is required to use custom fibre cables with different connectors at each end.

3.2.3.3 Fibre Optic Cable

The types of fibre cable are standard single-mode 9/125 μm , multi-mode 50/125 μm , custom single-mode FC/PC to ST-LP and custom multimode FC/PC to ST-LP. The first two cable lengths are 5 metres, and the second two are 10 metres. The FC/PC and ST-LP connectors are typically used in single-mode and multimode applications, respectively.

3.2.3.4 Achievable System Performance

It should be noted that the laser diode noise and photodiode receiver noise determine the achievable signal-to-noise of an optical link [24]. This paper found that vertical cavity lasers could achieve a high signal-to-noise ratio through direct modulation. This is a requirement for radio-over-

fibre applications, thereby utilising the inherent components properties for high linearity and a wide dynamic range.

Larsson et al [25] investigate the impedance characteristics of several vertical cavity devices. It is concluded that singlemode and multimode apertures have varied impedances. For a singlemode device, the differential resistance is 200 Ω due to a small current aperture, however for a multimode device, the differential resistance is 60 Ω due to a large current aperture. Thus, it is possible to see that multimode devices are a better option for direct modulation as RF inputs are usually 50 Ω , therefore resulting in a higher RF transfer efficiency without the need of impedance matching.

3.3 System Design

The literature research shows that the best design for the application is an intensity modulation and direct detection circuit. An illustrative circuit is shown in Figure 3.3.

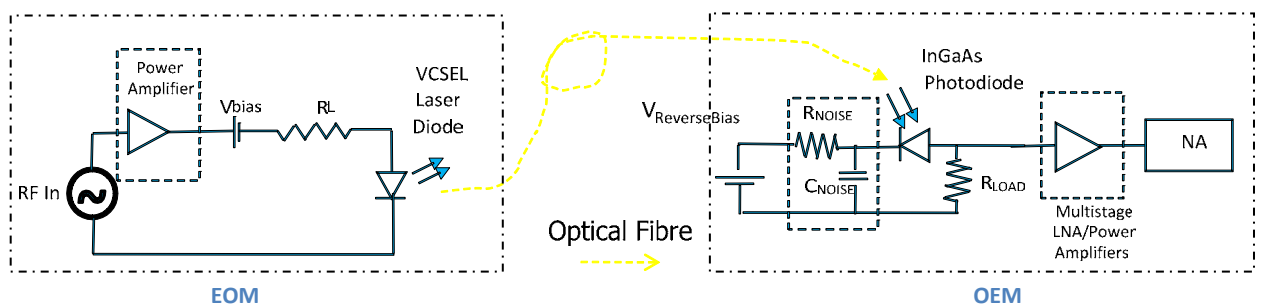


Figure 3.3 Simple Electro-Optical Modulator (EOM) and Opto-Electrical Modulator (OEM) circuit

The laser diode has a typical forward voltage of 1.75 Volts and a threshold current of 5 mA. The bias voltage available from the power supply is 5 Volts. Using Equation 10, the typical current limiting resistor is calculated as 650 Ω .

$$R_L = (V_{\text{bias}} - V_{\text{diode}}) / I_{\text{TH}} \quad \text{Equation 10}$$

where, R_L is the typical current limiting resistor, V_{bias} is the bias voltage from the PSU, V_{diode} is the laser diode forward voltage drop and I_{TH} is the threshold current for laser

The photodiode has a reverse bias voltage of 5 Volts, load resistance of 50 Ω , responsivity at 850 nm of 0.2 A/Watts and a junction capacitance of 1.0 pF. Thus, using Equation 11, the voltage output from the photodiode is at maximum 10 mV and typically 5 mV. Using Equation 12, the operating bandwidth is 3.18 GHz, which is sufficient for use at 2.45 GHz.

$$\text{Max } V_o = P_{\text{opt}} \times R_{\text{LOAD}} \times R(\lambda) \quad \text{Equation 11}$$

where, R_{LOAD} is the load resistance, V_o is the voltage output from the photodiode, P_{opt} is the received optical power and $R(\lambda)$ is the responsivity at the wavelength

$$f_{\text{BW}} = \frac{1}{2\pi \times R_{\text{LOAD}} \times C_j} \quad \text{Equation 12}$$

where, f_{BW} is the operating bandwidth, R_{LOAD} is the load resistance and C_j is the junction capacitance

An optical link budget is important to ensure an optical system operates correctly taking into account a design margin. The laser has a typical optical power of 500 μW or 3.01 dBm, typical fibre loss is 3.0 dB per km, each connector has a loss of 0.5 dB and a design margin of 3 dB. Equation 13 calculates the optical link budget and it is found that the photodiode receiver sensitivity must be at least -7.07 dBm or 196 μW .

$$\text{Fibre Output} = \text{Source Output} - (\text{Fibre \& Connector Losses} + \text{Design Margin}) \quad \text{Equation 13}$$

(in dB)

3.3.1 Electro-Optical Modulator Design

The design uses microstrip and consists of a 50 Ω line with a broadband bias decoupling network. Rogers Duroid 5880 of thickness 0.787 mm is used because it has a stable dielectric constant and a low loss tangent over the required frequency range. This attribute provides efficient RF power transfer from the RF input to laser output at 2.45 GHz. The purpose of the quarter-wave radial stub and quarter-wave short circuit stub is to provide DC bias decoupling and the purpose of the DC decoupling capacitor is to ensure no DC travelled down the RF input. The realised microstrip layout is shown in Figure 3.4.



Figure 3.4 Electro-Optical Modulator Microstrip layout

Safety circuits are incorporated to protect the laser from damage. Laser diodes are electrostatic discharge sensitive and voltage and current transients sensitive. Thus, the requirements for power supply conditioning using voltage & current regulation. A slow start up voltage and current is essential for laser protection. The design shown in Figure 3.5 is used for voltage regulation and transient suppression. The circuit consists of a voltage regulator, resistor, capacitor, varistor and a reverse voltage protection diode as shown in Figure 3.5.

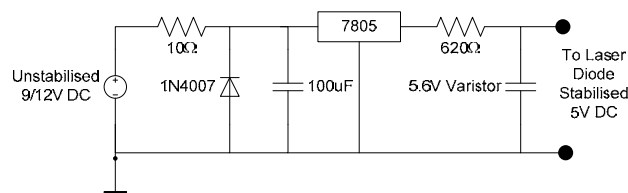


Figure 3.5 Stabilised voltage and current output

3.3.2 Opto-Electrical Modulator Design

The photodiode is less sensitive to electrostatic discharge, thus only a voltage regulator is required for the reverse bias voltage. The opto-electrical modulator circuit is shown in Figure 3.6.

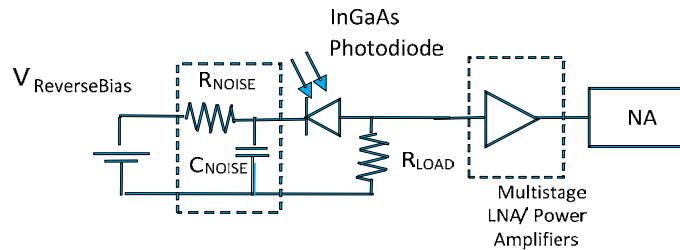


Figure 3.6 Opto-Electrical Modulator Circuit Diagram

The R_{noise} and C_{noise} are required by photodiodes for noise filtering. Multistage low noise amplifiers (LNA) or power amplifiers (PA) are required to equalise the loss of the fibre-optic system, therefore a number of amplifiers or variable gain amplifiers are normally required. A 0 dB gain is required for equalisation of system losses. The realised opto-electrical modulator circuits are shown in Figure 3.7 and Figure 3.8.

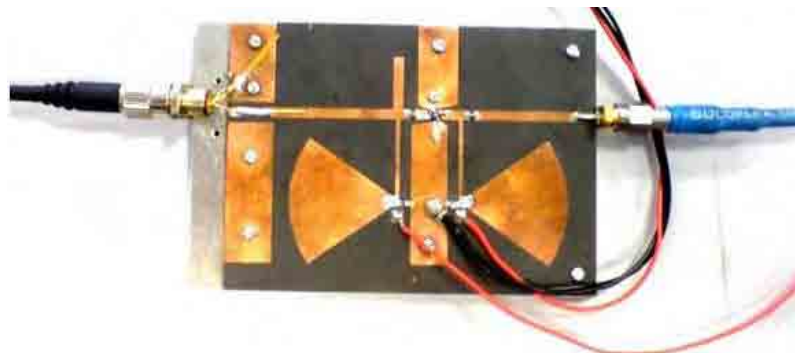


Figure 3.7 1-Stage OEM Microstrip Layout

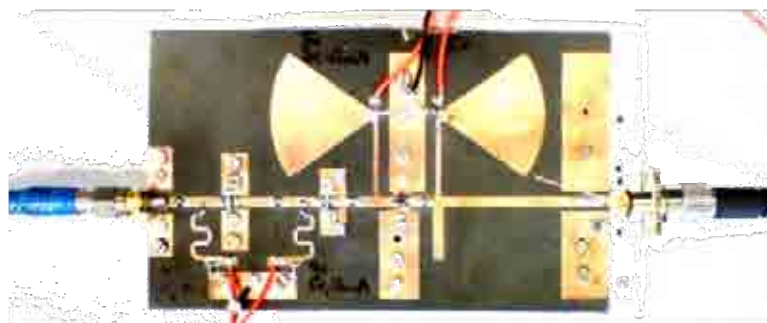


Figure 3.8 3-Stage OEM Microstrip Layout

3.4 Simulated Results

The radio-over-fibre system simulations are carried out using Ansoft Designer SV. The simulations predict the realised microstrip layout's performance as shown in Figure 3.4, Figure 3.7 and Figure 3.8. The laser diode and photodiode components used in the simulations are generic library components, thus simulations will not match measurements. However, they should show relative results when compared to the measurement results. The lowest forward current available on the library photodiode component is 28 mA, so all simulations start at this value and increase by 2 mA. The parameters are set to slope efficiency of 0.3, chip series resistance of 30Ω , bond wire inductance of 2 nH, responsivity of 0.2 A/W and chip capacitance of 1.2 pF. The simulations use S parameter (S2P) files provided by Avago for the amplifiers. An example of a configuration is outlined in Figure 3.9 and the detailed layout can be found in Appendix C. The other two configurations can be found in Appendix D and Appendix E. Appendix C shows graph results of bias current in 2 mA increments up to 50 mA. Appendix D and Appendix E only include the 28mA and 36mA bias current graphs. All three configurations use similar layouts, however the circuits use different amplifier combinations within the receiver.

Appendix C has a 1-stage amplifier photodiode receiver, using a MSA-0886 20dB Monolithic Microwave Integrated Circuit power amplifier (MMIC PA). The specification of MSA-0886 is found in Appendix F.

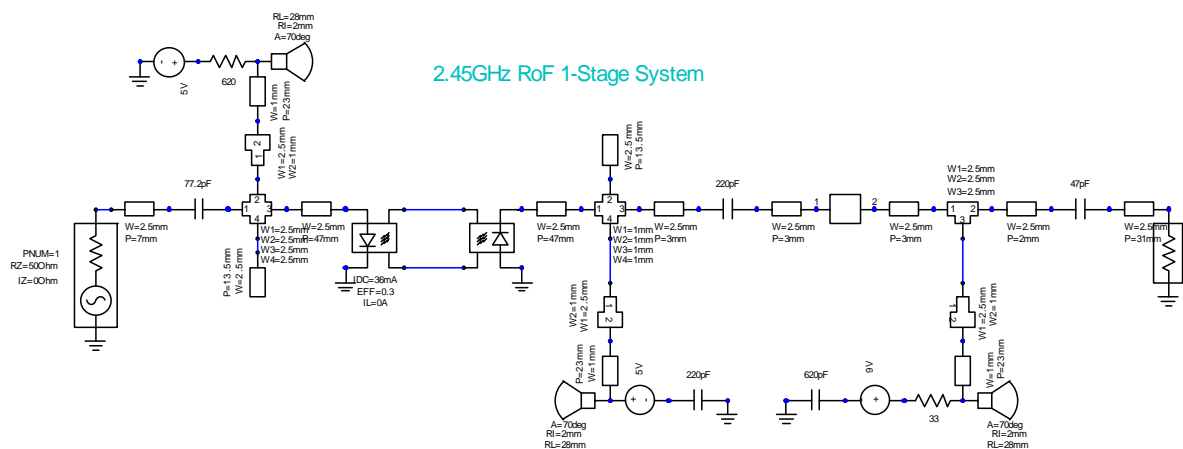


Figure 3.9 Overview of the radio-over-fibre system with 1-stage amplifier (MSA0886) (Appendix C)

Appendix D has a 3-stage amplifier photodiode receiver, using one MGA-81563 14 dB power amplifier and two MGA-86576 23 dB low noise amplifiers. The specifications of the MGA-81563 and MGA-86576 amplifiers are found in Appendix G and Appendix H, respectively.

Appendix E has a 3-stage amplifier photodiode receiver, using three MSA-0886 amplifiers.

The simulation is run from 10 MHz to 4 GHz and the respective S-Parameter results are shown in graphs. The graph is shown in Figure 3.10 as an example of 28mA laser bias and the results of the full bias range for the 1-stage and both 3-stage systems are shown in Figure 3.11.

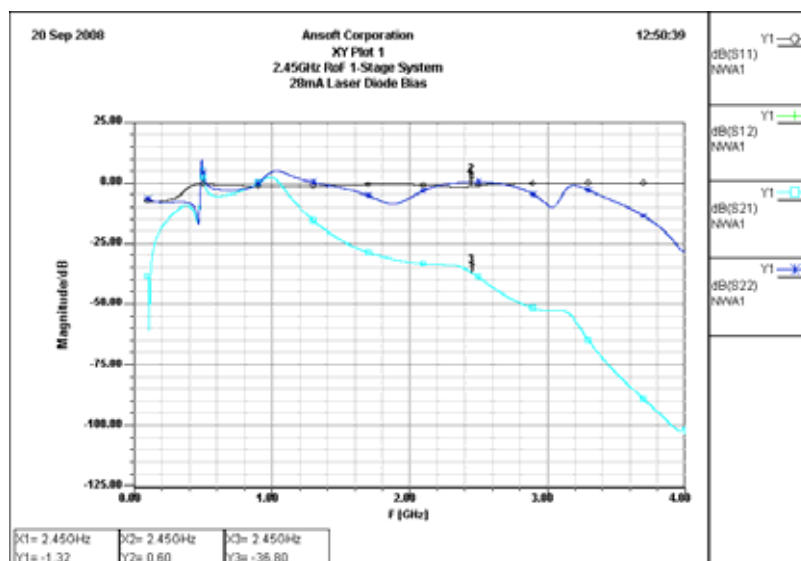


Figure 3.10 Example S-Parameter result of radio-over-fibre system with 1-stage amplifier at 28mA Bias (MSA-0886)

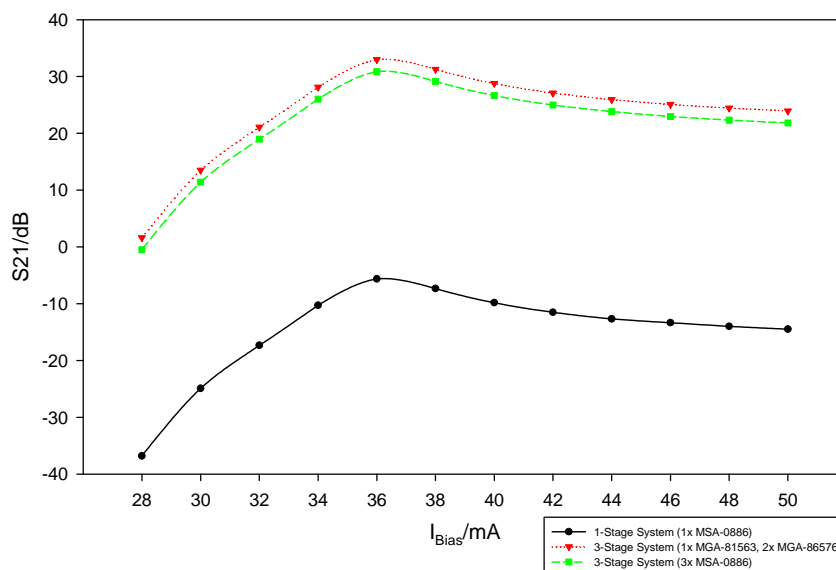


Figure 3.11 S-Parameter results of radio-over-fibre system with 1-stage and 3-stage amplifiers

The results of the 1-stage system show a gain increase from -36.8 dB to -5.63 dB, however this does not achieve the 0dB system gain required. The results of the 3-stage system (one PA and two LNA's) show a gain increase from 1.62 dB to 32.98 dB. The results of the 3-stage system (three PA's) show a gain increase from -0.49 dB to 30.86 dB. The two 3-stage systems appear to provide a 0 dB system gain. It is viewed that losses occur above a certain bias current. It is probable, that above a certain bias threshold current, the laser diode becomes saturated.

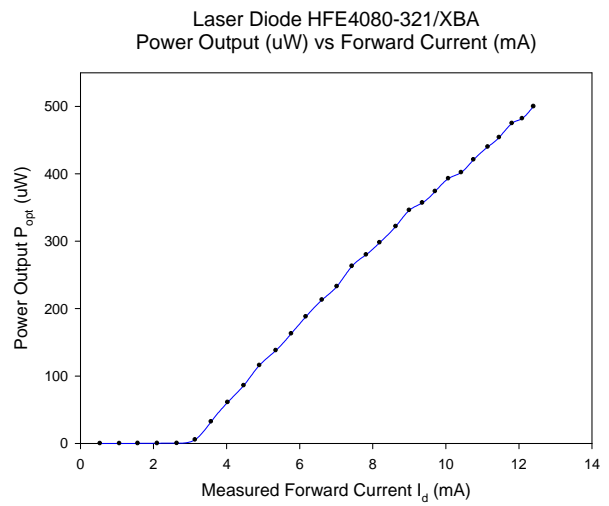
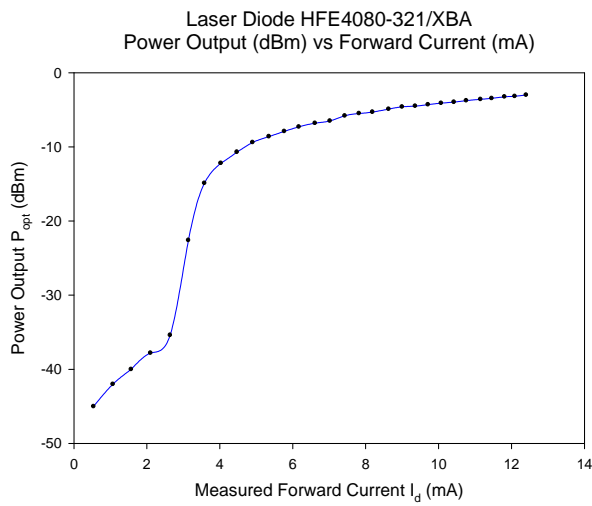
3.5 Measurement Results

The measurement set up uses a RF source (HP8648D Signal Generator), optical power sensor (Anritsu ML9001A) and portable spectrum analyser (R&S FSH3) as shown in Figure 3.12.



Figure 3.12 Measurement setup to characterise the laser diode

The laser diode is characterised to ensure the measured results match the datasheet. The laser diode characteristics of most importance are power output vs. forward current, laser diode spectral output and laser diode modulation response. The noise floor of the Anritsu optical power for the following measurement is -47 dBm or 19 nW. The measured results are shown in Figure 3.13 and Table 3.1.



(a)

(b)

Figure 3.13 Power Output (a) dBm and (b) uW vs. Forward Current (mA) for Laser Diode HFE4080-321/XBA

These results show that the maximum optical power output for this laser diode is 500 uW or -3.0 dBm, and does not exceed the maximum continuous forward current of 15 mA. This measurement is carried by varying the input current limiting resistor from 6.6 k Ω to 221 Ω as shown in Table 3.1.

Calculated R_d (Ω)	Calculated I_d (mA)	Measured I_d (mA)	Measured V_d (V)	Measured P_{opt} (dBm)	Measured P_{opt} (μ W)
6600	0.5	0.54	1.44	-45.0	0.031
3300	1.0	1.07	1.49	-42.0	0.058
2200	1.5	1.57	1.53	-40.0	0.099
1650	2.0	2.10	1.56	-37.8	0.166
1320	2.5	2.64	1.59	-35.4	0.291
1100	3.0	3.14	1.61	-22.6	5.5
945	3.5	3.58	1.62	-14.9	32.4
827	4.0	4.03	1.64	-12.2	61
735	4.5	4.47	1.66	-10.7	86
662	5.0	4.90	1.67	-9.4	116
502	5.5	5.35	1.68	-8.6	138
552	6.0	5.77	1.70	-7.9	163
509	6.5	6.17	1.71	-7.3	188
472	7.0	6.61	1.72	-6.8	213
441	7.5	7.02	1.73	-6.5	233
413	8.0	7.43	1.74	-5.8	263
389	8.5	7.82	1.76	-5.5	280
368	9.0	8.19	1.77	-5.3	298
348	9.5	8.63	1.78	-4.9	322
331	10.0	9.00	1.79	-4.6	346
315	10.5	9.36	1.80	-4.5	357
301	11.0	9.71	1.81	-4.3	374
288	11.5	10.07	1.81	-4.1	393
276	12.0	10.42	1.82	-4.0	402
265	12.5	10.76	1.83	-3.8	421
255	13.0	11.15	1.84	-3.6	440
245	13.5	11.46	1.85	-3.5	454
236	14.0	11.81	1.86	-3.3	475
228	14.5	12.09	1.87	-3.2	482
221	15.0	12.40	1.87	-3.0	500

Table 3.1 Results Table for Laser Diode HFE4080-321/XBA

The input RF modulation signal is calculated and shown in Table 3.2. This is required as intensity modulation varies the amplitude of the optical output and it is important to know the voltage amplitude of the input power.

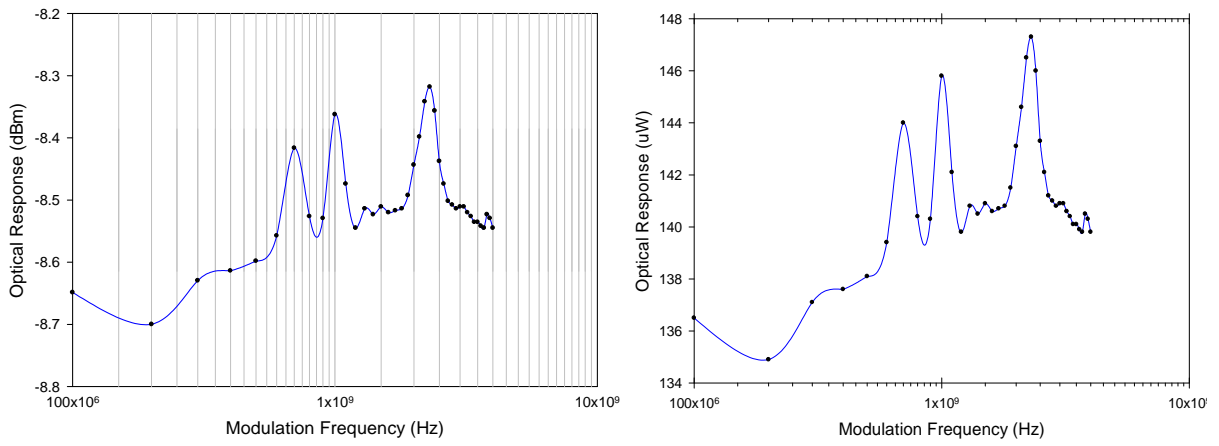


Figure 3.14 Laser Diode Frequency Modulation Response at $P_{RFin} = 0$ dBm

Figure 3.14 depicts how the optical output power varies with modulation frequency. The internal optical resonances account for the peaks and only vary by a maximum of 10 μ W, which can be considered negligible.

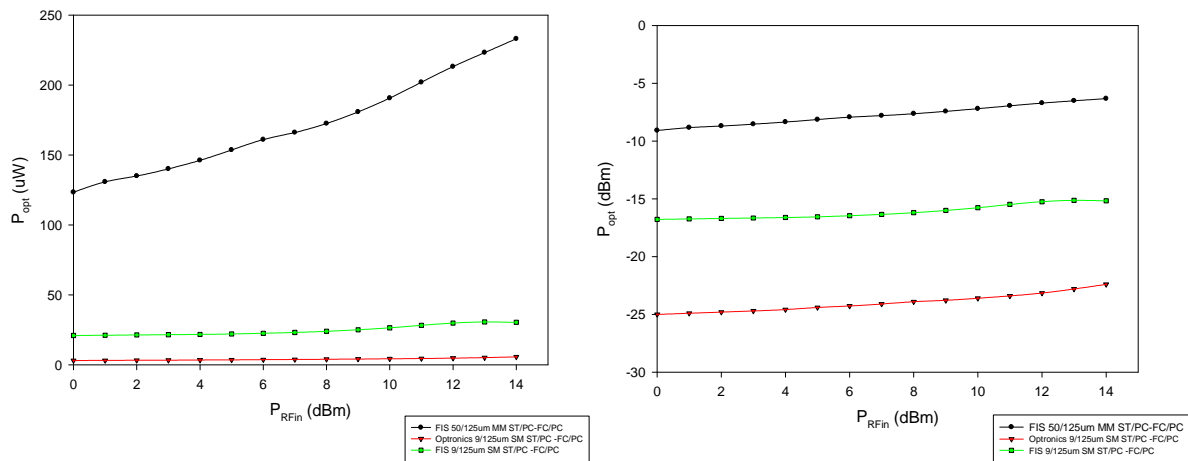


Figure 3.15 RF Modulation vs. Optical Power for differing Fibre Types



Figure 3.16 Fibre coupling measurement setup between fibre optic cables and laser diode

The graph in Figure 3.15 shows the coupling between different fibre optic cable and the laser diode. Figure 3.16 shows the measurement setup for the coupling for differing fibre types. The results show that the FIS 50/125 μm multimode ST/PC to FC/PC is the right fibre type for maximum coupling. This is no surprise as the laser is designed for multimode fibre operation, thus is efficient over multimode fibre. The laser diode is biased at 5.22 mA and 1.69 V and unmodulated.

The input RF modulation signal is converted from power into voltage and current in the Table 3.2. This using the knowledge that, $Z_0 = 50 \Omega$ and using Equation 14.

$$I_{\text{RFin}} = P_{\text{RFin}} / Z_0 \quad \text{Equation 14}$$

P_{RFin}	0dBm	3dBm	7dBm	8.5dBm	9.0dBm	9.5dBm	10dBm	10.5dBm	13dBm
P_{RFin}	1mW	2mW	5mW	7mW	8mW	9mW	10mW	11mW	20mW
V_{RFin}	0.224V	0.320V	0.500V	0.592V	0.632V	0.671V	0.707V	0.742V	1.000V
I_{RFin}	4.47mA	6.32mA	10.0mA	11.8mA	12.7mA	13.4mA	14.1mA	14.8mA	20.0mA

Table 3.2 Table of RF modulation signal in dBm/mW/V/mA

The radio-over-fibre performance is measured to characterise the system. The system employing the EOM and OEM with 1-stage MSA-0886 power amplifier and photodiode FG01 is shown in Figure 3.17.



Figure 3.17 Radio-over-Fibre System with 1-Stage MSA-0886 (FG04-1)

The component specification for the photodiode, FG04 can be found in Appendix B. The power amplifier has a device current of 33.1 mA, the noise floor of the spectrum analyser at 2.45 GHz is -53 dB and the fibre optic cable is a custom multimode fibre.

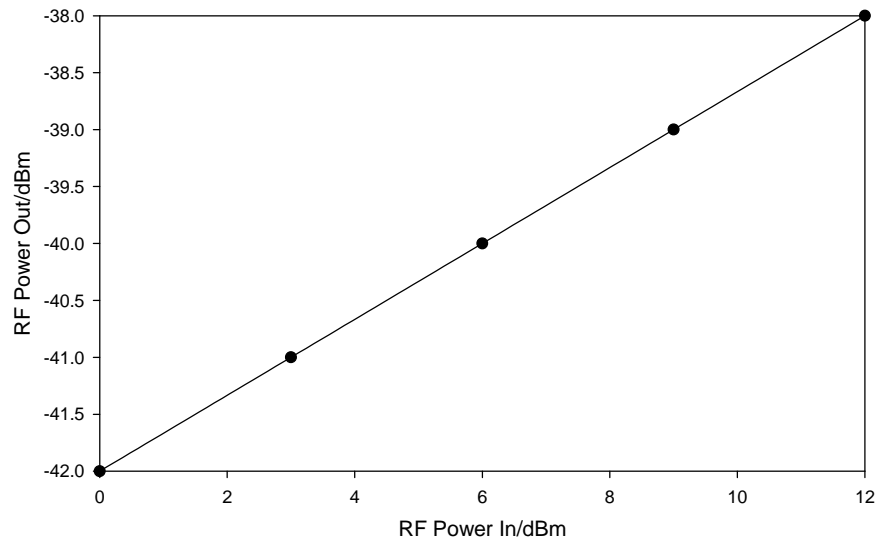


Figure 3.18 Measurement Results of 1-Stage System (MSA-0886/FG04-1)

The results in Figure 3.18 show a linear increase of power out with power in. Each 3 dB increase of RF Input power has 1 dB increase at the output. The system is operational but requires further amplification to reach a 0 dB system gain. Therefore, a 3-stage system is tested.

The 3-stage OEM consists of one MGA-81563, two MGA-86576 amplifiers and photodiode FG04-2 as shown in Figure 3.19.



Figure 3.19 Radio-over-Fibre System with 3-Stage 1x MGA-81563, 2x MGA-86576 (FG04-2)

The 815 power amplifier has a device current of 12.5 mA, the 865 power amplifier has a device current of 2.5 mA, the noise floor of the spectrum analyser at 2.45 GHz is -53 dB and the fibre optic cable is a custom multimode fibre.

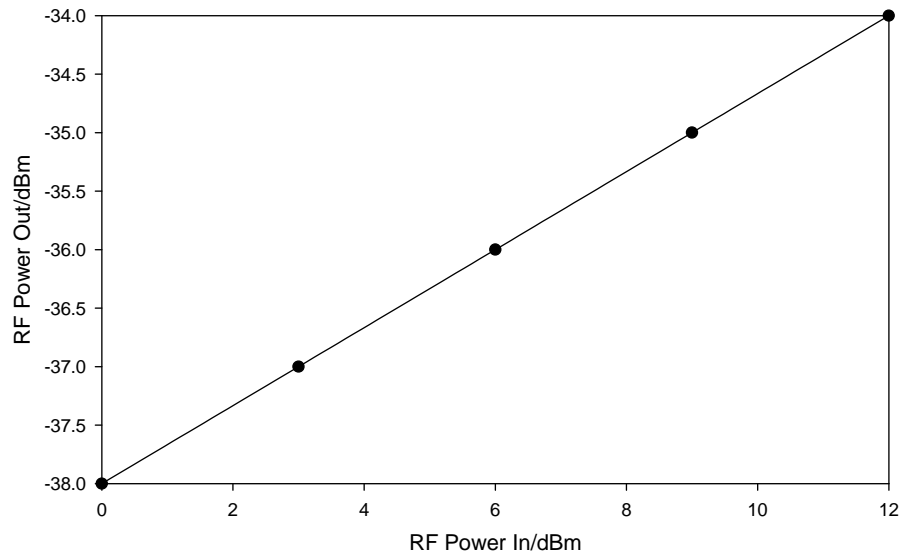


Figure 3.20 Results of 3-Stage System (1 x PA & 2 x LNA)

The results in Figure 3.18 show only a 4 dB gain over the previous 1-stage system. It indicates faulty amplifiers, which is expected from the low current drawn.

These amplifiers are replaced with three MSA-0886 20dB MMIC cascadable power amplifiers as shown in Figure 3.21 and the test results are shown in Figure 3.22.



Figure 3.21 Radio-over-Fibre System with 3-Stage 3x MSA-0886 (FG04-2)

The 866 power amplifiers have device currents of 22.3 mA, 20.2 mA and 21.5 mA, the noise floor of the spectrum analyser at 2.45 GHz is -49 dB and the fibre optic cable is a custom multimode fibre.

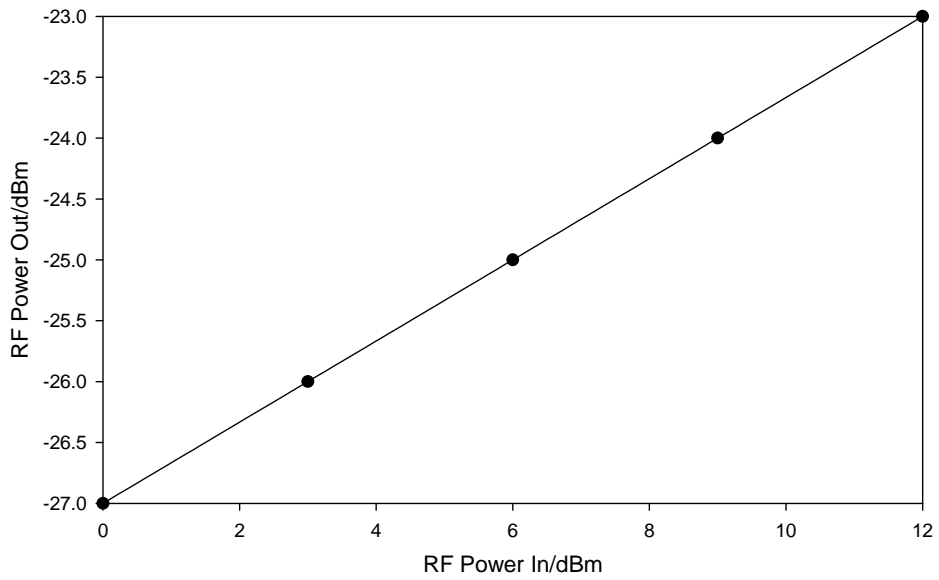


Figure 3.22 Results of 3-Stage System (3 x PA)

This 3-stage system has gain of 15 dB over the 1-stage system and 11 dB over the first 3-stage system. Therefore, it is probable that the impedance mismatch between photodiode and microstrip board accounts for the power loss or that the amplifier's were not driven with enough bias current and therefore lack performance.

For reference, a full set of graph measurement results can be found in Appendix I, Appendix J and Appendix K .

3.6 Conclusions

From the results, the radio-over-fibre system shows viability for the application. However, the system still requires further modification to improve system gain and efficiency. It is possible to design a smaller microstrip layout specifically for this design and insert several cascaded variable gain amplifiers in the opto-electrical modulator. The alternative to a microstrip design would be a mixed lumped/distributed element microstrip design. Using this approach the layout can be realised with smaller dimensions. A RF choke using a 5nH inductor with a series resonant frequency above 20 GHz has a bandwidth as large as 15 GHz. However, it should be noted that lumped elements also have inherent parasitic properties due to package size, lead inductance and capacitance whereby parasitic reactance increases with frequency. The distributed element design of such bandwidth would require two or three quarter-wave transformers.

The current design dimensions of 150 mm by 70 mm are too large to utilise for on-body measurements. Therefore, a commercial radio-over-fibre system, which has a minimum system gain of 0 dB and inherently small dimensions attributed to system-on-chip (SoC) design, is considered. This module is utilised for on-body measurements. This system will be characterised and discussed in Chapter 4.

CHAPTER 4

4 INTEGRATION AND CHARACTERISATION OF A COMMERCIAL RADIO-OVER-FIBRE SYSTEM VS. COAXIAL CABLE SYSTEM FOR OFF-BODY CHAMBER MEASUREMENTS

4.1 Introduction

In this Chapter, the integration of the commercial radio-over-fibre system within an enclosure is discussed and implemented. Thereafter, the system is characterised and performance is measured. The difference between radiation patterns using a coaxial cable system and a radio-over-fibre system in the anechoic chamber is measured, and the results are compared. The devices are a radio-over-fibre transceiver (OZ600), receiver (OZ450) and transmitter with a 20 dB LNA (OZ450). A 20 dB LNA is incorporated into the transmitter module to account for the possibility of low SNR conditions for high channel path variability (S21) for on-body measurements. The system characteristics are 20 dB system gain, wide bandwidth, small package outline, low noise laser, wide dynamic range and slow-start circuitry. The specifications can be found in Appendix N and Appendix O. Regulated power supplies are designed for the system. The next Chapter will discuss the on-body integration, simulations and measurements.

4.2 Power Supply Design

A regulated power supply may not necessarily be required but is integrated for safety of the modules. This is similar to the power supply design for the laser diode but uses a 12 Volt regulator instead and is designed for battery operation. It has a soft start, power supply conditioning and a current limiting resistor.

The current limiting resistor was chosen such that it does not exceed the maximum current allowed to module as per datasheet. The design requires the power supply board to be small and low

profile as to fit onto a pluggable 10-pin connector on the fibre modules. A veroboard design is implemented as it fits the requirements and is easy to implement, as per circuit diagram shown in Figure 4.1.

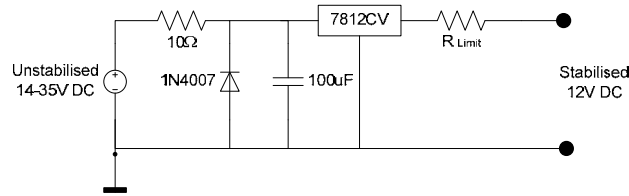


Figure 4.1 Power Supply for Commercial Radio-over-Fibre System Modules

For battery operation, it is important that the voltage at which the module becomes unusable because a loss of gain is identified. The input power for both systems are -10 dBm, the transceiver device current is 242 mA, the transmitter device current is 175 mA and the receiver device current is 139 mA. The batteries are two Duracell Procell MN1604 PP3 9 Volt with a capacity of 550 mAh. The voltage dropout against loss for both systems is shown in Figure 4.2.

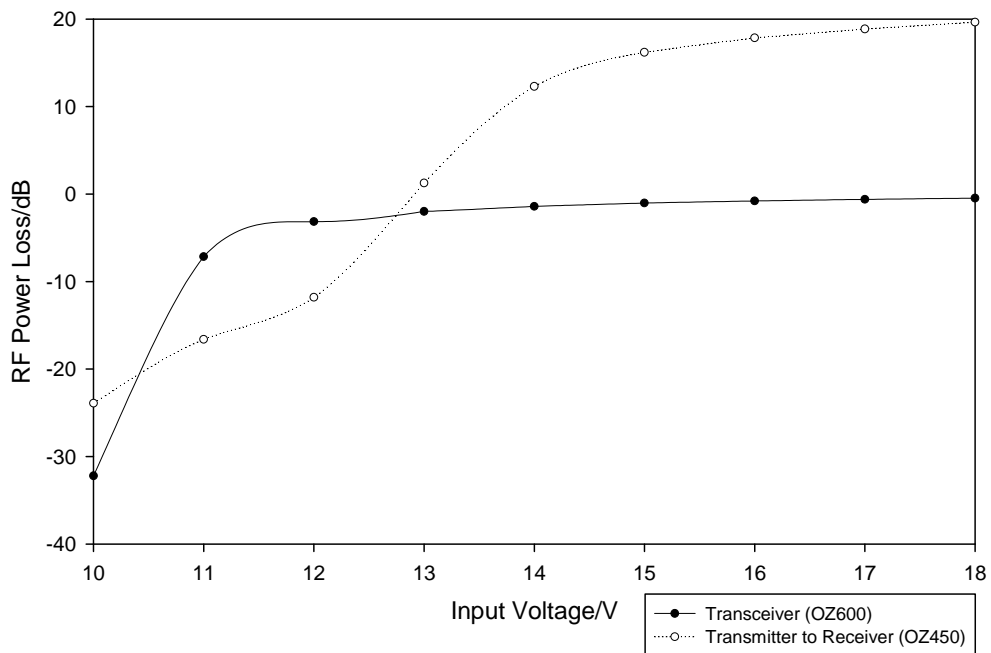


Figure 4.2 Loss of Gain with Voltage Dropout

Therefore, the minimum voltage for the transceiver before a reduction in gain by 1 dB was 15 V, although this was not important as this module is to be located next to the analyser and has the option for direct DC power. However, the voltage dropout was important for the separate modules as these are to be mounted on the body. The minimum voltage for the transmitter and receiver before reducing gain by 1 dB is 17 V, and thus proves a challenge. The resulting capacity of a 9 V cell is too low, 550 mAh, as compared to a 1.5 V cell, which is 2600 mAh. The use of two 9 V cells in series is required, as a minimum of 17 V are required to power the modules. The benefits of using low capacity 9 V cells instead of high capacity 1.5V cells are the weight and size. The battery pack needs to be small and light and 9V cells fit these criteria. However, the modules seem to be power hungry, drawing 314 mA between them, and the two 9 Volt series batteries are incapable of powering this system for long periods. Thus, direct DC power cables are fed to the on-body modules through a workbench power supply as shown in Figure 4.3.



Figure 4.3 DC Cables to OZ450 Radio-over-Fibre modules

This approach using direct power cables of 1 mm diameter has little or no effect on the measurement accuracy and as the power cables provide very low DC voltage, they do not affect high frequency signals.

4.3 Radio-over-Fibre System Characterisation

A photograph of the whole radio-over-fibre system is shown in the Figure 4.4.



Figure 4.4 Photos of whole system (Transceiver → Receiver → Transmitter → Transceiver)

Each subsystem is tested by feeding input power into the transmitter and measuring output power from the receiver. The two subsystems are labelled System Link 1 (transceiver to receiver) and System Link 2 (transmitter to transceiver).

4.3.1 System Link 1 (Transceiver to Receiver)

The signal generator outputs an RF carrier at 2.45 GHz to the OZ600 transceiver via RF cable. The transceiver modulates the signal onto an optical carrier to the OZ450 receiver via fibre optic cable. The receiver then demodulates the optical carrier and then amplifies the signal to 0 dB. This is received by the spectrum analyser and the measurement is taken.

4.3.1.1 Measurement Set Up

The measurement is set up as per Figure 4.5.

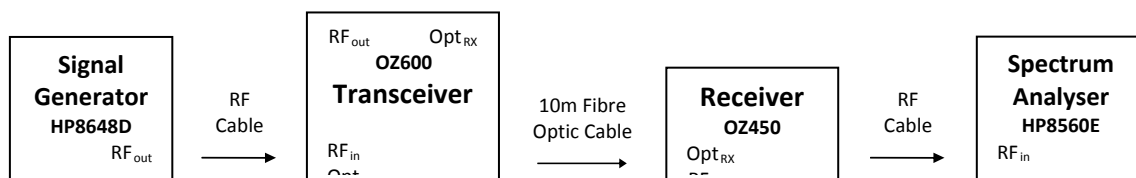


Figure 4.5 Diagram of the measurement set up for System Link 1

The fibre type is a single-mode 10m cable, measurement equipment are signal generator HP8648D and spectrum analyser HP8560E. The signal generator output power varies from -60 dBm to +10 dBm. The calibration data for the spectrum analyser is ref level cal #296 and the noise floor without optical is -73 dBm. The device current for the transceiver is 242 mA and for the receiver is 139 mA.

4.3.1.2 Measurement Results

Figure 4.8 shows the results of System Link 1 plotted on a graph.

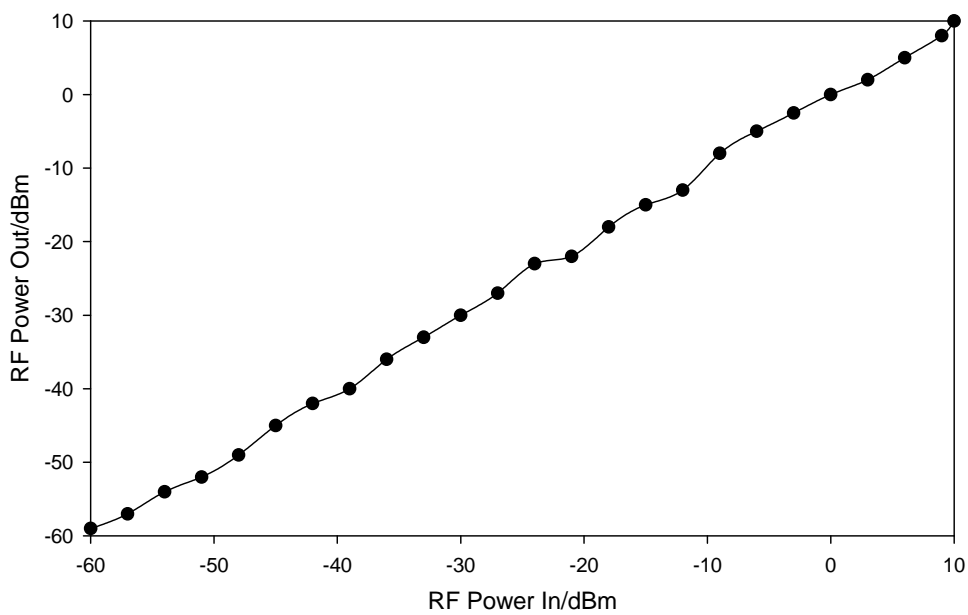


Figure 4.6 Results of the Transceiver to Receiver (System Link 1)

The results show good performance with a system gain/loss variation of no more than ± 1 dB. We can see the dynamic range of the system is 70 dB at minimum, which is ideal for on-body measurements.

4.3.2 System Link 2 (Transmitter to Transceiver)

The signal generator outputs an RF carrier at 2.45 GHz to the OZ450 transmitter via RF cable. The transmitter amplifies the RF signal before modulating the signal onto an optical carrier to the OZ600 transceiver via fibre optic cable. The transceiver then demodulates the optical carrier and then amplifies the signal. This is received by the spectrum analyser and the measurement is taken.

4.3.2.1 Measurement Set Up

The measurement is set up as per Figure 4.7.

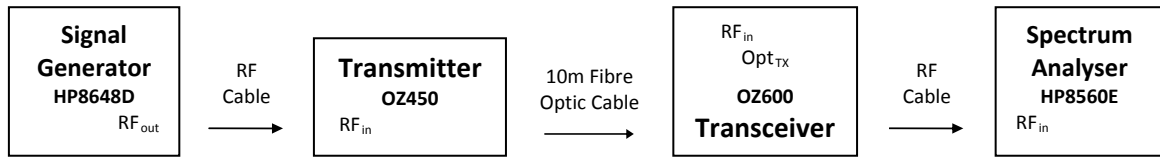


Figure 4.7 Diagram of the measurement set up for Transmitter to Transceiver (System Link 2)

The fibre type is a single-mode 10m cable, measurement equipment are signal generator HP8648D and spectrum analyser HP8560E. The signal generator output power varies from -80 dBm to +10 dBm. The calibration data for the spectrum analyser is ref level cal #296 and the noise floor without optical is -54 dBm. The device current for the transceiver is 242 mA and for the receiver is 175 mA.

4.3.2.2 Measurement Results

Figure 4.8 shows the results of System Link 2 plotted on a graph.

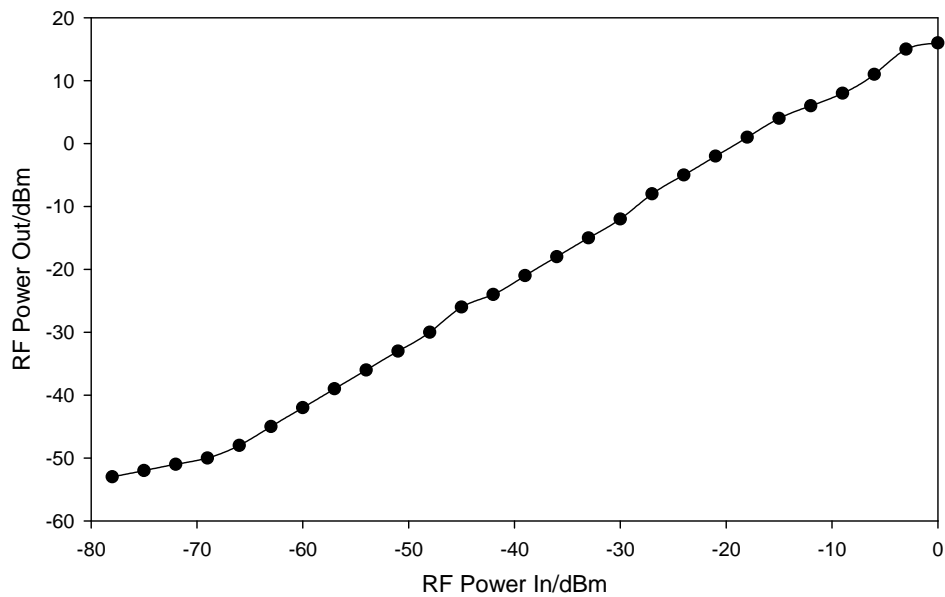


Figure 4.8 Results of the Transmitter to Transceiver (System Link 2)

The results show an acceptable performance with a system gain/loss variation of no more than ± 4.5 dB. The OZ450 transmitter has an internal gain of 20 dB from the built-in low noise amplifier. The results show a 3 dB loss above an input power of -10 dBm. Therefore, a maximum RF

input power limit of -10 dBm must be imposed. This occurs because the laser diode becomes saturated due to over amplification of the input RF signal. The dynamic range of the system is 69 dB at maximum.

4.3.3 Full System Link 1 and 2 Link Budget

A quantitative estimate of the RF link budget is required to characterise the full system shown in Figure 4.4. If the RF output from network analyser is 10 dBm then the output from the OZ450 receiver is 10 dBm due to the 0 dB gain of System Link 1. This power is transmitted through a pair of monopoles over the head to the belt on-body channel, which has a path loss of ≈ 50 dB [4]. Thereafter the signal power is -40 dBm at the belt monopole, which is then received by the OZ450 transmitter with 20 dB LNA. This amplifies the signal to -20 dBm due to the 20 dB gain of System Link 2, which is then received by the network analyser. The received signal power is well above the analyser noise floor, thus a lower power can be transmitted from the network analyser if required.

4.3.4 Temperature vs. Loss

Optical devices are prone to power variation due to their susceptibility to temperature change. This is exaggerated further through inserting the module within a closed box. A little loss is expected but the system should stabilise at the ambient operating temperature. This is tested by connecting the whole system together, transmitting a constant RF input power and measuring the RF output power using the Agilent Network Analyser 8720ES. The network analyser is calibrated for through (S21) measurements, essentially zeroing the results to measure system gain or loss only. The RF output power is measured over time and is shown as two plots on the graph in Figure 4.9.

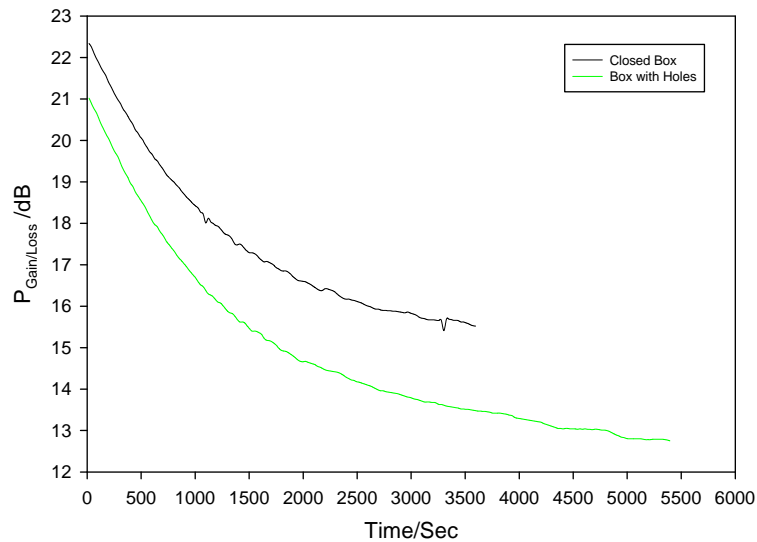


Figure 4.9 Gain Variation over Time for Commercial RoF System

It can be seen that the temperature variation is extreme, resulting in a loss of 6.9 dB over 60 minutes as per the black trace. With holes in the box, over 90 minutes the resulting loss is 8.35 dB as per green trace and continues to drop as time and temperature increases.

Figure 4.10 depicts the system with 40 dB attenuation, placed between the OZ450 transmitter and receiver to simulate a typical RF channel equivalent to the anechoic chamber antenna transmit to receive channel thereby ensuring unsaturated input power into the EOM.



Figure 4.10 40dB Attenuators in place of RF channel for controlled measurement analysis

Therefore, an external aluminium heatsink is connected as depicted in Figure 4.11(a) and the result is shown as the black trace in Figure 4.12. The system plateaus after 60 minutes of operation. Therefore, the implementation of an internal aluminium heatsink with ventilation holes, which creates convective air-cooling as depicted in Figure 4.11(b). The system temperature stabilisation improvement is shown by the red and green traces on Figure 4.12.

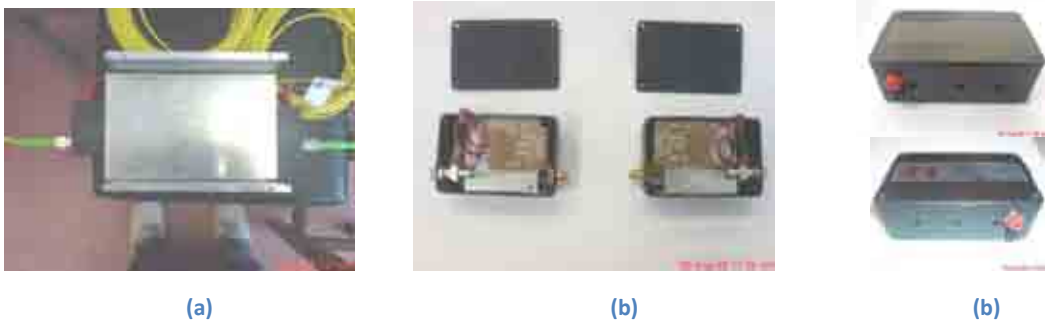


Figure 4.11 (a) External heatsink, (b) 4.5cm x 4.5cm internal heatsink and ventilation holes

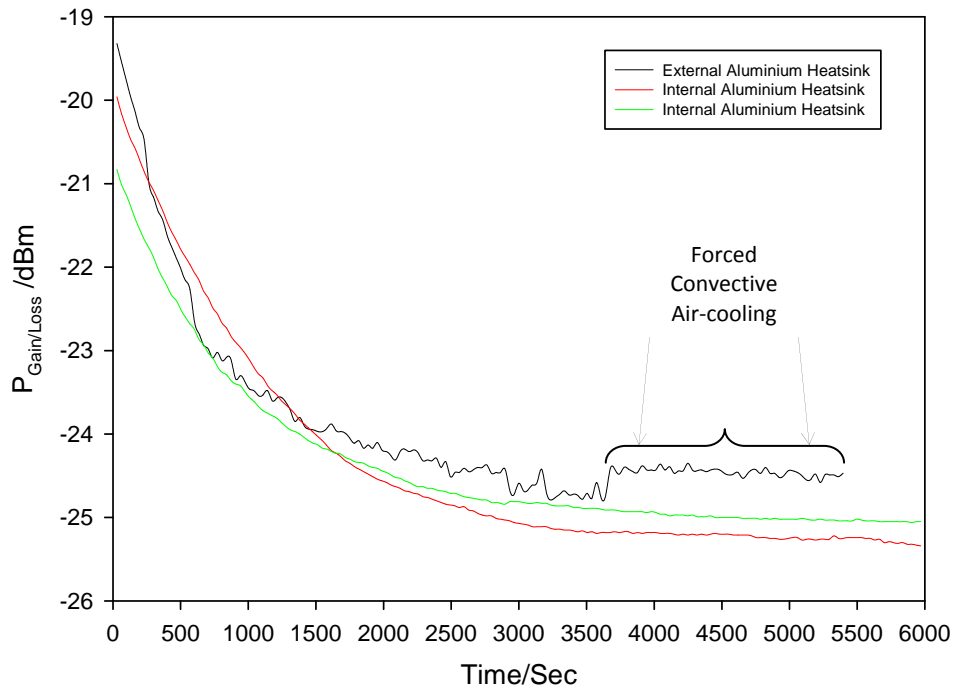


Figure 4.12 Gain/Loss over time for commercial RoF system 2 with 40dB attenuators

The results show that the system is stable after 60 minutes of operation, although when put on-body it may start to heat up due to the body heat imposed on the modules, instigating further loss. The fibre system must be switched on for 60 minutes prior to taking measurements to allow for the ambient temperature stabilisation as indicated by the red and green trace in Figure 4.12. The loss associated with the ambient temperature stabilisation is approximately 5 dB.

A cooling system with mini fans or thermoelectric cooler (TEC) could be implemented, as this would actively cool the system instead of the current passive method. If a thermoelectric cooler were considered the following design process would help to decide viability. The following design process uses quantitative estimates based on datasheets and practical measurements carried out

above. The cooler chosen for the design process is the Ferrotec single stage thermoelectric peltier cooler. The datasheet for the cooler can be found in Appendix M. The typical thermal resistance is 6 °C/Watts, the typical temperature differential is 20 °C/Watts, the system power dissipation is 3.0 Watts and a design maximum ambient temperature of 30 °C.

$$[(P_{in} + P_{sys}) \times T_{HR}] + T_{MA} = T_h$$

where, P_{in} is the max module input power, P_{sys} is max heat input to the housing and system power dissipation, T_{HR} is the housing temperature rise, T_{MA} is the maximum ambient temperature and T_h is the max housing temperature

Equation 15

From the cooler datasheet, the TEC dimension (3.2mm x 22.3mm x 22.3mm) is small enough to fit within the plastic housing and has a maximum cooling rate (Q_c Max) of 21 Watts. Using the graphs on the datasheet it is possible to determine the voltage and current required to provide a ΔT of 51 °C, and is found to be 9.0 V at 4.0 A. Using Equation 15, it is possible to determine the viability of the proposed cooler method. The datasheet also shows the coefficient of performance (CoP) which is the measure of cooling system efficiency given the input current. The current drawn is high but this can be reduced by using a different thermoelectric cooler with a higher cooling rate, which then decreases the amount of voltage and current required to achieve the same cooling efficiency. The type of cooler can be chosen to suit the application, such include two-stage, three-stage, centre-hole, multi-hole, round, thin-film and thermal cycling. The thermoelectric coolers or mini fans could be placed within the enclosures for increased heat transfer. By doing so the enclosure would not be any larger than the current profile and would not move the antenna further from the body surface. The accumulated heat within the plastic enclosure is calculated to be a maximum of 51 °C, therefore the emitted heat from the enclosure should be safe enough for direct contact with human skin for up to a maximum of 15 minutes, and for indirect contact then a longer period can be sustained. This was deduced using interpolated data from Royal Society for the Prevention of Accidents (ROSPA) [26]. It should be also noted that this would not affect the objective of low RF visibility, as the enclosure can be placed behind the antenna's ground plane making it almost invisible to RF as per Figure 1.3(c).

4.4 Monopole Design and Build

The monopole is designed and simulated in CST MWS with the model and return loss result shown in Figure 4.13.

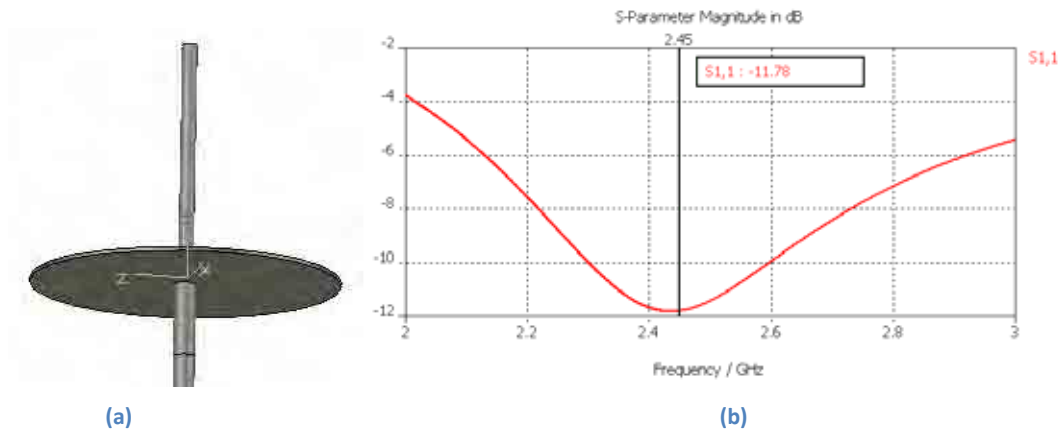


Figure 4.13 (a) 3D model and (b) return loss simulation result using CST MWS

The monopole antenna is designed and constructed using a copper wire conductor, round copper ground plane, SMA flange connector and a ferrule. The monopole is required to have the smallest possible ground size, as they are to be used on-body. As ground plane reduces in size so does the return loss. The quarter-wave ground plane of 3.06 cm at 2.45 GHz is the minimum in theory therefore 3.2 cm is used. The initial monopole design is shown in Figure 4.14.



Figure 4.14 Quarter-wave monopole

The measured return loss of the monopoles is -10.0 dB and -10.6 dB using the FSH3 spectrum analyser. In comparison, the simulation of the monopole shows a return loss of -11.78 dB, which is comparable to measured results. In addition, two monopoles with wider half wave ground plane of 6.12 cm are also constructed, each having a return loss of -31 dB and -26 dB. It should be noted that monopoles have an inherent impedance mismatch of $\approx 75\Omega$, when connected to network analyser.

4.5 Monopole Radiation Patterns with Coaxial Cable in the Anechoic Chamber

The next measurement was to assess the influence of coaxial cable. A radiation pattern is measured for a monopole with cables on the left and right in succession, with all four polarisations for the radiation pattern measured. The reference transmit antenna used is a Vivaldi antenna D1 as shown in Figure 4.15(a) in two polarisation positions; co-polarised and cross polarised. A bird's eye view diagram and corresponding photograph of the configurations is shown in Figure 4.15(b) to (e) and the radiation patterns are shown in Figure 4.16.

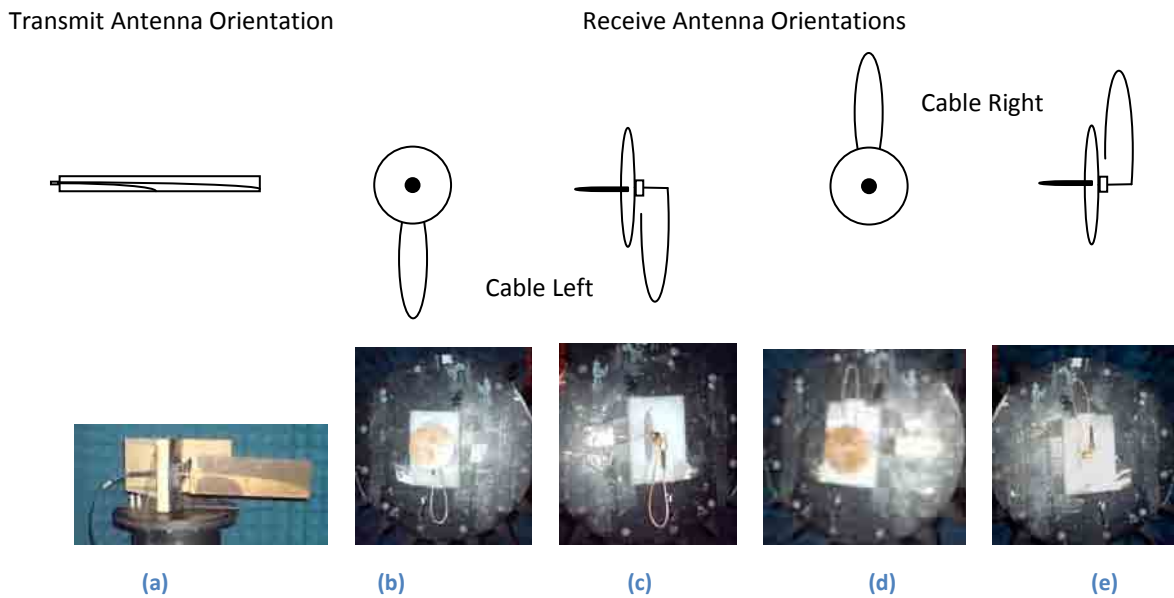


Figure 4.15 Bird's eye view diagrams above and photographs below showing coaxial cable orientation and antenna polarisation (a) Vivaldi reference antenna (b) cable left co-polarisation (c) cable left cross-polarisation (d) cable right co-polarisation (e) cable right cross-polarisation

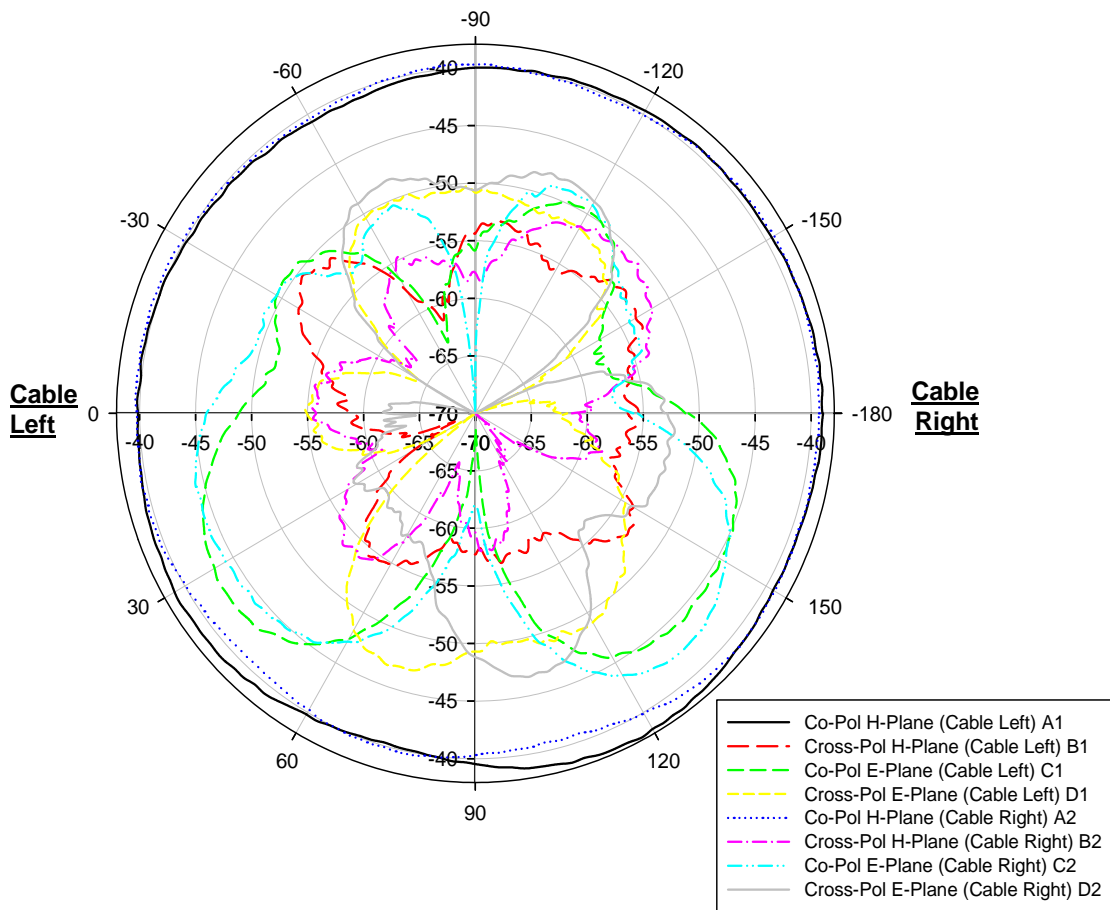


Figure 4.16 Influence of coaxial cable left vs. coaxial cable right on monopole antenna radiation pattern

The results shown in Figure 4.16 are labelled A1 to D1 in the legend for cable left orientations which can be found on the polar plot labelled cable left. This implies that the cable is positioned at this label relative to the polar plot. The second set of results is labelled A2 to D2 in the legend and relate to cable right orientations with the same implications of positioning relative to the polar plot. The following text uses A1 to D2 to refer to plots found in Figure 4.16.

The results show differences in patterns when cable is on either side of monopole. Comparing A1 and A2 shows a 2dB perturbation between 15° and 135°. Comparing B1 and B2 shows deep nulls at 25° and 135°, respectively, indicating the cable position at each respective null. Comparing C1 and C2 show a 4dB difference in pattern shown at 0° and 180°, respectively, indicating the cable position for each. D1 and D2 are difficult to compare due to differing patterns. From the cross-polarised H-plane (B1/2) and co-polarised E-plane (C1/2) results, it can be concluded that ingress, egress or reflections from the coaxial cable causes the antenna pattern to be perturbed. This

perturbation is lossy and is located where the coaxial cable has been placed. From the co-polarised H-plane ($A_{1/2}$) results, it can be concluded that the changing the cable position does change the radiation pattern, with the cable on the left being 2dB better than cable on the right as shown at 15° and 135° .

4.6 Comparison of Monopole Radiation Patterns using Coaxial Cable or Fibre Optic Cable in the Anechoic Chamber

Using the set up shown in Figure 4.17, the radiation pattern is measured with a coaxial system and a fibre system and Figure 4.18 shows the normalised H-plane co-polarised radiation pattern of the monopole.



(a)



(b)

Figure 4.17 (a) Coaxial system and (b) fibre system measurement set up with monopoles

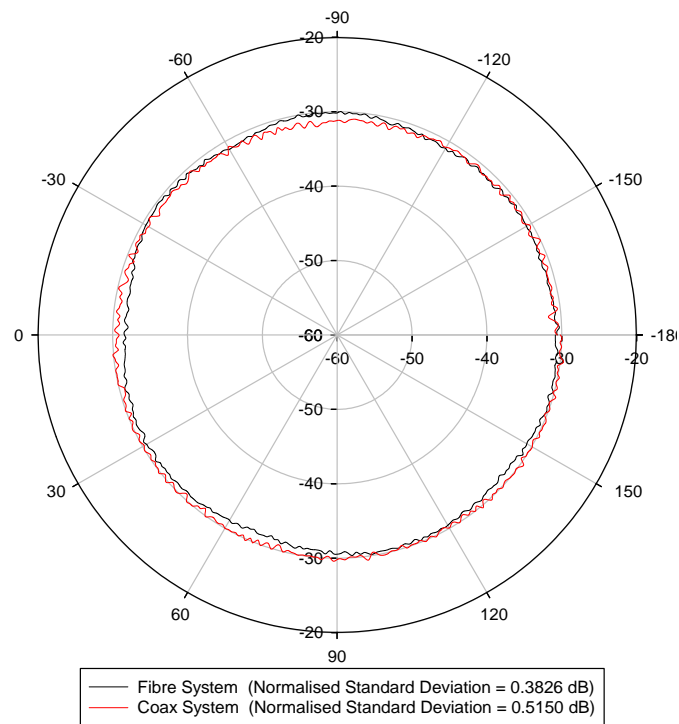


Figure 4.18 Normalised radiation pattern for coaxial cable and fibre optic cable in H-Plane Co-Polarised

The plotted results indicate that the fibre systems normalised standard deviation (σ) is less than the coaxial systems. This could be due to the fibre system appearing to react slower to signal variation hence a lower sample rate per degree and the coaxial system appears faster to react to signal variation hence a higher sample rate per degree. However, this is unlikely, as laser diode has a maximum rise/fall time of 370 pS (≈ 2.7 GHz). It is more likely that the fibre system is uninfluenced by coaxial cables thus the results are more accurate with less signal variation. In the case of the coaxial system, it is likely that coaxial cables are perturbing the radiation pattern through ingress, egress, reflection or vibration causing a high signal variation.

4.7 Conclusions

The fibre system has been fitted with convective coolers and show significant improvement over a closed enclosure. In addition, it is proposed that TEC cooling may provide better thermal stability. The fibre system is measured to have a dynamic range of 69 dB at maximum. The coaxial cable system has a dynamic range equal to that of the HP8722D network analyser of approximately 90 dB without cable losses. Discussion of Figure 4.16 earlier, measured up to 4 dB differences in radiation pattern where the coaxial cable is located. It is probable that the coaxial cable suffers from ingress and egress as well as constructive or destructive multipath near the coaxial cable and antenna. This also applies to the coaxial cable case for the co-polar radiation pattern discussed in Figure 4.18.

CHAPTER 5

5 SIMULATION AND MEASUREMENT RESULTS OF COMMERCIAL ROF SYSTEM VS. COAXIAL CABLE FOR ON-BODY MEASUREMENTS

5.1 Introduction

An active fibre system is employed for the purpose of on-body measurements. The on-body simulations use CST MWS with phantom Mike as described in Chapter 2.2.5 with two monopoles in the walking posture as shown in Figure 5.1. All measurements and simulations are carried out at 2.45 GHz. On-body simulations with coaxial cables and the fibre system are compared with measured results.

5.2 On-body Simulations – Comparison of Coaxial Cable vs. Fibre in CST MWS

The on-body simulations are carried out using CST MWS and phantom Mike as described in Chapter 2.2.5. Two monopoles are placed on-body, one on the right-hand-side of the belt and one on the right hand side of the head as shown in Figure 5.1. This configuration uses a line of sight (LOS) channel path and is used to simulate the Bluetooth-enabled mobile phone on belt to the Bluetooth headset on head.

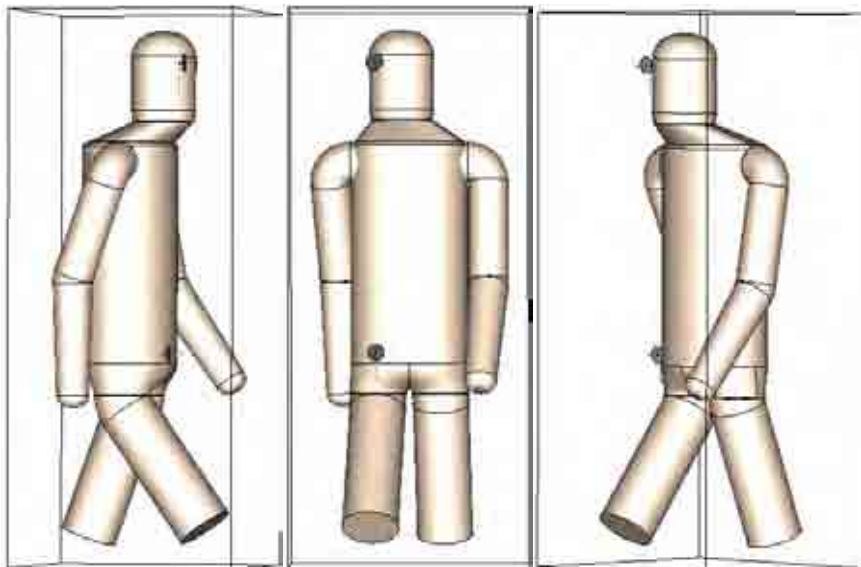


Figure 5.1 Mike phantom with two monopoles in CST MWS 2008

For simulation and measurement, the configuration is the same but the antenna feeds and cable orientation differ. The design of Mike with monopoles in CST requires accurate location and orientation of the monopoles and coaxial cables on the phantom. This involved designing monopoles in CST and importing them into the phantom model. The coaxial cable design is carried out in four phases to reduce measurement complexity, thus, simulation time. Simulation results for each phase can be found in Appendix P.

The first phase is to represent the coaxial cable with short solid PEC as the feed, this has the effect of simulating the outer shield as a cylindrical reflector of short length as shown in Figure 5.1. The second phase, the PEC is extended to full length coming down the body to the middle of the thigh. The third phase is to design a short piece of coaxial cable with centre conductor, dielectric and outer shield to feed the antenna. The fourth phase is to design the coaxial cable as third phase and connect associated bends, keeping the coaxial cable close to the body of full length. The fourth design phase requires the ports to be aligned to the primary axis in Cartesian coordinates due to simulation software limitations. The time-taken for simulations varies from 3 to 14 days, which is dependent on the size of the bounding box and mesh cell count. When Mike's full body is used then the simulation time is approximately 336 hours, which proves unacceptable within timescales.

Therefore, the feet, ankles and calves are removed from the design and the time taken to simulate the design is reduced to 72 hours. These body parts are removed, as they would have little impact on the channel path results, because they are significantly below the on-body channel path being measured. The simulation results of Mike stance using CST can be found in Appendix P in tabular form. The simulations are carried out on a Dell computer with an Intel® Core™2 Quad-core 2.4GHz Processor with 16GB RAM running Microsoft Vista Ultimate x64.

5.3 On-body Measurements – Comparison of Coaxial Cable vs. Fibre in the Anechoic Chamber

The subject used in the measurements was a male with height of 175 cm and weight of 75 kg. The measurements are carried out with two types of feed, coaxial cable and fibre optic cable. The monopoles placement is the same but the antenna feed and cable orientations differ.

For the coaxial cable on-body measurements, two Rhopase 1601 with a diameter of 4.06 mm and a length of 10 metres are employed as depicted in Figure 1.2(b). The datasheet for the Rhopase 1601 coaxial cable is found in Appendix Q.

For the fibre system, two 10-metre single-mode FC/APC fibre-optic cables are employed. The fibre modules (opto-electrical and electro-optical modulator with LNA) are also required to convert the optical signal into electrical signals for transmission through the RF channel as depicted in Figure 5.1.

The measurement results of both coaxial system and fibre system are shown in two different graph formats as shown in Figure 5.3 and Figure 5.4. Figure 5.3 shows the simulated and measured path-gain (S_{21}) variations as a function of time (60 seconds), whilst holding Mike's posture as depicted in Figure 5.1. The posture is a walking pose with left arm out farther than body, and right arm close to behind the body, with the legs vice versa. To counter the human errors and inaccuracies for the Mike stance, the stance is held still for the first 10 seconds, and then there are slight movements in the arms and head for the remaining 50 seconds thereby achieving an average. Figure

5.4 shows a simulated and measured mean plot of measured forward path-gain (S_{21}) at each repetition. A different measurement number in the mean plot denotes each repetition.

For the coaxial system, measurements are taken with different coaxial cable orientations relative to the head and body. The coaxial cable orientations relative to the head and body are labelled vertical front, vertical back, horizontal, diagonal and these configurations are depicted in Figure 5.2 and Figure 5.5. These different cable orientation measurements are important to capture, as this would enable comparisons of their relative merits for on-body measurements.



Figure 5.2 Photograph of measurement setup of vertical orientation coaxial cable with on-body Mike stance

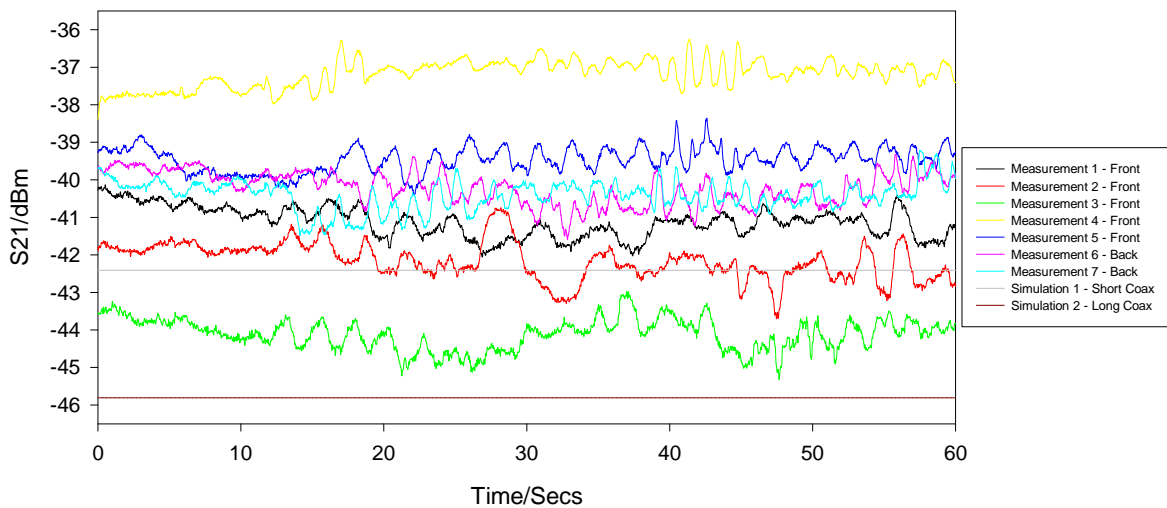


Figure 5.3 Measurement & simulation results of vertical alignment coaxial cable on-body over 60 seconds in Mike stance as per Figure 5.2

The graph in Figure 5.3 highlights the difficulty for on-body measurements using coaxial cable, as vast variability exists with 2 dB in difference on each repetition. The two straight lines show the simulated results using Mike and CST. It is clear that the measurement results are difficult to

compare with the simulated results. This could be due to many factors such as loose connectors, body movement, varying body tissue absorption rates, monopole alignment/location and network analyser drift due to heat. The mean plot against measurement number is shown in Figure 5.4.

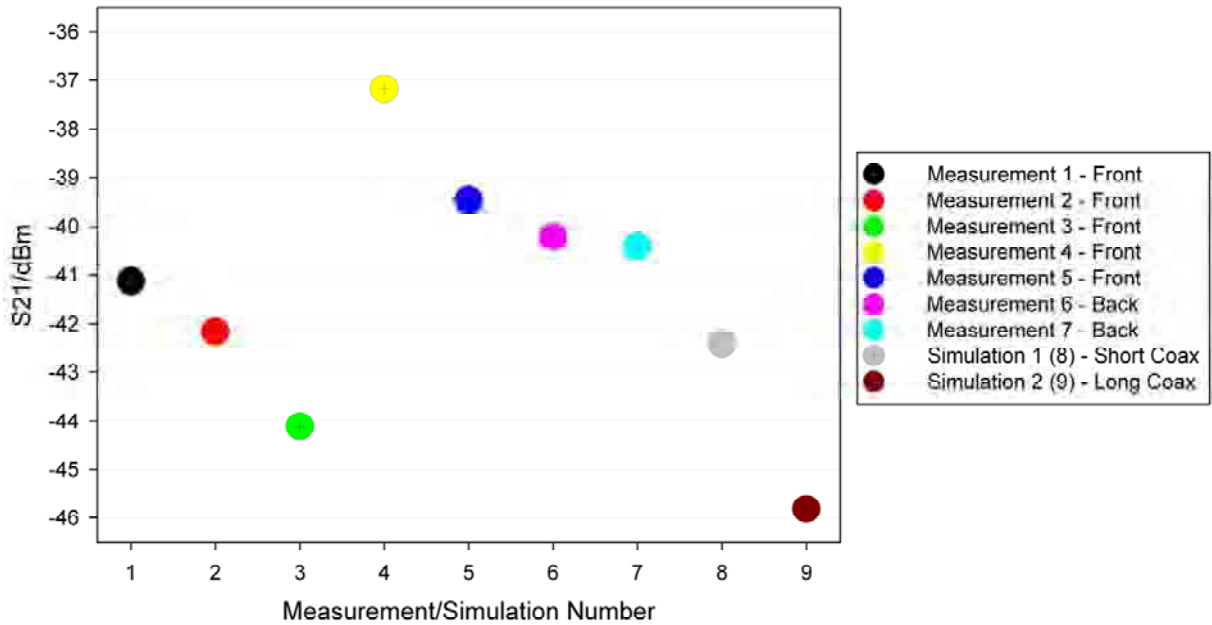


Figure 5.4 Mean plot measurement & simulation results of vertical alignment coaxial cable on-body in Mike stance as per Figure 5.2

The photographs in Figure 5.5 show the cable orientations of horizontal and diagonal coaxial cable relative to the head and body. The results for this configuration can be found in Figure 5.6 and Figure 5.7.

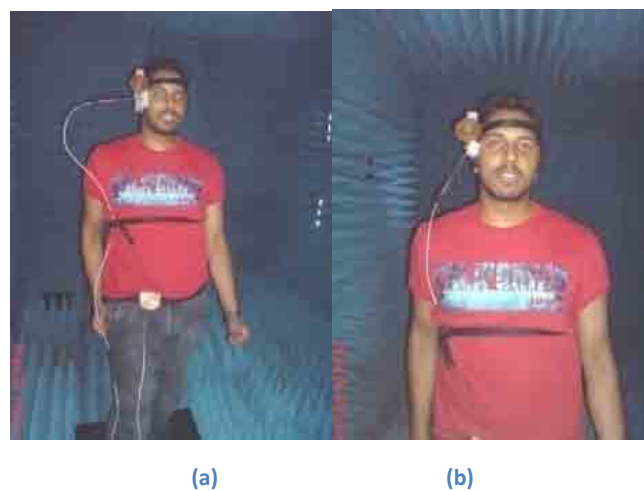


Figure 5.5 Photographs of measurement setup of (a) horizontal (90°) & (b) diagonal (45°) orientation coaxial cable with on-body in Mike stance

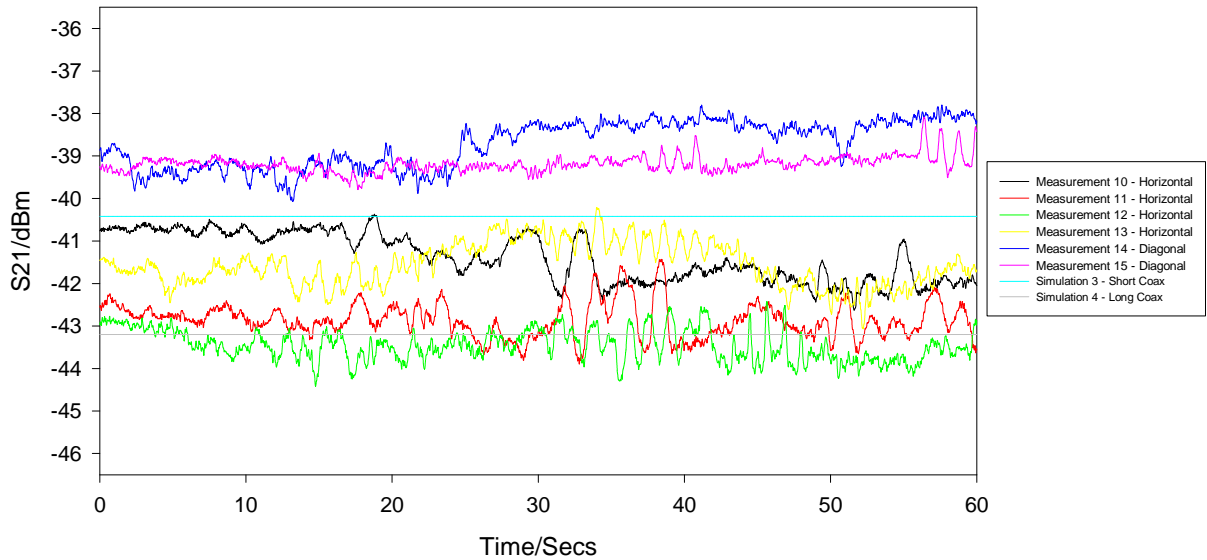


Figure 5.6 Measurement & simulation results of horizontal & diagonal orientation coaxial cable on-body over 60 seconds in Mike stance as per Figure 5.5

Simulation numbers 3 and 4 and the measurement numbers 10 to 15 in Figure 5.6 show general agreement, as the coaxial cables are horizontally or diagonally away from the channel path, hence less ingress, egress, reflections and multipath from the coaxial cable.

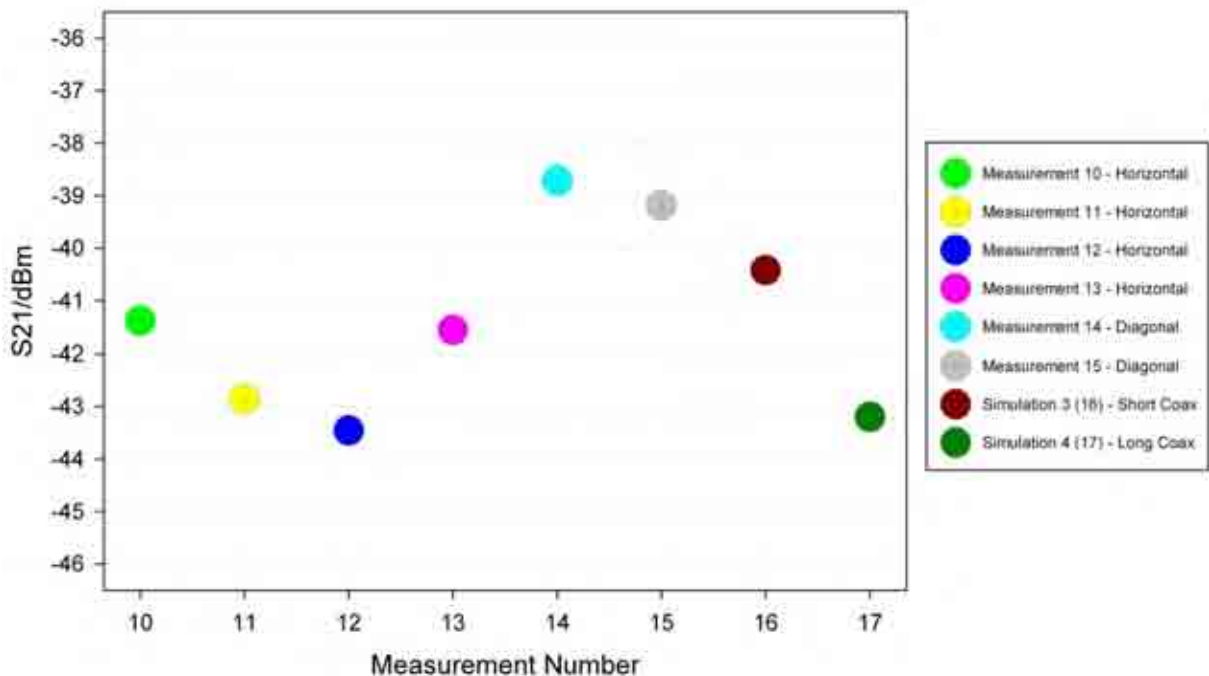


Figure 5.7 Mean plots of measurements & simulation results of horizontal & diagonal orientation coaxial cable on-body in Mike stance as per Figure 5.5

We can see from the simulation results that the shorter coaxial cable benefits from fewer reflections hence a 3 dB forward path gain (S_{21}) over the longer coaxial cable. The longer coaxial cable must suffer from ingress, egress, reflection, absorption and multipath, which contribute to this 3 dB loss in the forward path (S_{21}).

For the fibre system, the set up is shown in the photograph in Figure 5.8 and the fibre system results are shown in Figure 5.9 and Figure 5.10.

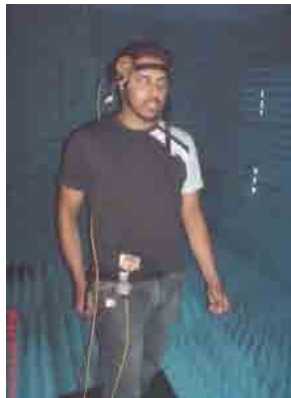


Figure 5.8 Photograph of measurement setup of fibre system on-body in Mike stance

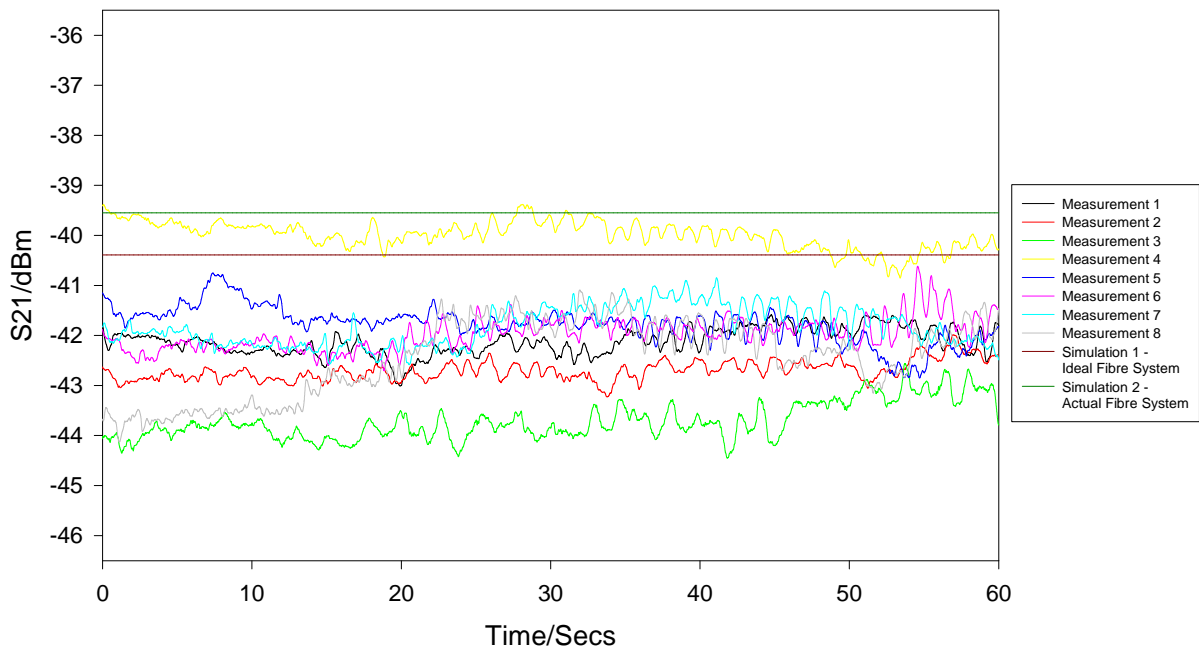


Figure 5.9 Measurement & simulation results 1 of fibre system on-body over 60 seconds in Mike stance as per Figure 5.8

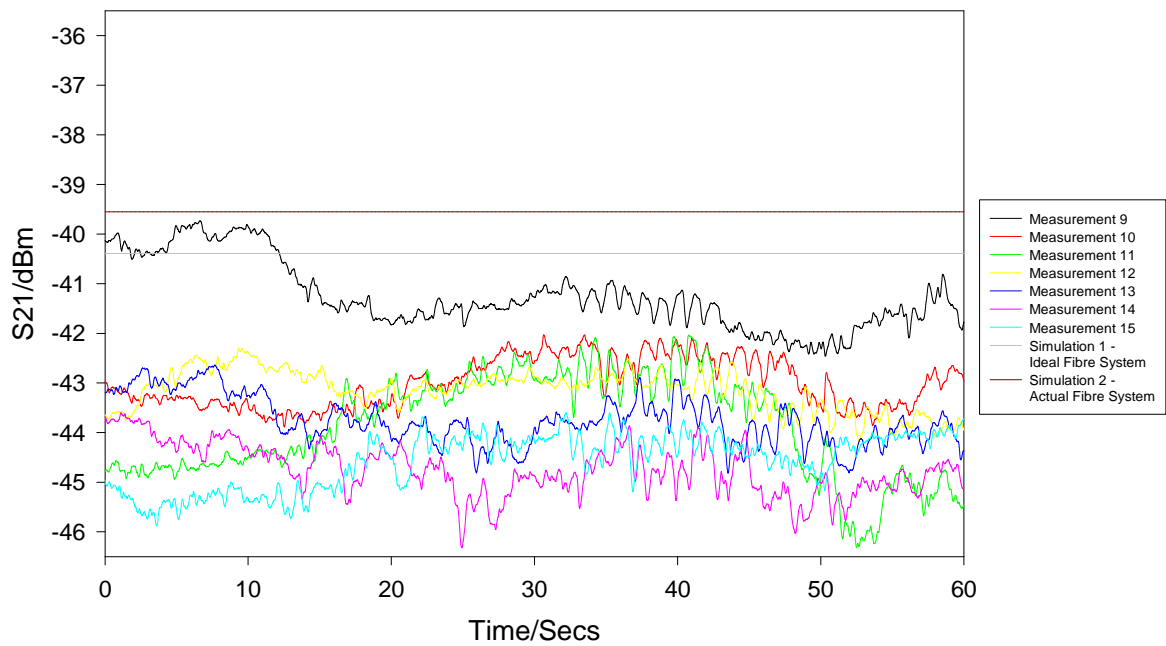


Figure 5.10 Measurement & simulation results 2 of fibre system on-body over 60 seconds in Mike stance as per Figure 5.8

At first glance, we can see a 4 dB variability which is less than the coaxial system case, which shows 6 dB variability. Comparisons of simulated result with measured results are difficult as only one trace satisfy the simulated results. The others measurements are several dB away. The reason for this loss is when the fibre modules are placed on the body, the operating temperature increases, thus gain falls. The rate at which the system gain falls is 1 dB every 5 minutes. To reduce this loss over time, active cooling could be integrated within the fibre system as proposed in the Chapter 4.3.4.

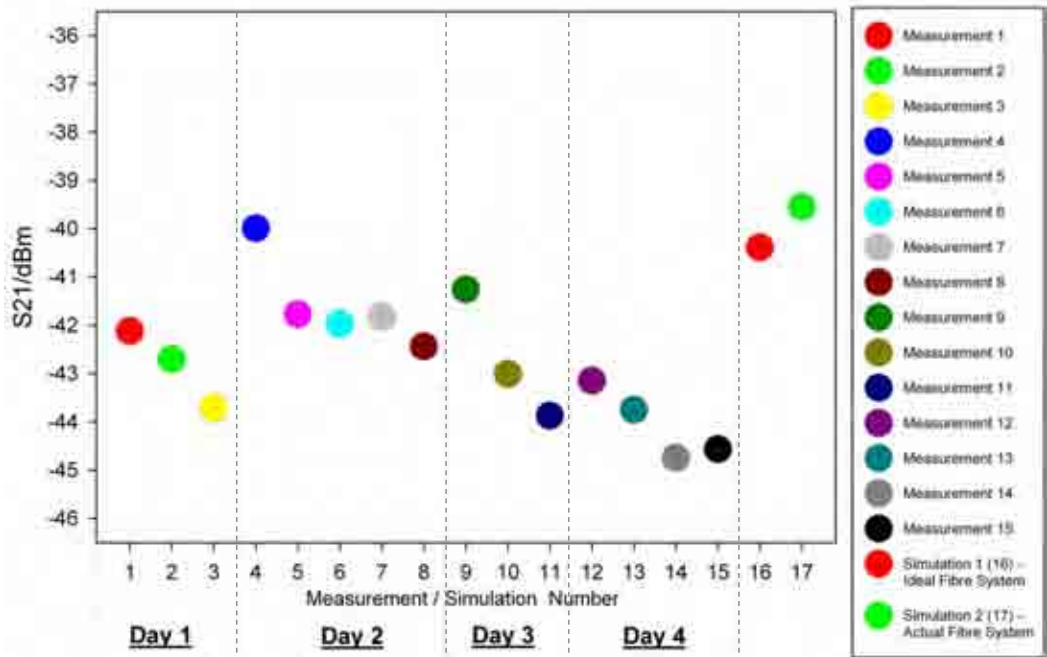


Figure 5.11 Mean plot of measurement & simulation results of fibre system on-body in Mike stance as per Figure 5.8

The mean plot in Figure 5.11 shows the trend of loss due to heat on each measurement repetition. Four groups have been identified which show a reduction in gain after each measurement number. Each group refers to one day of measurements, where the first measurement of the day has the most gain and reduces per sequential measurement. Fibre measurement numbers 5, 6 and 7 show exceptional agreement between them with only 0.3 dB in mean variation and this indicates the potential accuracy of repeatability achievable by this system. These three measurements were taken in succession with 2 minutes separating them. By taking them in quick succession the fibre module had near constant operating temperature attributing to greater measurement accuracy and good repeatability. This behaviour is expected because we have measured the fibre modules losing gain by an average of 0.2 dB every minute when it is mounted on the body, therefore by reducing the time between successive measurements it is possible to increase measurement accuracy and repeatability.

Figure 5.12 and Table 5.1 show the matching pair simulated and measured results for comparison. Figure 5.12 and Table 5.1 collate the matching pair simulated and measured results over 60 seconds, holding Mike's stance from Figure 5.3, Figure 5.6, Figure 5.9 and Figure 5.10. Figure 5.12

shows the mean plot of these results. The first measurement number shown on the graph refers to the actual coaxial or fibre measurement number, followed by a second measurement number in brackets, which refers to the sequential measurement or simulation number that has been assigned.

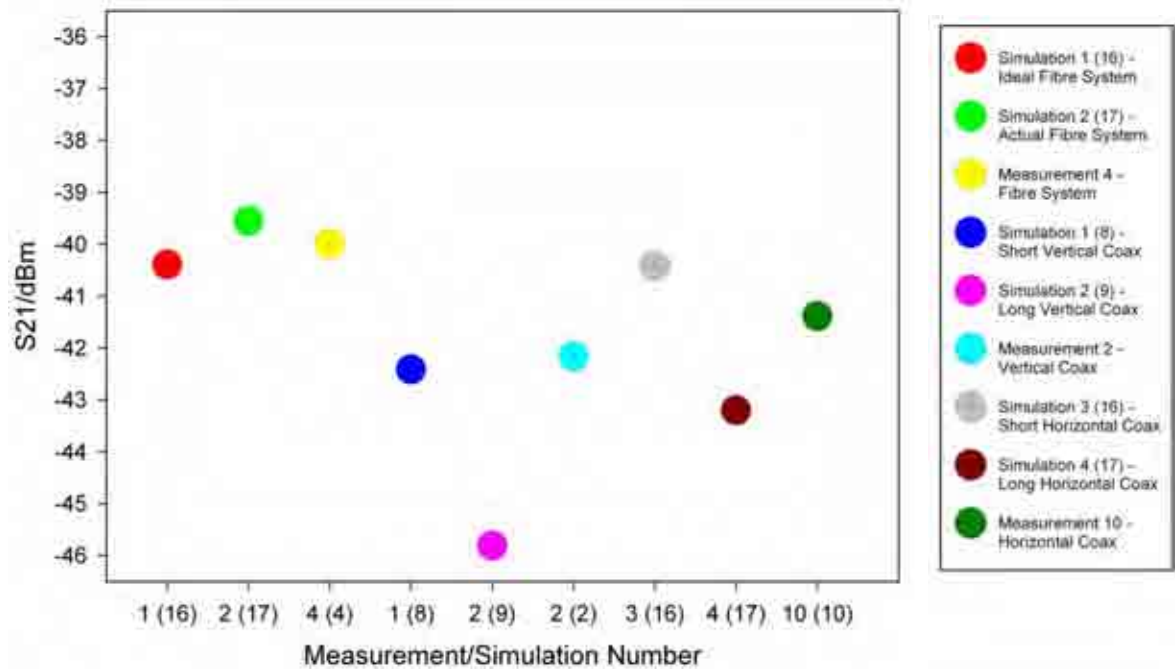


Figure 5.12 Mean plot of matched pair simulated & measured results of coaxial cable vs. fibre system on-body in Mike stance

The measured results for the fibre system meet both simulation results at least at one occasion. The measured results for the vertical coaxial system meets one of the two simulation results at least at one occasion. The measured results for the horizontal coaxial system meet both the simulation results at least at one occasion. If further repeatability studies for the fibre system were carried out, an increased number of the measured results would concur with the simulated results.

System Type	Coaxial	Coaxial	Coaxial	Coaxial	Fibre
Coaxial Cable Position	Vertical down Front of Body	Vertical down Back of Body	Horizontal	Diagonal	N/A
Corresponding Graphs	Figure 5.3	Figure 5.3	Figure 5.6	Figure 5.6	Figure 5.9 and Figure 5.10
Sample Data	5	2	4	2	15
$\Delta\langle S_{21} \rangle / \text{dB}$	6.94	0.20	2.07	0.47	4.75

Table 5.1 Tabular results of $\Delta\langle S_{21} \rangle$ for various measurement arrangements

($\Delta\langle S_{21} \rangle$ is the difference between max and min of the means shown in Figure 5.3, Figure 5.6, Figure 5.9 and Figure 5.10)

The statistical results in Table 5.1 show that delta mean S21 is a maximum of 6.94 dB for the coaxial system. The delta mean S21 for the fibre system is a maximum of 4.75 dB, which implies a better ability for accuracy and repeatable results even with thermal issues. However, the coaxial system with cable positions at vertical down back, horizontal or diagonal, show better repeatable results, however, the calculated results are only for a smaller number of samples of two and four, from which the statistics are calculated. For increased results validity, more than two samples are required. As a note, the fibre system also has consistent measurement results gain drift due to temperature increase, which also adversely affects the statistical results. It appears that if the temperature stability were improved the fibre system would have a lower delta mean S21.

The coaxial and fibre system are employed for on-body channel measurements, which vary in posture. The reason for such a measurement comes from an observed irregularity from the measurements carried out using a coaxial system. An observation of a slow rising gain is measured between each posture change and thus it is decided to employ the fibre system to see if the irregularity is due to the coaxial system. The 18 postures used in the measurement are; standing, body turned left, body turned right, body bent forward, head bent forward, head turned left, head turned right, arms stretched out to side, arms stretched above head, arms in front, forearms in front, arms move freely, sitting with arms hanging down, sitting comfortably hands on lap, sitting and

moving freely, standing, walking with arms to side and walking freely. Each posture was held for 20 seconds. The channel path results for varying posture are shown in Figure 5.13.

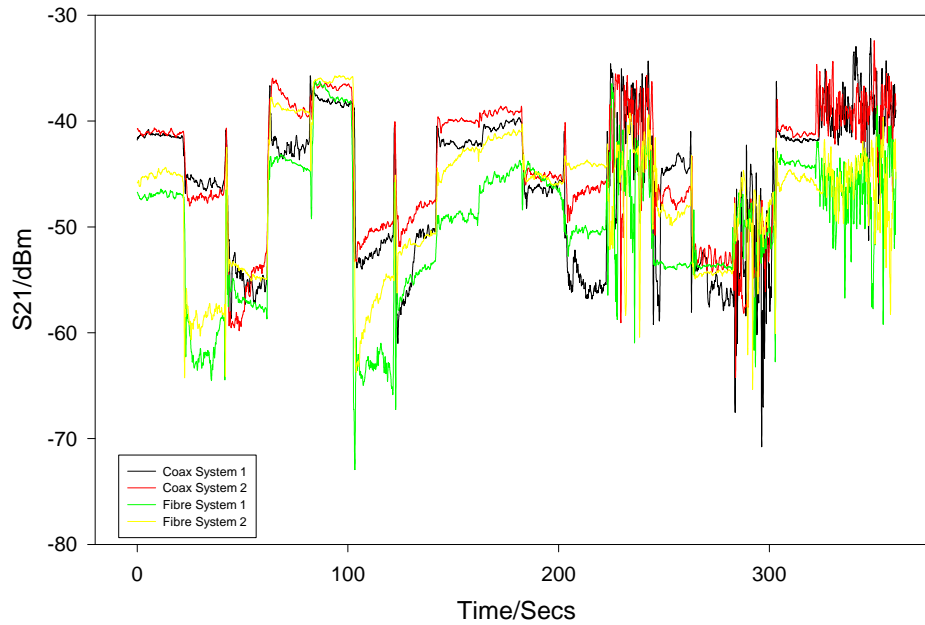


Figure 5.13 On-body measurement results of coaxial cable vs. fibre cable during an 18 posture set (IF bandwidth is 30 Hz)

By comparing the coaxial and fibre system's results, it is concluded that neither the coaxial nor the fibre system has any effect on the results. The phenomenon is likely to be attributed to the radio waves' interaction with body properties. This may occur due to muscles being tense during a posture, hence greater blood flow and more water content, which absorb microwaves at 2.45 GHz easily [27]. Another possible reason for this slow rising gain could be a property of the HP 8722D network analyser when using it with an intermediate frequency (IF) bandwidth of 30 Hz. However, it is known that a lower IF bandwidth results in lower system noise, thus greater the measurement accuracy, so this is unlikely. Another possible reason could be due to anechoic chamber multipath creating a non-quiet zone. Further investigation can be undertaken to conclusively understand such problems.

5.4 Conclusions

The investigation of fibre system in comparison to coaxial system appears to show a mean of 2.19 dB improvement in measurement accuracy however, the fibre system can be further modified to increase efficiency and stability. A power supply design flaw results in higher power consumption as some power is lost within the current limiting resistor and the regulator itself, thus creating heat. It is clear that efficiency is a problem however; a solution is to use a switched mode supply that provides pulses instead of constant DC followed by a low dropout regulator (LDO) and a low pass filter (LPF). This design would increase efficiency as switched mode supplies consume less power and the LDO utilises NPN transistors in a common collector configuration to provide a lower bias and lower voltage dropout. A standard linear regulator uses PNP transistors hence it requires 2 Volts typically before voltage dropout which is quite high and inefficient. Further improvements that could be made are to embed a miniature fan, a thermoelectric cooler or a more efficient heatsink into the fibre system enclosure. This would stabilise the temperature, allowing measurements to be more accurate. However, if any of these approaches were taken, the power consumption and occupied space would increase. It is important to take into account other adverse affects of these methods. Careful consideration must be taken, otherwise there is a possibility of affecting the overall RF visibility, as well as injecting noise or interference to the received signal.

CHAPTER 6

6 CONCLUSIONS AND SUGGESTIONS FOR FURTHER WORK

6.1 Conclusions

The main objective of this research was to design an alternative method to measure on-body channel paths. To undertake this task, several optical fibre methods are investigated and a system is designed to convert an RF signal into an optical signal, which is then converted back into an RF signal, and transmitted via an antenna over the on-body channel path. The process is then reversed to convert the optical signal back into an RF signal.

In Chapter 3, a radio-over-fibre system is designed, built and tested for the main objective and found to operate satisfactorily. The simulations carried out highlight that the 1-stage system would not perform as required, as the system gain would only reach a maximum of -5 dB. However, the 3-stage systems would perform well, with potentially very high system gains. The measurement results for the 1-stage system match the simulated results, although the results of the 3-stage system (three x MSA-0886) do not match the simulated results. The simulated results show that the system gain should be close to 0 dB, however, the measured result show -23.0 dB. It is deduced that the measurement result could be improved through impedance matching the photodiode to the microstrip layout, or better still a coplanar or stripline layout. The use of stripline or suspended stripline would be preferred due to the fact they provide better isolation, although cost and board thickness would be greater as compared to microstrip. Other methods for better design would be to incorporate variable gain amplifiers into the opto-electrical modulator to allow variation of system gain. In turn, this would equalise optical losses within the system. Another method would be to use mixed lumped/distributed element design, which would reduce layout dimensions. However, due to time constraints, improvements and modifications could not be made to the designed radio-over-fibre system, thus a commercial radio-over-fibre system was employed in Chapter 4.

The second objective was to compare the difference between the conventional coaxial cable measurement system and the novel radio-over-fibre measurement system. Chapter 4 concludes that some repeatability improvements are apparent when using a radio-over-fibre system over a conventional coaxial cable system for on-body measurements. It also found that performance and stability could be improved further through better thermal design. Thermal design techniques to improve heat dissipation include embedding a 40x40x10mm miniature fan, a finned copper heatsink, a metal enclosure, and/or a 12 V thermoelectric cooler (TEC) Peltier plate into the commercial radio-over-fibre modules. If a metal enclosure is used, then the body-mounted side must be insulated from the skin/body for health and safety of the user. Earlier, it was mentioned that these methods would not affect the requirement of low RF visibility. This is because the enclosure can be placed behind the antenna's ground plane making it less visible to RF.

The measurement results of the monopole radiation patterns in Figure 4.16 using the conventional coaxial cable measurement system show that perturbations in the radiation pattern are evident when the coaxial cable is placed in the near field of the monopole antenna. The co-polarised H-plane cable left vs. cable right comparison shows a 3 dB perturbation where the cables are located. The co-polarised E-plane cable left vs. cable right comparison also shows a 3 dB perturbation where the cables are located. The results from Zhang et al. [17], Benson et al. [18], Massey and Boyle [22] and Icheln et al. [23], all conclude that coaxial cables are EMI or RFI sensitive and it is impossible to definitively remove ingress, egress and shield multipath.

The co-polarised H-plane is investigated to compare the differences between the two measurement methods, coaxial cable and fibre optic cable as shown in Figure 4.18. The fibre system shows a lower standard deviation (σ) of 0.3826 dB with the fibre system as compared to 0.5150 dB of the coaxial system. This concurs findings from Lao et al. [12] and Fukasawa et al. [13] that a fibre system has a lower S21 deviation. The coaxial system suffers from variable loss and phase, spurious coupling and shield scattering which all contribute to the higher S21 deviation.

On-body simulations and measurements are also carried out and results are shown in Figure 5.3 to Figure 5.12. The measurements from the coaxial cable system show S21 variability of up to 6 dB, which accounts for loose connectors, body movement, varying body tissue absorption rates, monopole misalignment and varying distance, and network analyser drift due to heat. In addition, it is concluded that the measurements with coaxial cables are restrictive as any body movement results in the pulling of coaxial cables, causing the monopole alignment and distance to change. However, the coaxial system seems to improve when the coaxial cable is away from the main LOS channel path scenario, as per results shown in Table 5.1. Therefore, the results indicate that better accuracy results can be achieved with coaxial cable when the cable is “invisible” to the antenna and also the main channel path.

The measurements using the fibre optic system, show S21 variability on each repetition of up to 4 dB. However, this is accounted for and attributed to the fibre system gain drift due to heat build up within modules. If the enclosures remained at constant temperature, then the system would have accurate results with greater repeatability. From the comparison of coaxial and fibre measurement system results, a possible improvement of 2 dB or less is shown in fibre measurements in Figure 5.11 and Figure 5.12. Fibre measurement number 5, 6 and 7 from Figure 5.11 show that the fibre system can provide accurate results with 0.3 dB difference between their mean. In addition, using the fibre system, the fibre cables are light, flexible and loose, thus more manageable, less cumbersome and allow measurements to be taken simply and quickly.

Some on-body posture measurements are also carried out using a standard 18-posture set, for both the coaxial system and fibre system. It is concluded that the fibre system shows no conclusive improvement over the coaxial system for posture measurement, although the slow rising gain phenomena is likely to be due to the bodies’ properties or other undeterminable factors and is nothing to do with the fact that the coaxial cables were in close proximity to the body.

The issues with on-body measurements that are highlighted at the start of this thesis are; variable loss and phase when the body moves, generation of superfluous coupling and perturbation of the antenna radiation patterns. These issues are investigated and found to occur due to the type of coaxial cable employed for measurements. For good isolation, the braided coaxial cable must have low transfer impedance as discussed in Chapter 2.4.1.2. A high transfer impedance coaxial cable can be the root cause of superfluous coupling. Coaxial cables also suffer from variable phase when they are bent or deformed and this property is inherent in all coaxial cables. The cable type typically used for on-body measurements is thin and flexible. This poses a higher loss and variable phase, respectively. Due to the small diameter of the cables, they also greatly suffer from RFI ingress and egress. Albeit a small diameter, the metallic influence of the outer shield causes scattering and absorption of waves in the local vicinity creating multipath effects on the received signal.

To conclude, the radio-over-fibre system seems to work well with results showing a 2.19 dB mean improvement over a coaxial system. However, for improved accuracy and repeatable results, further modification of the power supply and thermal design would be required as suggested in Chapter 6.2.

6.2 Suggestions for Further Work

Possible future works that can be carried out to increase the accuracy and repeatability of on-body channel path measurements are:

- Impedance matching the components of the radio-over-fibre system, designing a mixed lumped/distributed element layout of the system for miniature size [28], and repeating on-body simulation and measurements to show improvements
- Designing a switched mode power supply and a closed-loop thermoelectric cooler for the commercial radio-over-fibre system, and repeating on-body simulation and measurements to show improvements of the system. Some important considerations to be taken into account whilst undertaking these tasks are whether the switch mode power supply counteracts the improved repeatability of the fibre system due to additive noise and interference
- Alternatively, a passive optical system could be employed as the module size becomes smaller and power consumption is minimised, however several off-body active optical amplifiers would be required. Such examples were employed by Kovacs et al. [29], for use on ultra wideband applications, although this only consisted of a single passive fibre optic link, instead of the proposed two cascaded fibre optic links. Kovacs et al. employed one passive fibre optic receiver, Discovery Semiconductors DSC50 with the rest of the link using coaxial cable. The key consideration to be made is whether the dynamic range of the passive system can achieve greater than 60 dB, as this is a prerequisite for on-body measurements.

REFERENCES

7 REFERENCES

- [1] Jovanov, E., et al., "A wireless body area network of intelligent motion sensors for computer assisted physical rehabilitation", *Journal of NeuroEngineering and Rehabilitation*, 2005.
- [2] Salonen, P., Rahmat-Samii, Y., and Kivikoski, M., "Wearable antennas in the vicinity of human body", in *Antennas and Propagation Society International Symposium, 2004 IEEE*. 2004. p. 467-70 Vol.1.
- [3] O'Reilly, R.M., "Cochlear implants". 2006 Apr 2008 [cited 2008 12 August]; Available from: <http://fugazi-dev3.kidshealth.org:8003/parent/medical/ears/cochlear.html>.
- [4] Hall, P.S. and Hao, Y., "Antennas and propagation for body-centric wireless communications / peter s. Hall, yang hao, editors". *Artech house antennas and propagation library*. 2006, Norwood, Mass.: Artech House. xiii, 291.
- [5] Ito, K., "Numerical and experimental human body phantoms", in *Antennas and Propagation for Body-Centric Wireless Communications, 2007 IET Seminar on*. 2007. p. 6-12.
- [6] Salim, T. and Hall, P.S., "Efficiency measurement of antennas for on-body communications", *Microwave and Optical Technology Letters*, 2006. 48(11): p. 2256-9.
- [7] Hall, P.S., et al., "Antennas and propagation for on-body communication systems", *Antennas and Propagation Magazine, IEEE*, 2007. 49(3): p. 41-58.
- [8] Kamarudin, M.R., "Design and performance of antennas for on-body communication channels and antenna diversity", in *AAEL. 2007, University of Birmingham: Birmingham*.
- [9] Nechayev, Y.I., et al., "On-body path gain variations with changing body posture and antenna position", in *Antennas and Propagation Society International Symposium. 2005, IEEE*. p. 731 - 4.
- [10] Bai, S., "Simulation of dynamics of on-body channels", in *AAEL. 2008, University of Birmingham: Birmingham*.
- [11] Gallo, M., et al., "Use of animation software in simulation of on-body communications channels at 2.45ghz", *Antennas and Wireless Propagation Letters, IEEE, 2007(Accepted for future publication)*: p. 85-8.
- [12] Lao, R.R., et al., "The use of electro-optical link to reduce the influence of rf cables in antenna measurement", in *Microwave, Antenna, Propagation and EMC Technologies for Wireless Communications, 2005 MAPE 2005 IEEE International Symposium on*. 2005. p. 427-30 Vol. 1.
- [13] Fukasawa, T., Shimomura, K., and Ohtsuka, M., "Accurate measurement method using fiber-optics for an antenna on a portable telephone", in *Wireless Communication Technology, 2003 IEEE Topical Conference on*. 2003. p. 138-9.

- [14] Cryan, W., et al., "A 2.4ghz wireless-over-fibre transmitter using a vcsel-based photonic active integrated antenna (phaia)", in *Microwave Conference, 2004 34th European*. 2004. p. 507-9.
- [15] Kaiser, K.L., "Transmission lines, matching, and crosstalk / kenneth I. Kaiser". 2006, Boca Raton, Fla. ; London: CRC. 1 v. (various pagings).
- [16] Pozar, D.M., "Microwave engineering / by david m. Pozar". 1990, Reading, Mass. ; Wokingham: Addison-Wesley. xvii,726.
- [17] Zhang, H.-x., et al., "A study on the electromagnetic leakage arising from braided shielding cable", in *Radio Science Conference, 2004 Proceedings 2004 Asia-Pacific*. 2004. p. 519-22.
- [18] Benson, F.A., Cudd, P.A., and Tealby, J.M., "Leakage from coaxial cables", *Science, Measurement and Technology, IEE Proceedings A*, 1992. 139(6): p. 285-303.
- [19] Raychem Wires and Cables, T.E.C., "Electrical screening", *elecscrn.pdf*, Editor. 2008, Tyco Electronics Corporation.
- [20] Hecht, J., (2007) "Photonic frontiers: Cranking up the bandwidth: The quest for high-speed vcsels". *Laser Focus World magazine*.
- [21] Sali, S., "Cable shielding measurements at microwave frequencies", *Electromagnetic Compatibility, IEEE Transactions on*, 2004. 46(2): p. 178-88.
- [22] Massey, P.J. and Boyle, K.R., "Controlling the effects of feed cable in small antenna measurements", in *Antennas and Propagation, 2003 (ICAP 2003) Twelfth International Conference on (Conf Publ No 491)*. 2003. p. 561-4 vol.2.
- [23] Icheln, C., Krogerus, J., and Vainikainen, P., "Use of balun chokes in small-antenna radiation measurements", *Instrumentation and Measurement, IEEE Transactions on*, 2004. 53(2): p. 498-506.
- [24] Marozsak, T., et al., 2002. "Direct modulated lasers in radio over fiber applications". *Microwave Photonics, 2002 International Topical Meeting on*.
- [25] Larsson, A., et al., 2004. "Broadband direct modulation of vcsels and applications in fiber optic rf links". *Microwave Photonics, 2004 MWP'04 2004 IEEE International Topical Meeting on*.
- [26] Jenkins, D., "Temperatures of touchable surfaces - a personal burn hazard". 2000 [cited 2010 12/12/10]; Available from: <http://www.rospa.com/homesafety/adviceandinformation/product/temperatures-touchable-surfaces.aspx>.
- [27] Bansal, R., "Handbook of engineering electromagnetics". 2004: CRC Press. 706.
- [28] Al-Raweshidy, H. and Komaki, S., "Radio over fiber technologies for mobile communications networks". *Universal personal communications*, ed. H. Al-Raweshidy and S. Komaki. 2005, Norwood, MA: Artech House. 420.
- [29] Kovacs, I., et al., 2004. "Ultra wideband radio propagation in body area network scenarios". *Spread Spectrum Techniques and Applications, 2004 IEEE Eighth International Symposium on*.

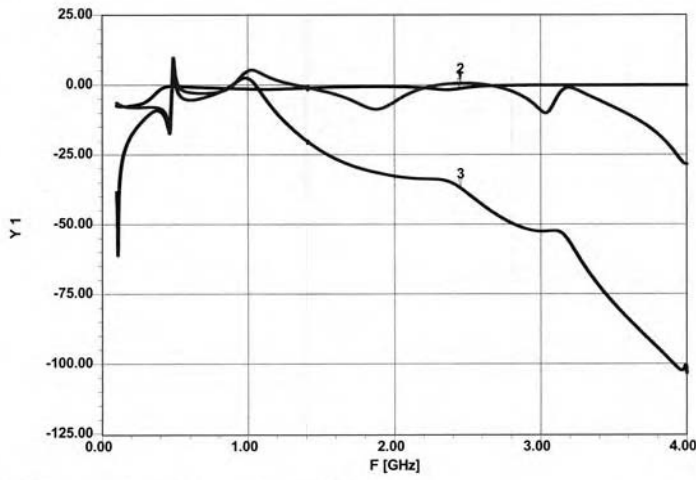
11 Jun 2008

Ansoft Corporation
XY Plot 1
Circuit1

12:17:28

2.45GHz RoF 1-Stage System

28mA Laser Diode Bias



X1= 2.45GHz Y1= -1.32
X2= 2.45GHz Y2= 0.61
X3= 2.45GHz Y3= -36.81

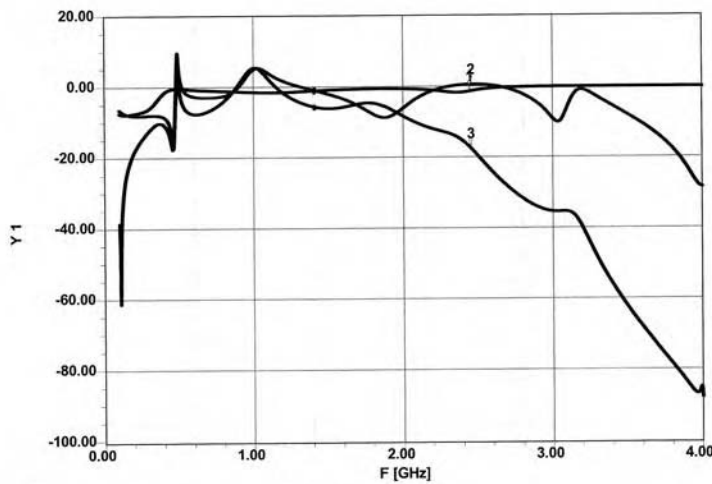
11 Jun 2008

Ansoft Corporation
XY Plot 1
Circuit1

12:22:23

2.45GHz RoF 1-Stage System

32mA Laser Diode Bias



X1= 2.45GHz Y1= -1.32
X2= 2.45GHz Y2= 0.61
X3= 2.45GHz Y3= -17.33

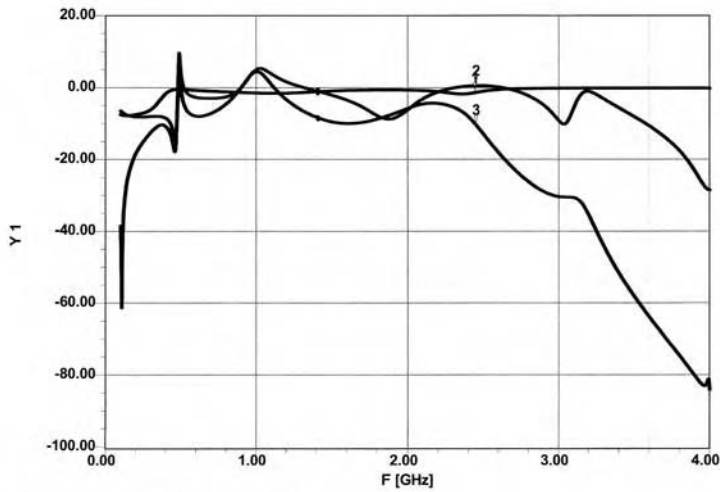
11 Jun 2008

Ansoft Corporation
XY Plot 1
Circuit1

12:25:56

2.45GHz RoF 1-Stage System

34mA Laser Diode Bias



X1= 2.45GHz X2= 2.45GHz X3= 2.45GHz
Y1= -1.32 Y2= 0.61 Y3= -10.29

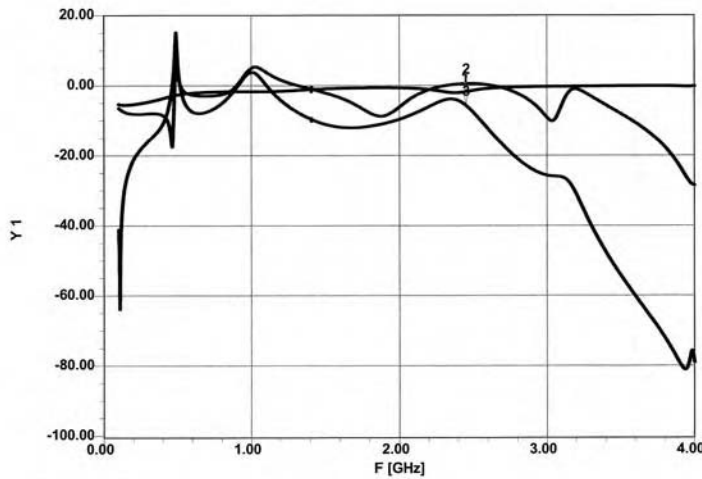
10 Jun 2008

Ansoft Corporation
XY Plot 1
Circuit1

15:20:33

2.45GHz RoF 1-Stage System

36mA Laser Diode Bias



X1= 2.45GHz X2= 2.45GHz X3= 2.45GHz
Y1= -1.72 Y2= 0.61 Y3= -5.63

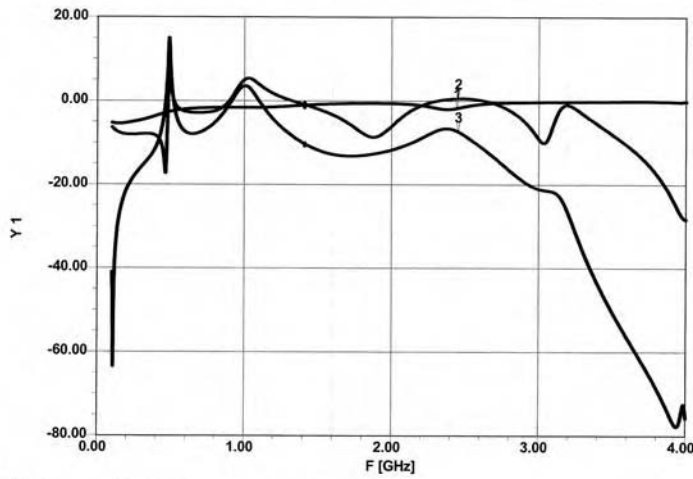
10 Jun 2008

Ansoft Corporation
XY Plot 1
Circuit1

16:33:16

2.45GHz RoF 1-Stage System

38mA Laser Diode Bi



X1= 2.45GHz
Y1= -1.73

X2= 2.45GHz
Y2= 0.61

X3= 2.45GHz
Y3= -7.33

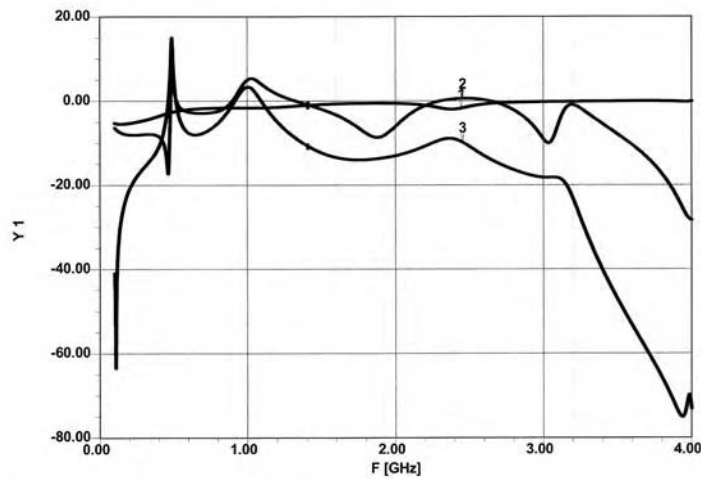
10 Jun 2008

Ansoft Corporation
XY Plot 1
Circuit1

16:41:24

2.45GHz RoF 1-Stage System

40mA Laser Diode Bi



X1= 2.45GHz
Y1= -1.73

X2= 2.45GHz
Y2= 0.61

X3= 2.45GHz
Y3= -9.81

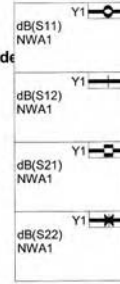
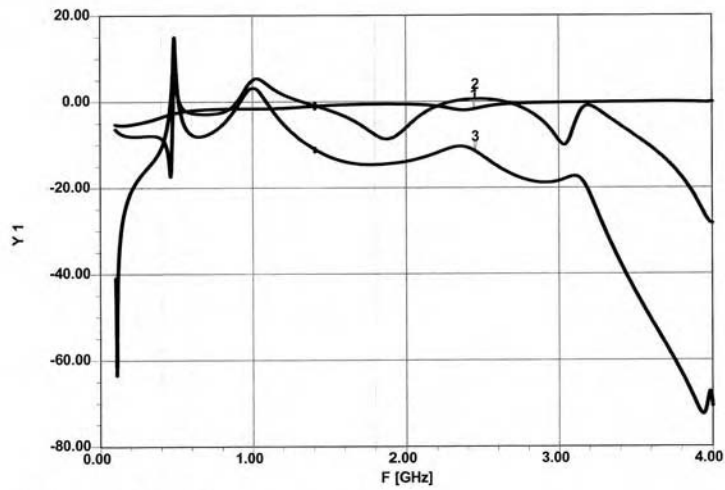
10 Jun 2008

Ansoft Corporation
XY Plot 1
Circuit1

16:43:26

42mA Laser Diode

2.45GHz RoF 1-Stage System



X1= 2.45GHz
Y1= -1.73

X2= 2.45GHz
Y2= 0.61

X3= 2.45GHz
Y3= -11.51

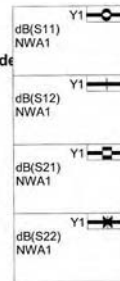
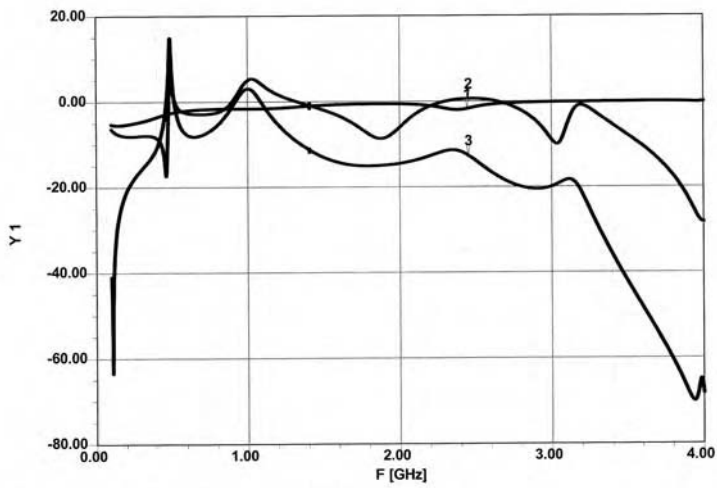
10 Jun 2008

Ansoft Corporation
XY Plot 1
Circuit1

16:45:19

44mA Laser Diode

2.45GHz RoF 1-Stage System



X1= 2.45GHz
Y1= -1.73

X2= 2.45GHz
Y2= 0.61

X3= 2.45GHz
Y3= -12.68

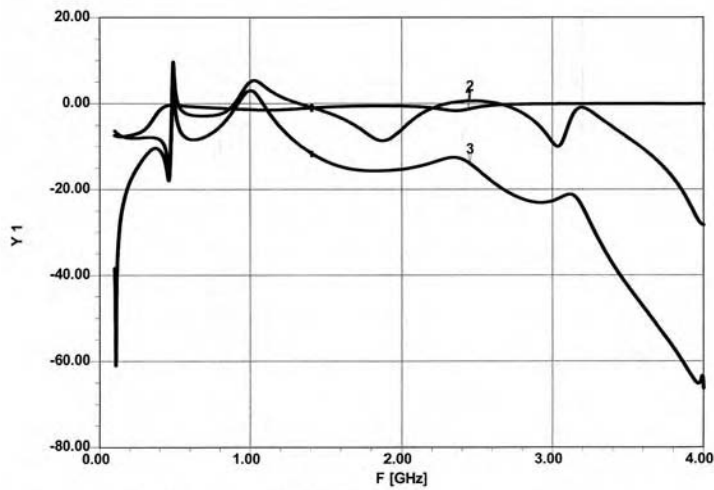
10 Jun 2008

Ansoft Corporation
XY Plot 1
Circuit1

17:09:54

2.45GHz RoF 1-Stage System

48mA Laser Diode Bias



X1= 2.45GHz Y1= -1.32
X2= 2.45GHz Y2= 0.61
X3= 2.45GHz Y3= -13.99

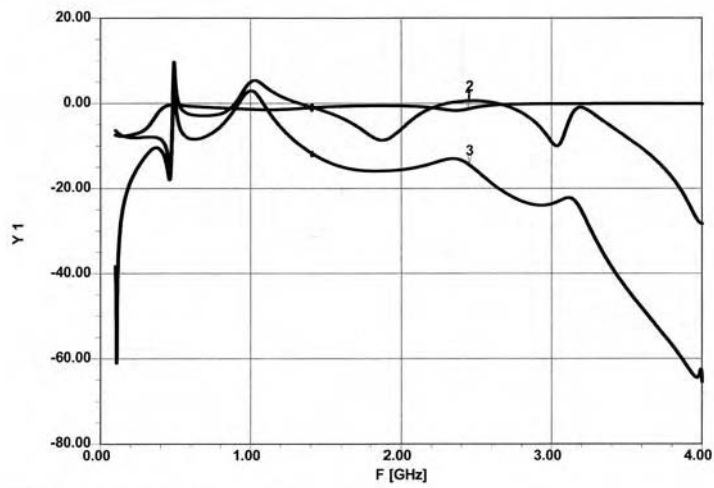
10 Jun 2008

Ansoft Corporation
XY Plot 1
Circuit1

17:16:26

2.45GHz RoF 1-Stage System

50mA Laser Diode Bias



X1= 2.45GHz Y1= -1.32
X2= 2.45GHz Y2= 0.61
X3= 2.45GHz Y3= -14.49

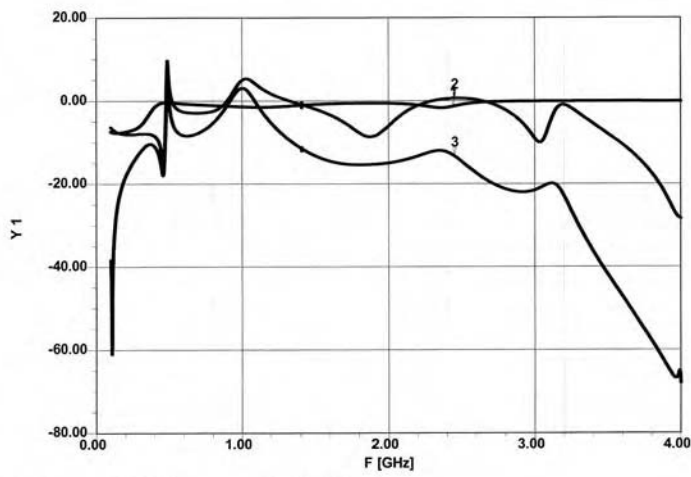
10 Jun 2008

Ansoft Corporation
XY Plot 1
Circuit1

17:06:43

2.45GHz RoF 1-Stage System

46mA Laser Diode Bias



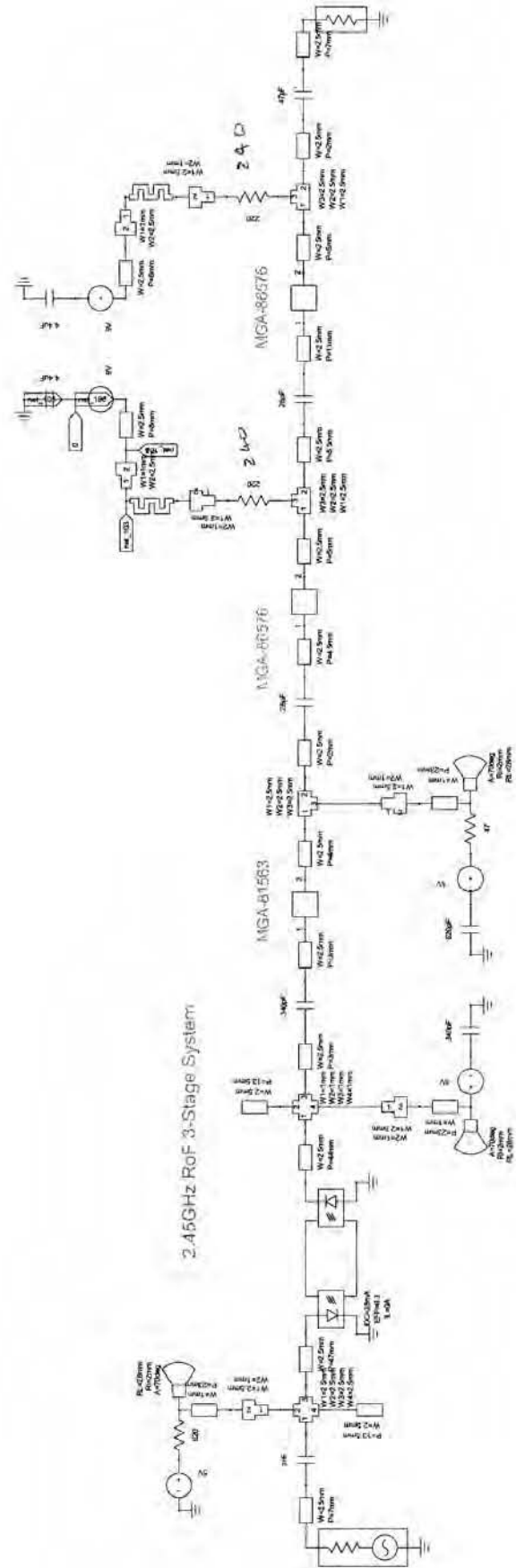
Y1	○
dB(S11)	
NWA1	
Y1	—
dB(S12)	
NWA1	
Y1	□
dB(S21)	
NWA1	
Y1	×
dB(S22)	
NWA1	

X1= 2.45GHz
Y1= -1.32

X2= 2.45GHz
Y2= 0.61

X3= 2.45GHz
Y3= -13.35

APPENDIX D



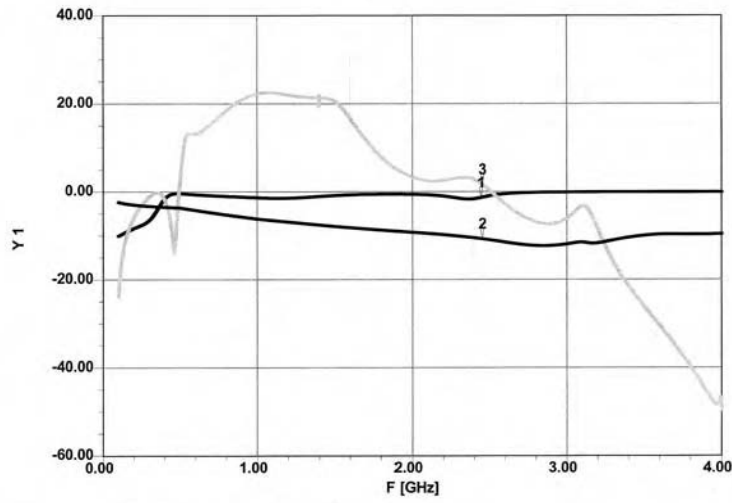
11 Jun 2008

Ansoft Corporation
XY Plot 1
Circuit1

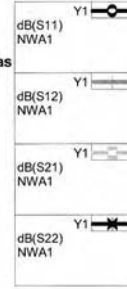
12:39:07

2.45GHz RoF 3-Stage System

28mA Laser Diode Bias



X1= 2.45GHz Y1= -1.33
X2= 2.45GHz Y2= -10.72
X3= 2.45GHz Y3= 1.65



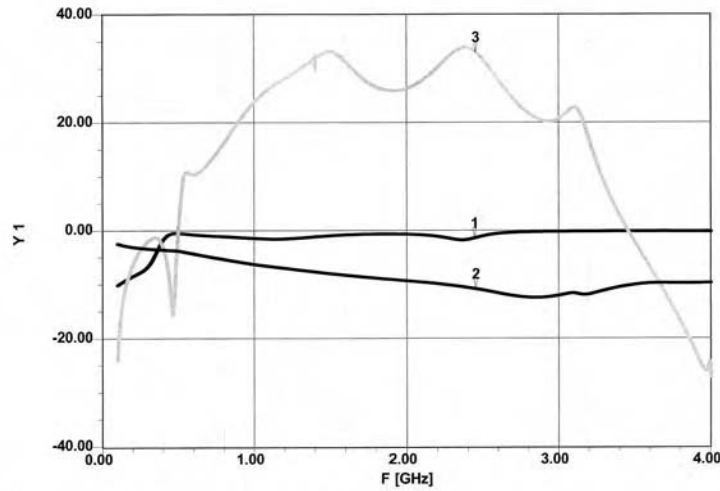
11 Jun 2008

Ansoft Corporation
XY Plot 1
Circuit1

12:36:58

2.45GHz RoF 3-Stage System

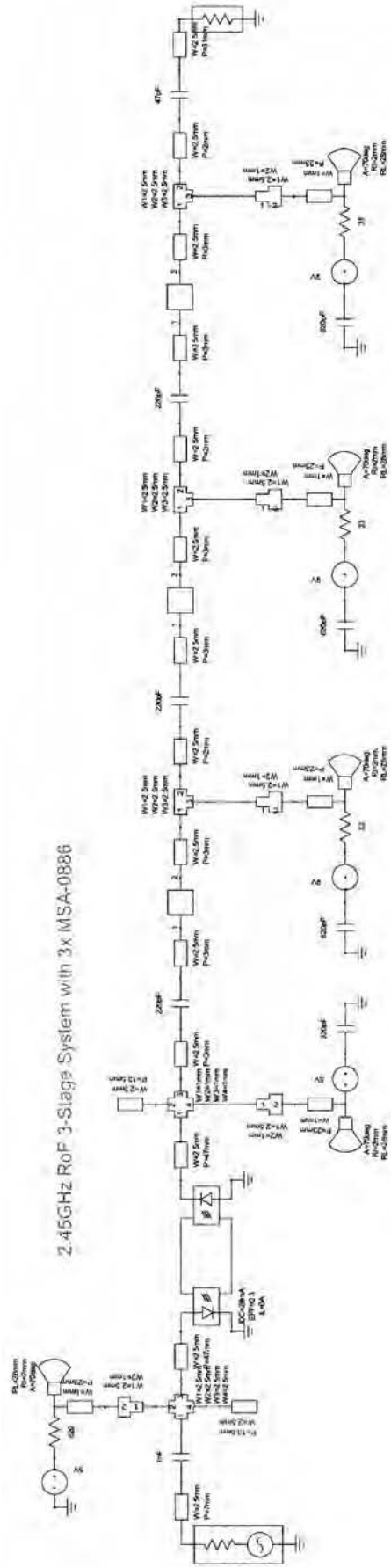
36mA Laser Diode Bias



X1= 2.45GHz Y1= -1.32
X2= 2.45GHz Y2= -10.72
X3= 2.45GHz Y3= 33.01



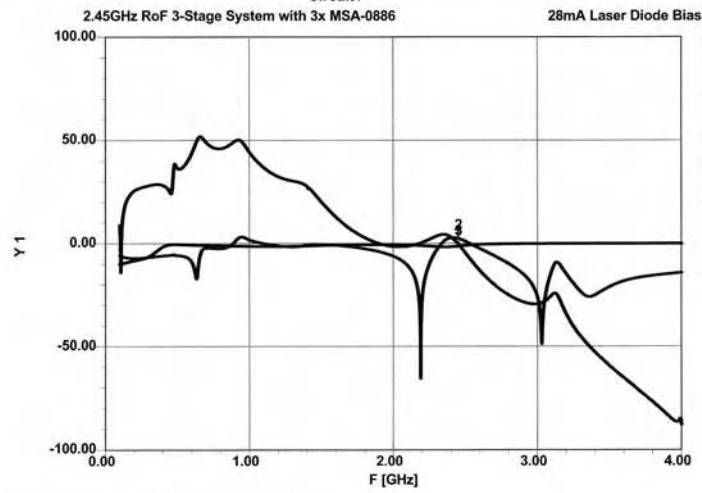
APPENDIX E



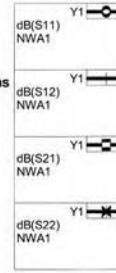
11 Jun 2008

Ansoft Corporation
XY Plot 1
Circuit1

12:40:04



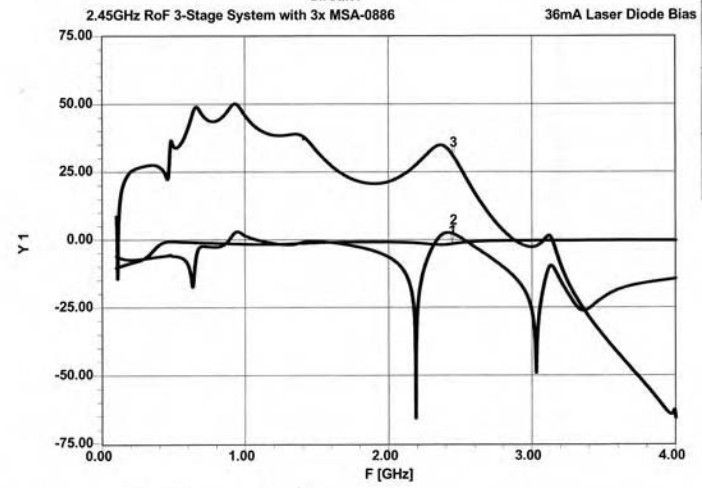
X1= 2.45GHz X2= 2.45GHz X3= 2.45GHz
Y1= -1.33 Y2= 2.36 Y3= -0.46



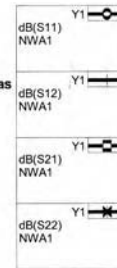
11 Jun 2008

Ansoft Corporation
XY Plot 1
Circuit1

12:37:22



X1= 2.45GHz X2= 2.45GHz X3= 2.45GHz
Y1= -1.32 Y2= 2.36 Y3= 30.89

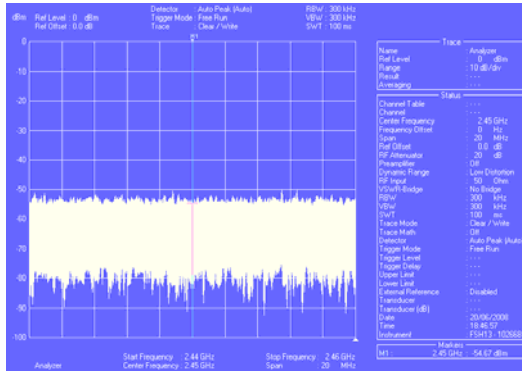


APPENDIX I

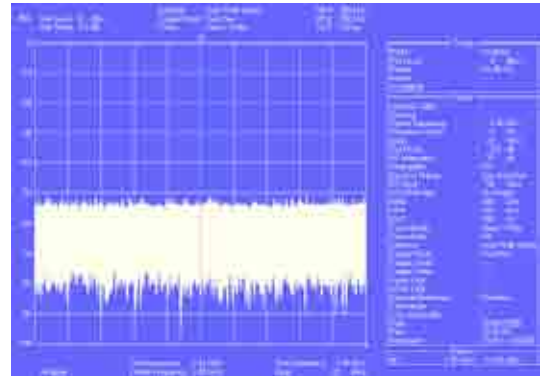
Measurement Results of 1-Stage MSA-0886 System (FG04-1)

R&S FSH3 Noise Floor

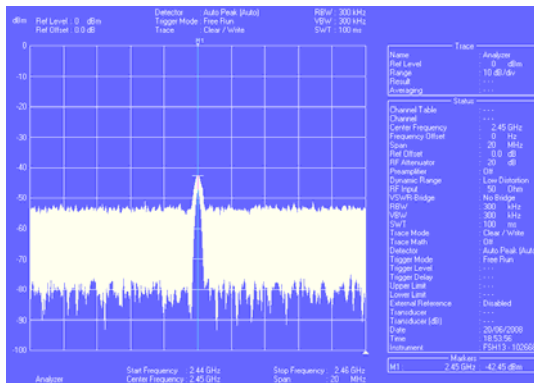
at $f_c=2.45\text{GHz}$, Span=20MHz



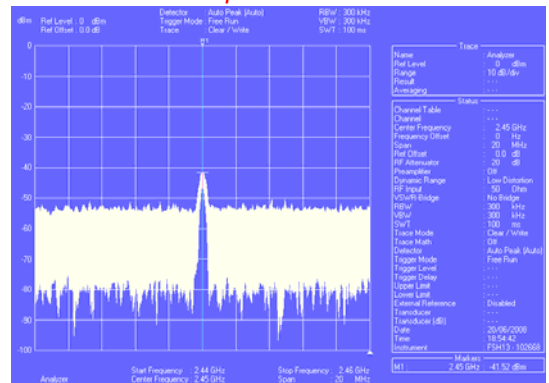
Coupled NF= -53dB (No measured coupling)



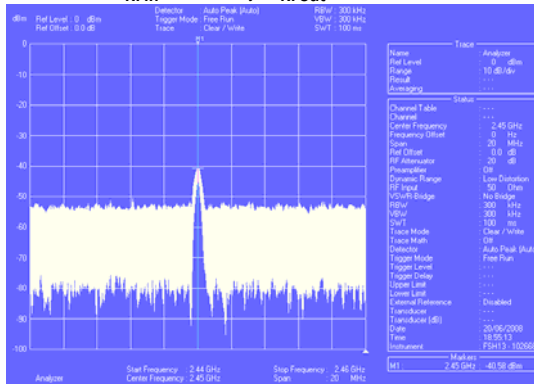
Uncoupled NF= -53dB



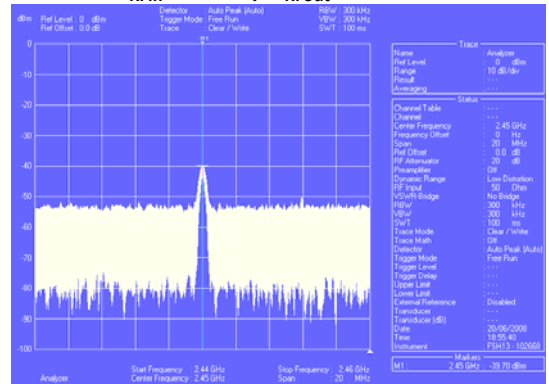
$P_{RFIn} = 0\text{dBm}$, $P_{RFout} = -42\text{dBm}$



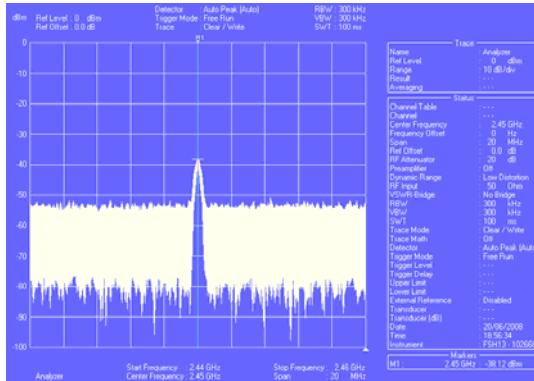
$P_{RFIn} = 3\text{dBm}$, $P_{RFout} = -41\text{dBm}$



$P_{RFIn} = 6\text{dBm}$, $P_{RFout} = -40\text{dBm}$



$P_{RFIn} = 9\text{dBm}$, $P_{RFout} = -39\text{dBm}$



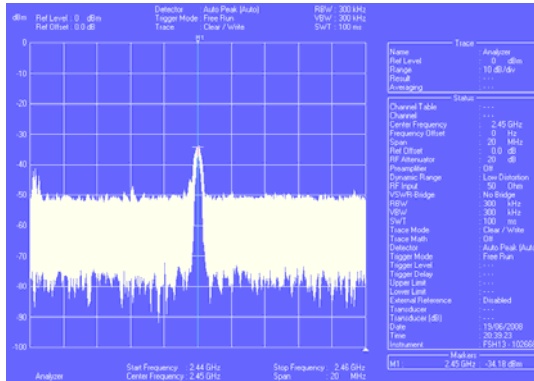
$P_{RFIn} = 12\text{dBm}$, $P_{RFout} = -38\text{dBm}$

APPENDIX J

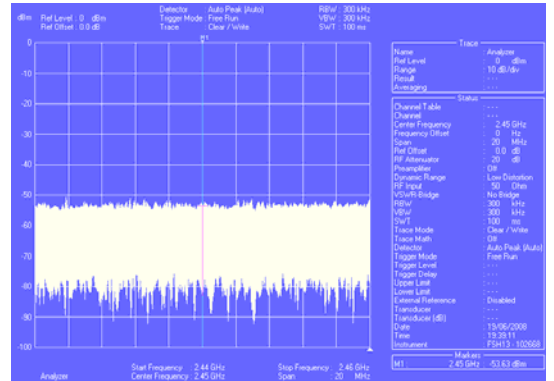
Measurement Results of 3-Stage 1 x MGA-815 & 2 x LNA MGA-865 System (FG04-2)

R&S FSH3 Noise Floor

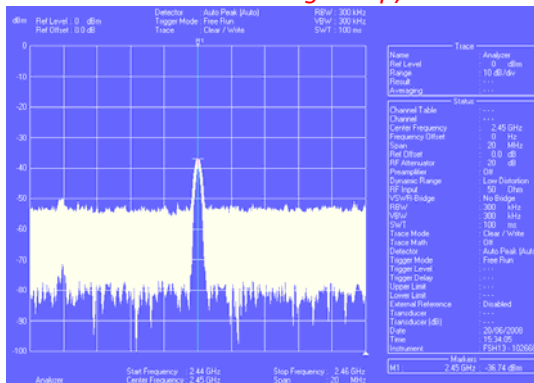
at $f_c=2.45\text{GHz}$, Span=20MHz



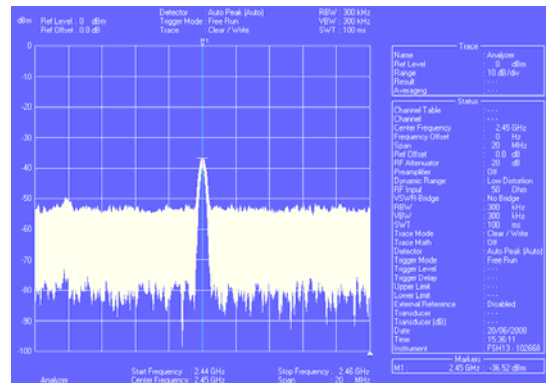
Coupled NF= -32dB (High proximity coupling due to 60dB 3-Stage Amp)



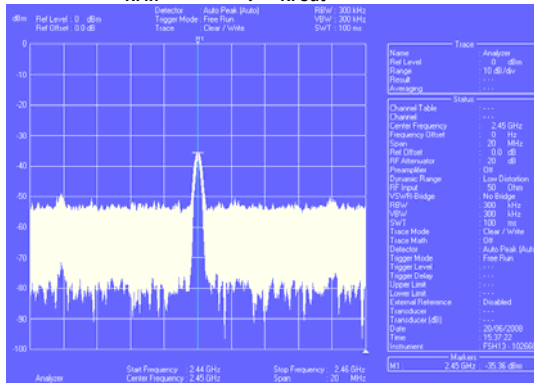
Uncoupled NF= -53dB



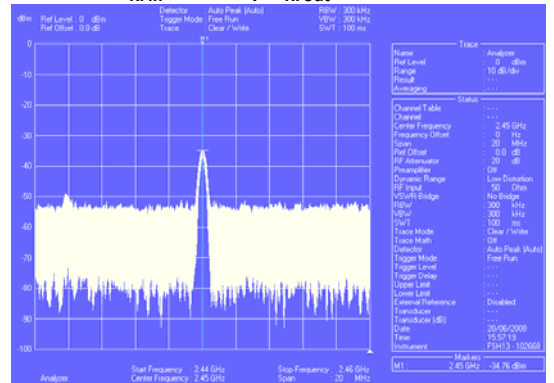
$P_{RFIn} = 0\text{dBm}$, $P_{RFout} = -38\text{dBm}$



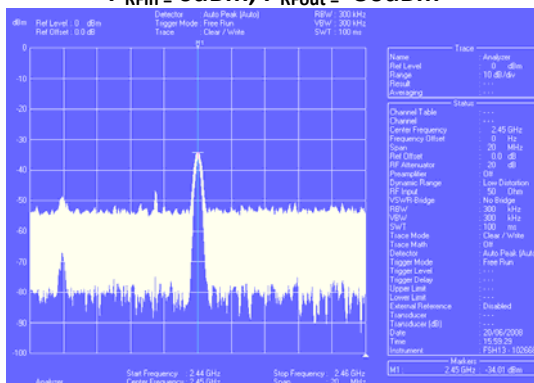
$P_{RFIn} = 3\text{dBm}$, $P_{RFout} = -37\text{dBm}$



$P_{RFIn} = 6\text{dBm}$, $P_{RFout} = -36\text{dBm}$



$P_{RFIn} = 9\text{dBm}$, $P_{RFout} = -35\text{dBm}$



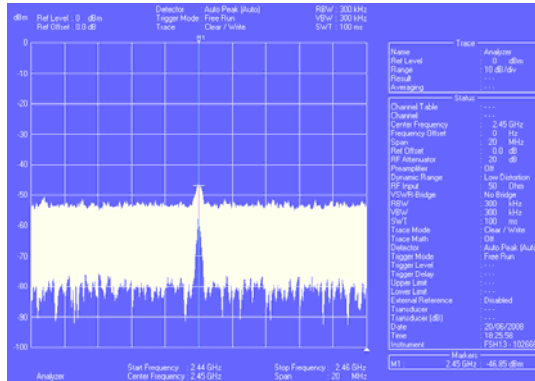
$P_{RFIn} = 12\text{dBm}$, $P_{RFout} = -34\text{dBm}$

APPENDIX K

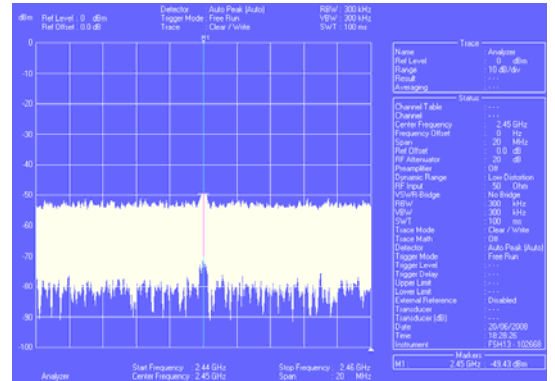
Measurement Results of 3-Stage 3 x MSA-0886 System (FG04-2)

R&S FSH3 Noise Floor

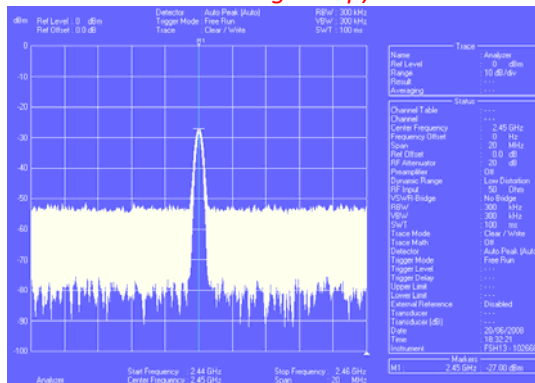
at $f_c=2.45\text{GHz}$, Span=20MHz



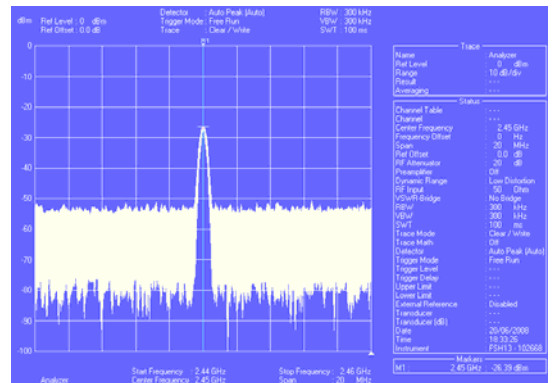
Coupled NF= -46dB (3dB proximity coupling due to 3-Stage Amp)



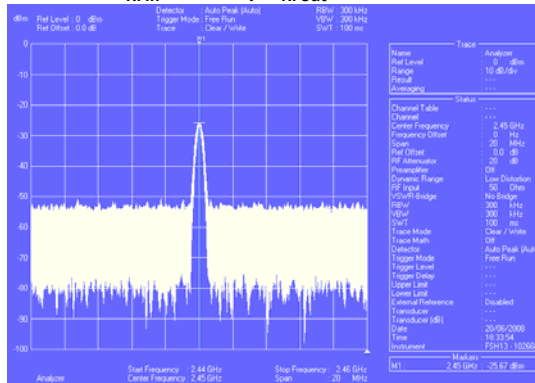
Uncoupled NF= -49dB



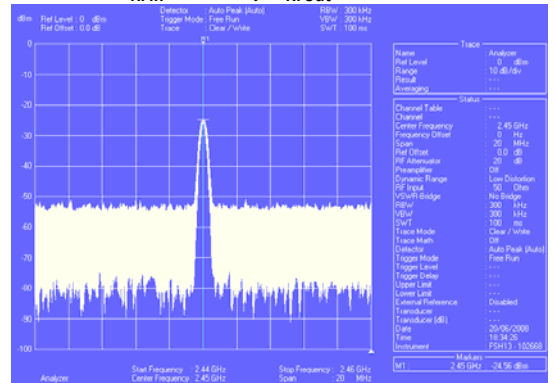
$P_{RFin} = 0\text{dBm}$, $P_{RFout} = -27\text{dBm}$



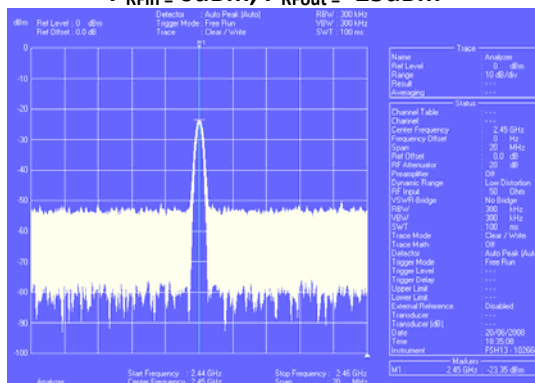
$P_{RFin} = 3\text{dBm}$, $P_{RFout} = -26\text{dBm}$



$P_{RFin} = 6\text{dBm}$, $P_{RFout} = -25\text{dBm}$



$P_{RFin} = 9\text{dBm}$, $P_{RFout} = -24\text{dBm}$



$P_{RFin} = 12\text{dBm}$, $P_{RFout} = -23\text{dBm}$

APPENDIX L

Commercial RoF System with unregulated 12V DC						
OZ600 Transceiver						
Loopback P Gain/Loss		OZ600 Specification:				
10m FC/APC - FC/APC 9/125um		Max RFin	10dBm	Id (typ)	240mA	
NA HP8722D		Max PoptIn	4mW	Measured Id	242mA	
		Max Vdc	12.5V	Id (max)	320mA	
		Min Vdc	11.5V	Poptout (typ)	1.6mW	
				Lambda	1310nm	
	No Optical	With Optical				
PRFin (dBm)	PRFout (dBm)	PRFout (dBm)	PGL (dB)			
-10	-37	-7.1	2.90			
OZ600 Tx to OZ450 Rx				OZ450 Tx to OZ600 Rx		
(System Link 1)				(System Link 2)		
Id (OZ600) = 242mA				Id (OZ600) = 242mA		
Id (OZ450 Rx) = 139mA				Id (OZ450 Tx) = 175mA		
10m FC/APC - FC/APC 9/125um				10m FC/APC - FC/APC 9/125um		
Sig Gen HP8648D				Sig Gen HP8648D		
Spec Anal 8560E - NF= -70dBm				Spec Anal 8560E - NF= -70dBm		
NF (No Optical/RF)= -73dBm				NF (With Optical/No RF)= -64dBm		
hence Laser Bias Gain = 73dBm-64dBm = 9dB						
PRFin (dBm)	PRFout (dBm)	PGL (dB)		PRFin (dBm)	PRFout (dBm)	PGL (dB)
-60	-59.0	1.0		-78	-53	25.0
-57	-57.0	0.0		-75	-52	23.0
-54	-54.0	0.0		-72	-51	21.0
-51	-52.0	-1.0		-69	-50	19.0
-48	-49.0	-1.0		-66	-48	18.0
-45	-45.0	0.0		-63	-45	18.0
-42	-42.0	0.0		-60	-42	18.0
-39	-40.0	-1.0		-57	-39	18.0
-36	-36.0	0.0		-54	-36	18.0
-33	-33.0	0.0		-51	-33	18.0
-30	-30.0	0.0		-48	-30	18.0
-27	-27.0	0.0		-45	-26	19.0
-24	-23.0	1.0		-42	-24	18.0
-21	-22.0	-1.0		-39	-21	18.0
-18	-18.0	0.0		-36	-18	18.0
-15	-15.0	0.0		-33	-15	18.0
-12	-13.0	-1.0		-30	-12	18.0
-9	-8.0	1.0		-27	-8.0	19.0
-6	-5.0	1.0		-24	-5.0	19.0
-3	-2.5	0.5		-21	-2.0	19.0
0	0.0	0.0		-18	1.0	19.0
3	2.0	-1.0		-15	4.0	19.0
6	5.0	-1.0		-12	6.0	18.0
9	8.0	-1.0		-9	8.0	17.0
10	10.0	0.0		-6	11.0	17.0
hence -1 to +1dB System Gain/Loss				-3	15.0	18.0
				0	16.0	16.0
				hence 16-25dB System Gain		

APPENDIX P

Coaxial System & Commercial RoF System

Comparison of Simulation and Measurement Results in Mike Stance

Simulation results attained using CST MWS with Mike phantom
 Measured results attained through measurements in anechoic chamber
 Transmitting from monopole on head to monopole on waist at 2.45 GHz

Matched Pair Simulation & Measurement
--

<u>Ideal Fibre System</u>			
Simulation 1		Measurement	
S11	S21	S11	S21
-17.74	-40.39	N/A	N/A

<u>Actual Fibre System</u>				
Simulation 2				
S11	S21			
-18.49	-39.55			
Measurement No.	Measurement over 60 Secs			
	S21 Min	S21 Mean	S21 Max	S21 Std Dev
1	-43.01	-42.12	-41.58	0.27
2	-43.23	-42.70	-41.99	0.20
3	-44.45	-43.71	-42.56	0.37
4	-40.85	-39.99	-39.38	0.28
5	-42.85	-41.77	-40.75	0.36
6	-42.70	-41.97	-40.62	0.31
7	-42.58	-41.82	-40.85	0.39
8	-44.13	-42.44	-41.09	0.76
9	-42.46	-41.26	-39.73	0.69
10	-43.89	-43.01	-42.03	0.49
11	-46.32	-43.87	-42.04	1.02
12	-44.18	-43.15	-42.30	0.40
13	-44.81	-43.75	-42.64	0.48
14	-46.32	-44.74	-43.60	0.51
15	-45.88	-44.57	-43.60	0.55
Total Fibre System Mean:	<u>-46.98</u>	<u>-45.78</u>	<u>-44.63</u>	<u>0.51</u>
Total Fibre System Δ<S21>	<u>-44.74</u>	<u>4.75</u>	<u>-39.99</u>	

<u>Vertical Coaxial System in Front</u>								
<u>Short Solid PEC Simulation</u>		<u>Short Coax Simulation 1</u>		<u>Long Solid PEC Simulation</u>		<u>Long Coax Simulation 2</u>		
S11	S21	S11	S21	S11	S21	S11	S21	
-15.67	-42.18	-14.82	-42.41	-19.74	-41.06	-21	-45.81	
Measurement No.	Measurement over 60 Secs							
	S21 Min	S21 Mean	S21 Max	S21 Std Dev				
1	-42.06	-41.12	-40.13	0.40				
2	-43.70	-42.16	-40.75	0.49				
3	-45.32	-44.11	-42.97	0.42				
4	-38.39	-37.17	-36.25	0.36				
5	-40.40	-39.46	-38.36	0.33				
Mean :	-41.97	-40.81	-39.69	0.40				
Δ<S21>	-44.11	6.94	-37.17					

<u>Vertical Coaxial System down Back</u>				
<u>Short Simulation</u>		<u>Long Simulation</u>		
S11	S21	S11	S21	
N/A	N/A	-13.74	-42.43	
Measurement No.	Measurement over 60 Secs			
	S21 Min	S21 Mean	S21 Max	S21 Std Dev
6	-41.58	-40.22	-39.32	0.44
7	-41.48	-40.41	-39.21	0.39
Mean :	-41.53	-40.31	-39.27	0.41
Δ<S21>	-40.41	0.20	-40.22	

<u>Horizontal Coaxial System</u>				
<u>Short</u> Simulation 3		<u>Long</u> Simulation 4		
S11	S21	S11	S21	
-15.3	-40.42	-19.7	-43.2	
Measurement No.	S21 Min	S21 Mean	S21 Max	S21 Std Dev
8	-42.62	-41.38	-40.37	0.56
9	-43.89	-42.86	-41.44	0.41
10	-44.41	-43.46	-42.42	0.37
11	-43.07	-41.56	-40.21	0.51
Mean :	-43.50	-42.31	-41.11	0.46
$\Delta<S21>$	-43.46	2.07	-41.38	

<u>Diagonal Coaxial System</u>				
<u>Short</u> Simulation		<u>Long</u> Simulation		
S11	S21	S11	S21	
N/A	N/A	N/A	N/A	
Measurement No.	S21 Min	S21 Mean	S21 Max	S21 Std Dev
12	-40.07	-38.71	-37.80	0.55
13	-39.79	-39.19	-38.09	0.19
Mean :	-39.93	-38.95	-37.95	0.37
$\Delta<S21>$	-39.19	0.47	-38.71	

Total Coax

System Mean: **-41.73** **-40.60** **-39.50** **0.41**

Total Coax System $\Delta<S21>$ **6.94**

Total Fibre System $\Delta<S21>$ **4.75**